ATMOSPHERIC TURBULENCE WITHIN AND ABOVE A CONIFEROUS FOREST

By

Xuhui Lee

B. Sc. (Meteorology) Nanjing Institute of Meteorology, China

M. Sc. (Micrometeorology) Nanjing Institute of Meteorology, China

A THESIS SUBMITTED IN PARTIAL FULFILLMENT OF

THE REQUIREMENTS FOR THE DEGREE OF

DOCTOR OF PHILOSOPHY

in

THE FACULTY OF GRADUATE STUDIES

DEPARTMENT OF SOIL SCIENCE

We accept this thesis as conforming

to the required standard

THE UNIVERSITY OF BRITISH COLUMBIA

January 1992

© Xuhui Lee, 1992

In presenting this thesis in partial fulfilment of the requirements for an advanced degree at the University of British Columbia, I agree that the Library shall make it freely available for reference and study. I further agree that permission for extensive copying of this thesis for scholarly purposes may be granted by the head of my department or by his or her representatives. It is understood that copying or publication of this thesis for financial gain shall not be allowed without my written permission.

Department of SOIL SCIENCE

The University of British Columbia
Vancouver, Canada

Date April 22, 1992

DE-6 (2/88)

Abstract

An experiment to study the exchange processes within and above an extensive coniferous forest of Douglas-fir trees was conducted on Vancouver Island during a two-week rainless period in July and August 1990. The stand, which was planted in 1962, thinned and pruned uniformly in 1988, had a (projected) leaf area index of 5.4 and a height of h = 16.7 m. The experimental site was located on a 5° gentle slope. The primary instrumentation included two eddy correlation units which were operated in the daytime to measure the fluctuations in the three velocity components, air temperature and water vapour density. One unit was mounted permanently at a height of 23.0 m (z/h = 1.38) and the other at various heights of (z/h in brackets) 2.0 (0.12), 7.0 (0.42), 10.0 (0.60), and 16.7 m (1.00) with two to three 8-hour periods of measurement at each level. Profiles of wind speed and air temperature were measured continuously during the experimental period at heights of 0.9, 2.0, 4.6, 7.0, 10.0, 12.7, 16.7 and 23.0 m using sensitive cup anemometers and fine wire thermocouples, respectively. Radiation regimes and air humidity were measured both above and beneath the overstory of the stand.

The vertical structure of the stand affected, to a great extent, the vertical distributions of the velocity statistics (wind speed, variance, turbulence intensity, Reynolds stress, skewness and kurtosis), air temperature, sensible and latent heat fluxes. The effect was also evident in the quadrant representation of the fluxes of momentum, sensible heat and water vapour. Negative Reynolds stress persistently occurred at the lower heights of the stand (z/h = 0.12 and 0.42). The negative values were related to the local wind speed gradients and it is believed that the longitudinal pressure gradient due to land-sea/upslope-downslope circulations was the main factor responsible for the upward

transport of the momentum at these heights. Energy budget was examined both above and beneath the overstory of the stand. The sum of sensible and latent heat fluxes above the stand accounted for, on average, 83% of the available energy flux. Beneath the overstory, the corresponding figure was 74%. On some days, energy budget closure was far better than on others. Counter-gradient flux of sensible heat constantly occurred at the canopy base (z/h = 0.42), invalidating the conventional gradient-diffusion relationship or K-theory at this height. Near the forest floor, however, K-theory with a far-field eddy diffusivity appeared to work satisfactorily. The daytime profiles of the dimensionless potential temperature, $\Delta\theta/\theta_*$, where the characteristic temperature, θ_* was defined as the ratio of the kinematic sensible heat flux to the square root of the vertical velocity variance both measured above the stand (z/h = 1.38), were found to be well stratified by H_g/H_T, the ratio of the sensible heat flux measured near the forest floor (z/h = 0.12) to that measured above the stand (z/h = 1.38). The profile of $\Delta\theta/\theta_*$ was simulated by combining the random flight technique for the dispersion of sensible heat from the elevated canopy source and the gradient-diffusion model with a far-field diffusivity for the dispersion from the ground-level source. The simulated profile agreed reasonably well with the measured one. The simulation results suggested that the profile of $\Delta\theta/\theta_*$ was not sensitive to the shape of the wind speed profile.

Table of Contents

List of Symbols

A	plant element area density (m^2/m^3)
A_{T_a}	amplitude of the diurnal course of air temperature (°C)
C_d	effective drag coefficient of plant elements
C_e	scalar concentration for an elementary point source
C_p	scalar concentration for a plane source
D	spacing among trees (Chapter 2, D = 4.2 m for the stand at Browns River)
D	saturation deficit (Chapter 3, kPa)
$\overline{D}$	arithmetic average of the daytime saturation deficit (kPa)
F_e	vertical scalar flux[1] for an elementary point source
F_g	scalar flux from the forest floor
$F_{i,H}$	flux fraction of sensible heat or water vapour in the quadrant-hole analysis
F_p	vertical scalar flux for a plane source
G	soil heat flux (W/m^2)
H	hole size in the quadrant-hole analysis
H	sensible heat flux (W/m^2)
H'	hole size above which half of the eddy flux occurs (Chapters 2 and 3)

[1]The term 'flux' in this dissertation is an abbreviation for 'flux density' as commonly used in micrometeorology literature.

H'	sensible heat flux simulated for finite fetches (Chapter 4, W/m^2)
H_g	sensible heat flux from the forest floor (W/m^2)
H_T	total sensible heat flux from the stand (W/m^2)
$I_{i,H}$	conditioning function in the quadrant-hole analysis
K	diffusivity in Batchelor's diffusion equation (m^2/s)
Kr_u	kurtosis of the u velocity component
Kr_v	kurtosis of the v velocity component
Kr_w	kurtosis of the w velocity component
K_f	far field eddy diffusivity (m^2/s)
L	Monin-Obukhov length, defined as $-\dfrac{u_*^3 \rho c_p T_a}{kgH(1+0.07/\beta)}$ (m)
M	number of fluid particles released in the ensemble experiment
$M_{\mathrm{cross}}(z)$	net number of fluid particles that cross height z in the ensemble experiment
P	transition probability density of the vertical position of a marked fluid particle
P_s	shear production term in Reynolds stress budget
P_w	wake production term in Reynolds stress budget
R_n	net radiation flux (W/m^2)
S	rate of heat storage in the layer between the 0 and 23.0 m heights per unit ground area (Chapter 3, W/m^2)
S	global solar irradiance (horizontal surface) (Appendix E, W/m^2)
$S(z)$	source density or flux divergence of sensible heat or water vapour (Chapter 3)
$S(z)$	source density of sensible heat (Chapter 4, W/m^3)

$\overline{S}$ daytime average global solar irradiance (horizontal surface, W/m^2)

Sk_u skewness of the u velocity component

Sk_v skewness of the v velocity component

Sk_w skewness of the w velocity component

$S_{i,H}$ fraction of Reynolds stress in the quadrant-hole analysis

S_l rate of latent heat storage in the air between the 0 and 23.0 m heights per unit ground area (W/m^2)

S_{nb} rate of heat storage in needles and branches per unit ground area (W/m^2)

S_s rate of sensible heat storage in the air between the 0 and 23.0 m heights per unit ground area (W/m^2)

St Strouhal number (= 0.21)

S_t rate of heat storage in tree trunks per unit ground area (W/m^2)

T average time interval (= 30 min)

T_a air temperature (°C)

$\overline{T_a}$ daytime average air temperature (°C)

$\overline{T'^2}$ variance of air temperature (°C^2)

T_L Lagrangian integral time scale (s)

T_{nb} temperature of needles and branches (°C)

T_t turbulent transport term in Reynolds stress budget

T_* characteristic air temperature, defined as $\overline{w'T'}/u_*$ (°C)

U 30-minute averaged wind speed measured with cup anemometers (Chapter 2, m/s)

U 30-minute averaged wind speed measured with hot wire anemometers (Appendix E, m/s)

$\overline{U}$	daytime average wind speed measured with cup anemometers (m/s)
U_r	wind speed measured with a hot wire anemometers at height z_r (m/s)
V	30-minute averaged equivalent cup wind speed for sonic anemometers, defined as $\overline{\sqrt{u_1^2 + v_1^2}}$ (m/s)
$< X_m >$	total streamwise distance traversed by marked fluid particle m in the ensemble experiment (m)
Z	vertical position of a marked fluid particle in the ensemble experiment (m)
a_T	constant in the Monin-Obukhov scaling of σ_T (= 0.9)
a_w	constant in the Monin-Obukhov scaling of σ_w (= 1.9)
a_{ρ_v}	constant in the Monin-Obukhov scaling of σ_{ρ_v} (= 1.1)
c_{nb}	specific heat of needles and branches (J/(°C kg))
c_p	specific heat of air at constant pressure (J/(°C kg))
d	displacement height (Chapter 2, $d = 0.7h$)
d	effective source height (Chapter 3, m)
d	diameter of the tree trunk (Appendix E)
f	vertical gradient of the variance of the Eulerian vertical velocity (m/s^2)
f_{Fi}	component of the form drag vector exerted on a unit mass of air
f_{Vi}	component of the viscous drag vector exerted on a unit mass of air
h	height of the stand at Browns River (= 16.7 m)
i	turbulence intensity
i_u	turbulence intensity for the u velocity component
i_v	turbulence intensity for the v velocity component

i_w	turbulence intensity for the w velocity component
k	von Karman constant (= 0.4)
m	mass of needles and branches per unit volume of air (kg/m^3)
n	natural frequency (Hz)
p	atmospheric pressure (kPa)
r_a	aerodynamic resistance to water vapour and sensible heat diffusion (s/m)
r_c	bulk canopy resistance (s/m)
$\overline{r}_c$	daytime mean canopy resistance (s/m)
$\overline{r}_h$	daytime average relative humidity
r_m	aerodynamic resistance to momentum transfer (s/m)
s	slope of the saturation vapour pressure at air temperature (kPa/°C)
t	time (s)
t_f	a migration time, defined as x_f/u (s)
$t_{i,H}$	time fraction in the quadrant-hole analysis
u	longitudinal velocity component (m/s)
u	streamwise velocity component (Appendix E, m/s)
u_1	one of the two horizontal components of the instantaneous velocity vector in the instrument coordinate system (m/s)
$\overline{u'^2}$	variance of the u velocity component (m^2/s^2)
u_i	component of the velocity vector in tensor notation (m/s)
u_i	a set of uniform random numbers in the range 0–1 (Chapter 4)
u_{ref}	wind speed at the reference location (m/s)
u_*	friction velocity, defined as $\sqrt{-\overline{u'w'}}$ (m/s)

$-\overline{u'w'}$	kinematic Reynolds stress (m^2/s^2)
v	lateral velocity component (m/s)
v_1	one of the two horizontal components of the instantaneous velocity vector in the instrument coordinate system (m/s)
$\overline{v'^2}$	variance of the v velocity component (m^2/s^2)
w	vertical velocity component (m/s)
w	velocity component perpendicular to the slope surface (Appendix E, m/s)
w_1	Lagrangian vertical velocity of a marked fluid particle at release (m/s)
$\overline{w'^2}$	variance of the w velocity component (m^2/s^2)
$\overline{w'^2_E}$	variance of the Eulerian vertical velocity (Chapter 4 and Appendix D, m^2/s^2)
w_n	Lagrangian vertical velocity of a marked fluid particle at step n (m/s)
$w(z_o, t)$	Lagrangian vertical velocity of a marked fluid particle (m/s)
$\overline{w'T'}$	covariance between the vertical velocity component and air temperature or kinematic sensible heat flux (°C m/s)
$\overline{w'_1T'_2}$	covariance between the vertical velocity component of unit 1 and air temperature of unit 2 (°C m/s)
$\overline{w'\rho'_v}$	covariance between the vertical velocity component and water vapour density or water vapour flux ($g/(m^2s)$)
$\overline{w'_2\rho'_{v1}}$	covariance between the vertical velocity component of unit 2 and water vapour density of unit 1 ($g/(m^2s)$)

$\overline{(w'T')_2}$	kinematic sensible heat flux measured with unit 2 (°C m/s)
$\overline{(w'\rho_v')_1}$	water vapour flux measured with unit 1 (g/(m^{2}s))
x	longitudinal component of position vector (m)
x_1	horizontal position of a marked fluid particle at release (m)
x_f	horizontal position of the leading edge of a plane source (m)
x_i	position vector in tensor notation (m)
x_n	horizontal position of a marked fluid particle at step n (m)
x_p	fetch (m)
y	lateral component of position vector (m)
z	height or vertical component of position vector (m)
z_1	vertical position of a marked fluid particle at release (m)
z_n	vertical position of a marked fluid particle at step n (m)
z_o	height of the source for a marked fluid particle (Appendix D, m)
z_o	effective roughness length of the ground surface (Appendix E, m)
z_r	reference height (= 23.0 m for the stand at Browns River)
z_r	reference height (= 2.0 m for the stand near Woss)
z_*	height of roughness sublayer (m)
α	coefficient in the Langevin equation (Appendix D)
β	Bowen ratio
Δt_n	time step at step n (s)
$\Delta\overline{T}_a$	change over a 30-minute interval in air temperature averaged over the layer between the 0 and 23.0 m heights (°C)

$\Delta\overline{T}_{nb}$	change over a 30-minute interval in the average temperature of needles and branches (°C)
$\Delta\overline{\rho}_v$	change over a 30-minute interval in water vapour density averaged over the layer between the 0 and 23.0 m heights (g/m^3)
$\Delta\theta$	potential temperature difference, defined as $\theta - \theta(z_r)$ (°C)
γ	psychrometric constant (kPa/°C)
λ	latent heat of vaporization of water (J/kg)
λ	coefficient in the Langevin equation (Appendix D)
λE	latent heat flux (W/m^2)
ν	kinematic viscosity (m^2/s)
Ω	McNaughton and Jarvis's Omega factor
ω	diurnal angular frequency ($= \pi/12$ rad/h)
Φ	term of the interaction between velocity and pressure fields in Reynolds stress budget
ϕ	phase angle of the diurnal course of air temperature (rad)
$\phi_{\alpha\alpha}$	power spectrum of quantity α
ρ	air density (g/m^3)
ρ_v	water vapour density (g/m^3)
ρ_{v*}	characteristic water vapour density, defined as $\overline{w'\rho_v'}/u_*$ (g/m^3)
σ_T	square root of the variance of air temperature (°C)
σ_u	square root of the variance of the u velocity component (m/s)
σ_w	square root of the variance of the w velocity component (m/s)
σ_w^2	variance of Lagrangian vertical velocity (Chapter 4 and Appendix D, m^2/s^2)
σ_Z	mean depth of plume or square root of the variance of the vertical position of a marked fluid particle (m)

σ_{ρ_v}	square root of the variance of water vapour density (g/m^3)
τ	time scale for parameterizing Φ (s)
θ	potential air temperature (°C)
θ_c	contribution of the canopy source to potential air temperature (°C)
θ_g	contribution of the ground-level source to potential air temperature (°C)
θ_*	characteristic potential temperature, defined as $\dfrac{H_T}{\rho c_p \sigma_w(z_r)}$ (°C)
ξ	Gaussian white noise
ξ_n	a set of Gaussian random numbers with zero mean and unit variance
$'$	departure from temporal or ensemble average
$''$	departure from spatial average
$\overline{}$	temporal or ensemble averaging operator
$<>$	spatial averaging operator

List of Tables

List of Figures

To my wife, Yuhong

Acknowledgements

I wish to acknowledge the University Graduate Fellowships of B.C. and research and teaching assistantships in the Soil Science Department of University of B.C. The funding for the research work was provided through grants from the Natural Science and Engineering Research Council of Canada, Canadian Forest Products Inc. and MacMillan Bloedel Limited.

During my Ph.D. program I have been helped by many people. In particular, I wish to extend my sincere thanks to Dr. T.A. Black, my supervisor, for his steering role and participation in the field experiments, his constructive comments on drafting the dissertation and his great friendship, and to his family for their kindness in many ways. I also wish to thank Dr. M.D. Novak for his encouragement and his interest in my research over the years. Thanks also go to Drs. T.M. Ballard and I.S. Gartshore for being in my supervisory committee and for their assistance; Bob Sagar, Jing-Ming Chen and Rick Ketler for their friendship and help with the experiments; Ralph Adams for designing the hot wire anemometer system for the old growth experiment; Al Mcleod and John Harwijne for their help in selecting the research sites; and last, but not least, David Loh and John Janmaat for their help in the field experiments.

Chapter 1

Introduction

The understanding of forest canopy-atmosphere exchange is of great importance to a variety of scientific issues, such as global and regional CO_2 and water balances, and the transport, dispersion and deposition of air borne pollutants. The conventional gradient-diffusion relationship, or K-theory, has been used for many years to study the exchange processes near the surface of the earth. However, experimental studies in the past two decades have shown that turbulent exchange in the upper part of and immediately above forests and plant canopies of other types is dominated by large intermittent eddies. Because the sizes of these eddies are comparable to canopy height, which is the scale of scalar concentration and velocity gradients, the validity of K-theory is questionable. In recent years, much attention has been directed to alternative approaches, such as random flight simulations in a Lagrangian framework (e.g. Leclerc *et al.* 1988, Legg *et al.* 1986, Legg and Raupach 1982) and higher order closure models (Meyers and Paw U 1986, Wilson 1988, Wilson and Shaw 1977). These theories are, however, still at an early stage of development. More experimental studies are required to provide data for testing and further development of the theories.

Recently experiments have been conducted on atmospheric turbulence in forest stands of various tree species, e.g. in mixed deciduous forests of oak and hickory trees (Baldocchi and Meyers 1988) and of mainly aspen and red maple trees (Shaw *et al.* 1988), in a forest of pine trees (Denmead and Bradley 1985), and in forests of aspen, pine and spruce trees (Amiro 1990a and 1990b). In this work, a coastal coniferous forest of Douglas-fir trees on Vancouver Island was selected as the site for a turbulent exchange experiment.

Douglas-fir is an important tree species in the northwest coastal region of North America. In western Oregon, Washington and British Columbia, Douglas-fir occupies about 15.8 million hectares (Oliver *et al.* 1986). The evapotranspiration process from Douglas-fir stands has been studied extensively using the energy balance approach with the guidance of Monteith's big leaf model (Monteith 1965) or its improved versions (e.g. Kelliher *et al.* 1986, Tan and Black 1976, McNaughton and Black 1973, Fritschen *et al.* 1985). Yet relatively little is known about the turbulent characteristics of the air flow and the exchange processes within and above forests of this type. The overall goal of the study reported here is to examine in detail the turbulence regimes and the exchange processes within and immediately above this selected stand. The study was part of a collaborative research project which aimed to develop silvicultural prescriptions that would satisfy timber production objectives while creating black-tailed deer winter range on the Island. It is also intended to contribute to an improved understanding of the exchange processes in forest environments in general.

This dissertation consists of three papers. The first paper (Chapter 2) is limited to the statistical properties of the velocity field within and above the stand. The second paper (Chapter 3) concentrates on the eddy fluxes of sensible heat and water vapour within and above the stand. The third paper (Chapter 4) analyses the profiles of air temperature using Lagrangian theories for scalar dispersion. The conclusions of the dissertation are presented in Chapter 5. Supplementary results and discussions can be found in the Appendices.

References

Amiro, B.D.: 1990a, 'Comparison of turbulence statistics within three Boreal forest canopies', *Boundary-Layer Meteorol.* **51**, 99-121.

Amiro, B.D.: 1990b, 'Drag coefficients and turbulence spectra within three Boreal forest canopies', *Boundary-Layer Meteorol.* **52**, 227-246.

Baldocchi, D.D. and Meyers, T.P.: 1988, 'Turbulence structure in a deciduous forest', *Boundary-Layer Meteorol.* **43**, 345-364.

Denmead, O.T. and Bradley, E.F.: 1985, 'Flux-gradient relationships in a forest canopy', in Hutchison, B.A. and Hicks, B.B. (eds.), *The Forest-Atmospheric Interaction*, D. Reidel Publishing Co., Dordrecht, 421-442.

Fritschen, L.J., Gay L. and Sympson J.: 1985, 'Eddy diffusivity and instrument resolution in relation to plant height', in Hutchison, B.A. and Hicks, B.B. (eds.), *The Forest-Atmospheric Interaction*, D. Reidel Publishing Co., Dordrecht, 583-590.

Kelliher, F.M., Black, T.A. and Price, D.T.: 1986, 'Estimating the effects of understory removal from a Douglas-fir forest using a two-layer canopy evapotranspiration model', *Water Resource Research*, **22**, 1891-1899.

Leclerc, M.Y., Thurtell, G.W. and Kidd, G.E.: 1988, 'Measurements and Langevin simulations of mean tracer concentration fields downwind from a circular line source inside an alfalfa canopy', *Boundary-Layer Meteorol.* **43**, 287-308.

Legg, B.J. and Raupach, M.R.: 1982, 'Markov-chain simulation of particle dispersion in inhomogeneous flows: The mean drift velocity induced by a gradient in Eulerian velocity variance', *Boundary-Layer Meteorol.* **24**, 3-13.

Legg, B.J., Raupach, M.R. and Coppin, P.A.: 1986, 'Experiments on scalar dispersion within a plant canopy. Part III: An elevated line source', *Boundary-Layer Meteorol.* **35**, 277-302.

McNaughton, K.G. and Black, T.A.: 1973, 'A study of evapotranspiration from a Douglas-fir forest using the energy balance approach', *Water Res. Res.* **9,** 1579-1590.

Meyers, T. and Paw U, K.T.: 1986, 'Testing of a higher-order closure model for modeling airflow within and above plant canopies', *Boundary-Layer Meteorol.* **37,** 297-311.

Oliver, C.D., Hanley, D.D. and Johnson, J.A.: 1986, *Douglas-fir: Stand Management for the Future*, College of Forest Resources of University of Washington, Seattle, Washington.

Price, D.T. and Black, T.A.: 1990, 'Effects of short-term variation in weather on diurnal canopy CO_2 flux and evapotranspiration of juvenile Douglas-fir stand', *Agric. For. Meteorol.* **50,** 139-158.

Shaw, R.H., Den Hartog, G. and Neumann, H.H.: 1988, 'Influence of foliar density and thermal stability on profiles of Reynolds stress and turbulence intensity in a deciduous forest', *Boundary-Layer Meteorol.* **45,** 391-409.

Tan, C.S. and Black, T.A.: 1976, 'Factors affecting the canopy resistance of a Douglas-fir forest', *Boundary-Layer Meteorol.* **10,** 475-488.

Wilson, J.D.: 1988, 'A second-order closure model for flow through vegetation', *Boundary-Layer Meteorol.* **42,** 371-392.

Wilson, R.N. and Shaw, R.H.: 1977, 'A higher order closure model for canopy flow', *J. Appl. Meteorol.* **14,** 1197-1205.

Chapter 2

Statistical Properties of the Velocity Field

2.1 Introduction

The description of turbulence statistics is a prerequisite to understanding turbulent transport of water vapour, carbon dioxide, trace gases, heat and particles within and beneath forest canopies and in the surface layer above the forest stands. Velocity statistics are required either as inputs to canopy flow models (e.g. Shaw and Wilson 1977) and Lagrangian dispersion models (e.g. Chapter 4) or for testing these models. The asymmetric and intermittent nature of the flow within the stand affects the release and deposition of spores (Aylor 1991), while high turbulence intensity of the flow may play an important role in enhancing heat loss from wild animals (Sagar *et al.* 1991). Thermal stability was reported to influence some of the statistics within forests (Shaw *et al.* 1988, Leclerc *et al.* 1991), and its influence on the flux-gradient relationships immediately above forests has been frequently observed to be different from that for smooth surfaces (e.g. Raupach 1979).

This Chapter is limited to the statistical properties of the velocity field within and above the selected Douglas-fir stand. The objectives of this Chapter are: (1) to document the stability regimes using the Monin-Obukhov length scale and to examine the applicability of Monin-Obukhov scaling above the stand; (2) to describe the statistics of the velocity field, including mean wind speed, Reynolds stress, variance, turbulence intensity, skewness, and kurtosis, with discussion of the mechanism of momentum transfer in the lower part of the stand; and (3) to quantify the intermittency and identify the kinds of turbulent motion which dominate momentum transfer using the quadrant-hole conditional sampling technique.

2.2 Experimental Methods

2.2.1 Site Description

The experiment was performed in late July and early August, 1990 in a coniferous stand near Browns River located approximately 10 km west of Courtenay on Vancouver Island, 125°10′W, 49°42′N, at an elevation of 450 m (Appendix F). The overstory species is Douglas-fir (*Pseudotsuga menziesii* Franco), planted in 1962. In 1988, it was thinned to 575 stems/ha and pruned to a height of approximately 6 m uniformly over a 600 m × 600 m plot. The forest floor was littered with dead branches and tree trunks, with a little understory vegetation (salal, Oregon grape and huckleberry) less than 0.5 m tall. The average trunk diameter at a height of 1.3 m was 0.20 m. A visual inspection from the instrument tower provided an estimate of 16.7 m for the height of the stand (h). Surrounding the plot are unthinned and unpruned stands of Douglas-fir trees of similar age and height which extend several kilometres.

The profile of the leaf area density of the stand was obtained from intensive destructive sampling on four trees of selected sizes. A branch was sampled every two whorls. The base diameter of all branch on the four trees and the diameter at a height of 1.3 m of 250 trees were measured. The area of needle samples pressed between two glass plates was measured with a video-camera image analysis system (Skye Instruments Ltd., Liandrindod Wells, UK). Leaf area density of the stand was obtained from the relationships between dry needle weight (dried for 8 hours at 80°C) and the projected needle area, between branch diameter and dry needle weight, and between tree diameter and foliage area per tree. The profile of leaf area density is presented in Figure 2.1. The total (projected) leaf area was 5.4.

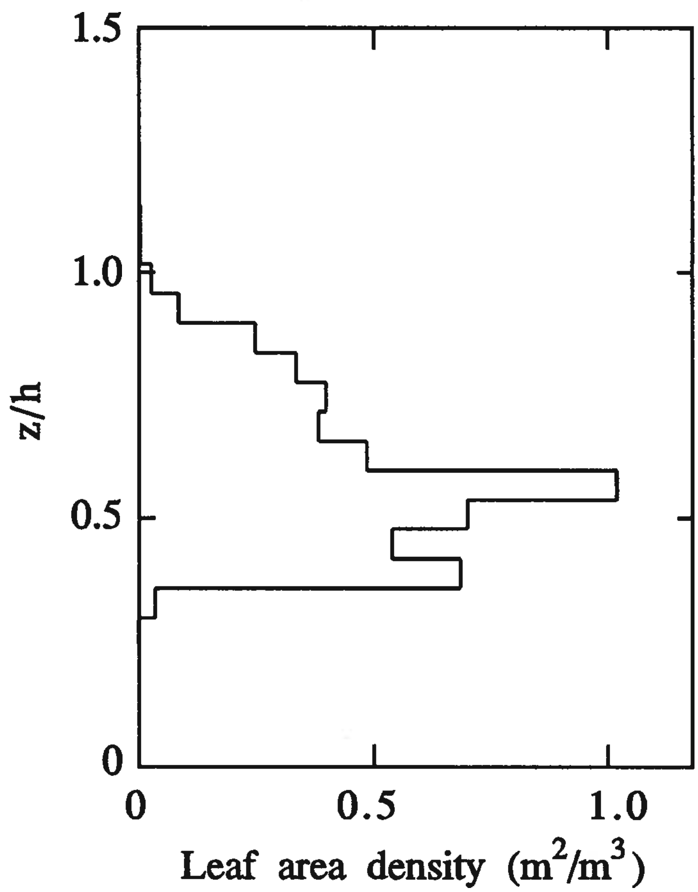

Figure 2.1: Profile of leaf area density of the Douglas-fir stand at Browns River. The total (projected) leaf area index was 5.4.

Table 2.1: Average values of weather variables at z/h = 1.38 for the period 06:00–18:00 PST, the period of operation of the eddy correlation units, and the relative height of the lower eddy correlation unit (z/h) for the Douglas-fir stand at Browns River. $\overline{S}$, $\overline{U}$, $\overline{T_a}$ and $\overline{r_h}$ represent global solar irradiance (horizontal surface), wind speed measured with a cup anemometer, air temperature and relative humidity (average water vapour pressure divided by saturated water vapour pressure at $\overline{T_a}$), respectively. The height of the stand (h) was 16.7 m.

Date	Period Hour (PST)	z/h	$\overline{S}$ W/m²	$\overline{U}$ m/s	$\overline{T_a}$ °C	$\overline{r_h}$ %	Sky
19 Jul	11:30–18:00	0.12	655	2.1	22.8	37	clear
20 Jul	09:30–16:30		646	2.1	24.7	28	clear
26 Jul	09:00–16:30		501	1.8	16.4	73	partly cloudy
27 Jul	11:00–17:30	0.42	637	2.4	17.6	61	clear
28 Jul	08:30–16:00		622	1.7	21.2	51	clear
29 Jul	12:00–19:00	0.60	619	1.7	24.7	39	clear
30 Jul	09:00–16:30		578	2.0	24.5	44	clear
31 Jul	12:30–17:30	1.00	524	1.8	19.3	64	mainly clear
1 Aug	09:00–17:00		548	1.9	16.5	64	partly cloudy

The experimental site is located on an east-facing slope with an inclination angle of approximately 5°. The coastline is located at 12 km to the east of the site and is oriented in a SE–NW direction. About 350 m to the east of the instrument tower, the pruned plot ends and the slope becomes steeper (12°). About 60 m to the west of the tower, there is a very narrow silvicultural access road; beyond this the canopy is rather sparse. Further to the west, at a distance of approximately 500 m, is a small hill. During the daytime, the wind blows constantly from the NE to NEE sector as a result of sea-to-land and upslope winds. In the night-time, the wind direction shifts 180°.

The most recent rainfall event prior to the experiment occurred on 6 July, 1990. The weather remained mostly clear during the experimental period. Table 2.1 lists the daytime average values of weather variables for the nine days of the experiment.

2.2.2 Instrumentation and Data Collection

Micrometeorological measurements were made mainly from a 25 cm wide, 24 m tall guyed triangular open-lattice steel tower (Appendix A). Two eddy correlation units, which measured the fluctuations in the three velocity components, air temperature and water vapour density, were mounted 1.5 m from the tower. The first unit (hereafter referred to as the upper unit) consisted of one 3-dimensional sonic anemometer (Applied Technologies Inc., Boulder, CO, Model BH-478B/3, 25 cm path length), one fine wire thermocouple (chromel-constantan, 13 μm in diameter) and one krypton hygrometer (Campbell Scientific Inc., Logan, UT, Model K20, 0.795 cm path length). This unit was operated permanently at a height of 23.0 m ($z/h = 1.38$) during the experimental period. The second unit (hereafter referred to as the lower unit) consisted of one 3-dimensional sonic anemometer/thermometer (Applied Technologies Inc., Model SWS-211/3V, 10 cm path length) and one krypton hygrometer (Campbell Scientific Inc., Model K20, 1.021 cm path length). It was operated at the following heights (z/h in brackets): 2.0 (0.12), 7.0 (0.42), 10.0 (0.60), and 16.7 m (1.00) (see Table 2.1).

The analogue voltage signal from the thermocouple of the upper unit was amplified by an amplifier (Neff Instrument Corp., Duarte, CA, Model SC019) with a gain of 2000 and a bandwidth of 10 Hz. The six analogue signals (five from the upper unit and one from the hygrometer of the lower unit) were sent to an A/D board built in the electronics of the sonic anemometer/thermometer of the lower unit, resulting in a total of ten channels of digital data with a sampling rate of 9.9 Hz. The data were sent via a serial port to a lap-top XT micro-computer (Zenith Data Systems Corp., St. Joseph, MI, Model ZWL-184-02 Supersport with 20 Mb hard drive), and transferred to 80 Mb data cartridge magnetic tapes using a tape backup system (Colorado Memory Systems Inc., Loveland, CO, Model DJ-10), usually after a period of about 8 hours of continuous data collection, for subsequent analysis. In addition, the analogue signals from the upper unit were sampled in parallel at 10 Hz by a data logger (Campbell Scientific Inc., Model 21X with extended software II), which gave on-line calculations of the most important mean statistics for the purpose of monitoring the performance of the unit.

Turbulence statistics were calculated over 30-minute intervals after the experiment. A two-way coordinate rotation was applied to the statistics above and on top of the stand, following the procedure of Tanner and Thurtell (1969), and a one-way coordinate rotation was applied to the statistics inside the stand, following the procedure of Baldocchi and Hutchison (1987).

Air temperature and wind speed were measured continuously over the whole experimental period with fine wire thermocouples (chromel-constantan, 26 μm in diameter) and sensitive cup anemometers (C.W. Thornthwaite Associates, Centerton, NJ, Model 901-LED), respectively, at heights of 0.9, 2.0, 4.6, 7.0, 10.0, 12.7, 16.7, and 23.0 m. Supporting measurements included humidity, wind direction, and radiation (net, global and diffuse irradiances) above the stand and near the forest floor (see Chapter 3 for details). The data logging for these instruments was accomplished by five additional data loggers (Campbell Scientific Inc., Models 21X and CR5). All data logging systems were synchronized to within a few seconds.

Eddy correlation sensors were pointed into the prevailing wind directions in the daytime. Only the turbulence data collected in the daytime were considered for analysis.

2.2.3 Inter-comparison of Instruments

On 31 July and 1 August 1990, the lower unit was operated at the height of the tree tops (z/h = 1.00). Figure 2.2 shows the 30-minute covariances measured at z/h = 1.00 plotted against those measured at z/h = 1.38. There was good agreement between the two units in the measurement of $\overline{w'T'}$, the covariance between the vertical velocity component (w)

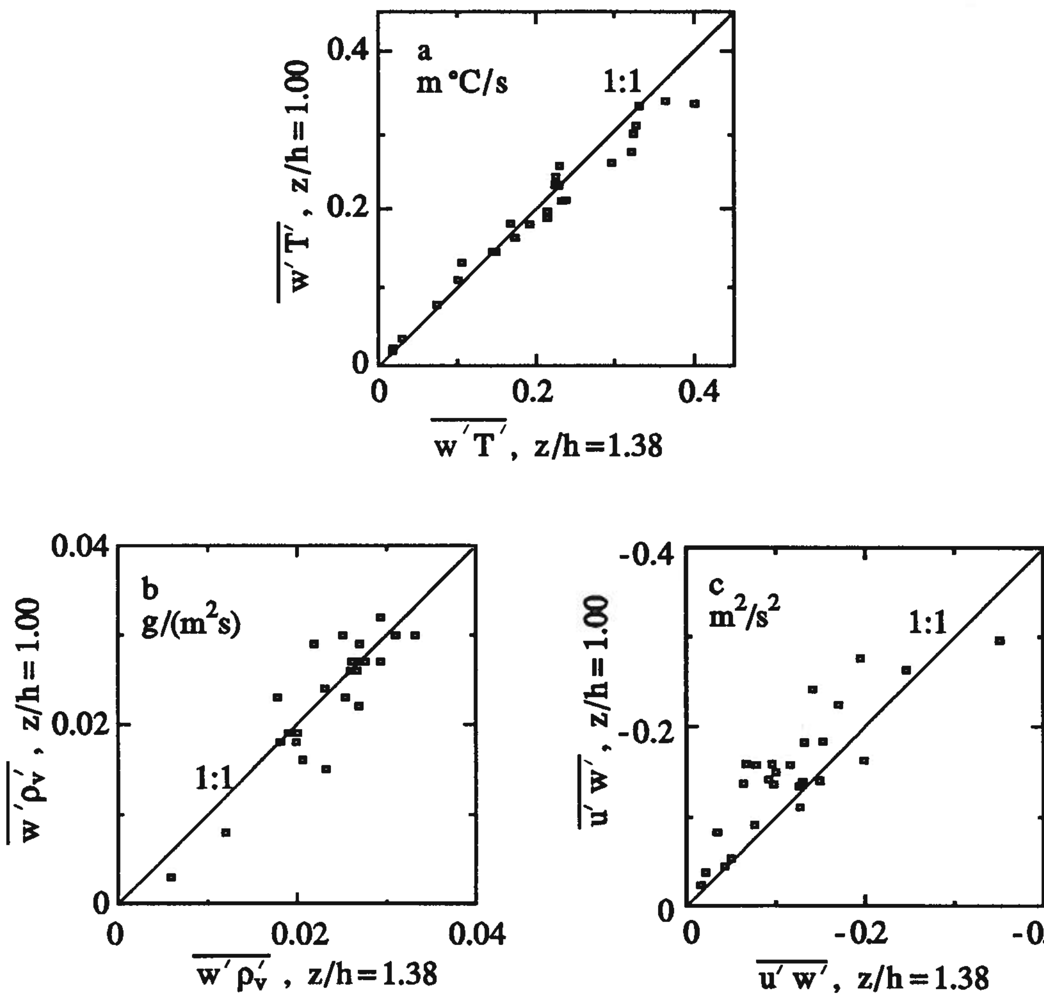

Figure 2.2: Covariances of w and T (a), w and ρ_v (b), and w and u (c) measured at z/h = 1.00 versus those measured at z/h = 1.38 for the Douglas-fir stand at Browns River on 31 July and 1 August 1990.

and air temperature (T). For $\overline{w'\rho_v'}$, the covariance between w and water vapour density (ρ_v), the scatter was somewhat larger, but overall was about the 1:1 line. A reduction of 20% was observed in $-\overline{u'w'}$, the covariance between the longitudinal velocity component (u) and w or the kinematic Reynolds stress, from z/h = 1.00 to z/h = 1.38. The decrease in Reynolds stress with increasing height was also observed by Baldocchi and Meyers (1988) over a deciduous forest, with a higher reduction rate of 48% from z/h = 1.00 to z/h = 1.45. They suggested that one of the reasons for the decrease was the vertical divergence of Reynolds stress associated with the pressure perturbations and convergence of streamlines due to topographic effects, which was also likely to be a contributing factor in the present study. As pointed out later, the longitudinal pressure gradient due to land-sea/upslope-downslope circulations might also contribute to the vertical divergence of Reynolds stress.

In order to compare the measurements made by the sonic anemometers with the measurements made by the cup anemometers, the equivalent average 'cup' wind speed, V was calculated for the sonic anemometers for every 30-minute period using

$$V = \overline{\sqrt{u_1^2 + v_1^2}}$$

where u_1 and v_1 are the two horizontal components of the instantaneous velocity vector, and the overbar denotes temporal averaging. The results are summarized in Figure 2.3. The correlations between V and U, the 30-minute average wind speed measured with cup anemometers, were very good, indicating a stable performance of the instruments. But overall the value of U was higher than that of V, which was likely the result of overspeeding of the cup anemometers in turbulent flow (Coppin 1982).

The two eddy correlation units were compared over a smooth bare field on level ground on 3 and 5 October, 1991. The details are given in Appendix C.

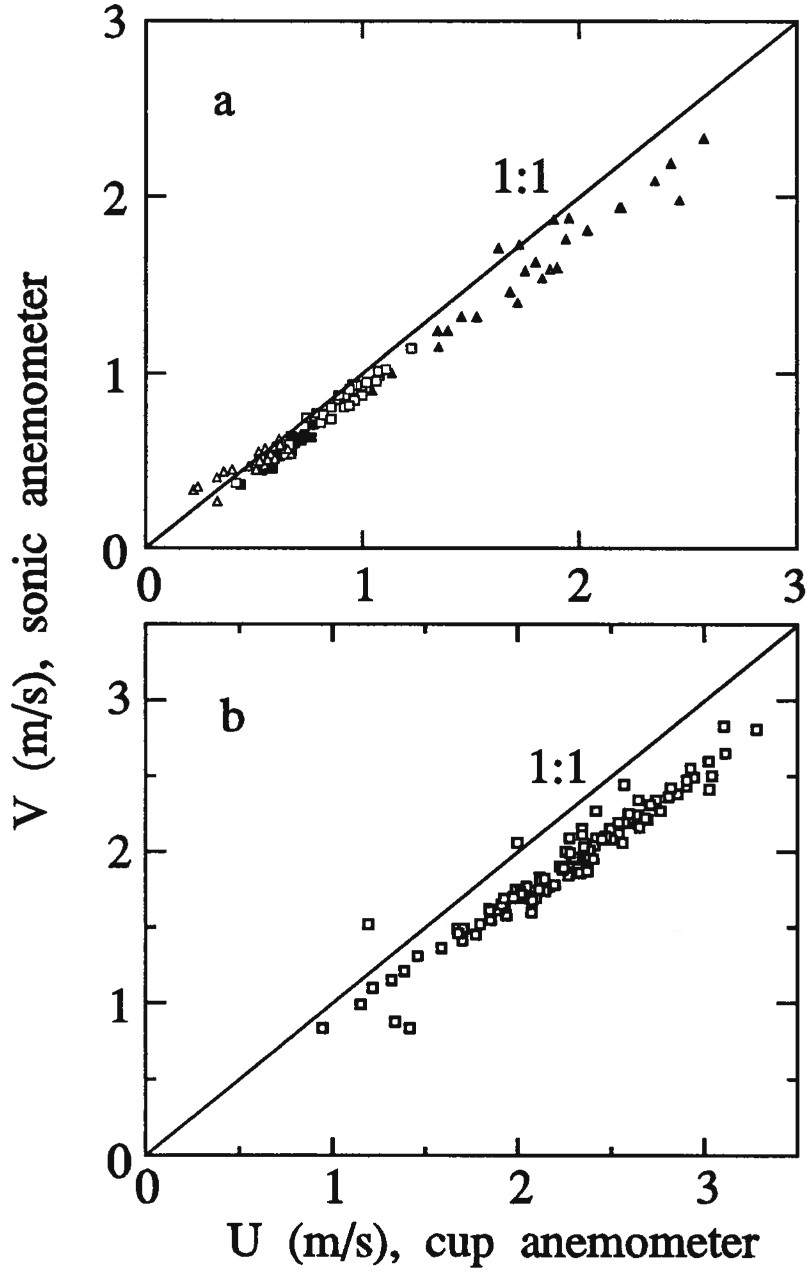

Figure 2.3: Comparison of equivalent 'cup speed' V measured by sonic anemometers with wind speed U measured by cup anemometers in the Douglas-fir stand at Browns River during the entire experimental period in 1990: (a) lower unit at z/h = 0.12 (□), 0.42 (■), 0.60 (△) and 1.00 (▲) and (b) upper unit at z/h = 1.38.

2.3 Results and Discussion

2.3.1 Monin-Obukhov Similarity above the Stand

The surface boundary layer over an extensive plant canopy can be considered as two parts: the upper part, the inertial sublayer (Tennekes 1973) in which the flux-gradient relationships established on the basis of Monin-Obukhov similarity are obeyed, and the lower part, the roughness sublayer (Raupach *et al.* 1980) or transition sublayer (Garratt 1980), which is close to and within the canopy itself (Raupach and Thom 1981). Three kinds of the surface influence in the roughness sublayer have been identified: First, there exists horizontal inhomogeneity, dramatically demonstrated by the horizontal variations in the wind profile over artificial canopies in wind tunnels (Mulhearn and Finnigan 1978, Raupach *et al.* 1986), although there does not appear to be any measurements of either wind speed or scalar concentrations over outdoor canopies reported to confirm this feature. Second, the transfer processes in the roughness sublayer are greatly enhanced, with the enhancement effect greater for scalars than for momentum. This feature was attributed to a 'wake production effect' (Thom *et al.* 1975). It has been observed over a variety of forests (Garratt 1978 and 1980, Shuttleworth 1989, Thom *et al.* 1975, Raupach 1979, Denmead and Bradley 1985, Hogstrom *et al.* 1989), over a model canopy in a wind tunnel (Raupach *et al.* 1980), and over bushland (Chen and Schwerdtfeger 1989). Third, counter-gradient fluxes can occur in the roughness sublayer under certain circumstances (Chen and Schwerdtfeger 1989).

Garratt (1980) proposed a scaling law, $z_* - d = 3D$, for momentum flux, where z_* is the height (above the ground surface) of the roughness sublayer, d is the height of the displacement plane (assumed to be 0.7 h in the present study, see Jarvis *et al.* 1976) and D is the spacing of roughness elements. The mean tree spacing in the stand of the present study is about 4.2 m. Based on Garratt's proposal, the top two measurement levels (z/h

=1.00 and 1.38) were located within the roughness sublayer. With sensible heat flux being the dominant output component of the energy budget of the stand (Chapter 3) and relatively low wind speed, the stability parameter, $(z-d)/L$, where L is the Monin-Obukhov length, was typically of large magnitude, the value varying mainly between -0.20 and -5.0 at z/h = 1.38. Eddy diffusivities under these moderately to strongly unstable conditions, calculated from the profile measurements at z/h = 1.00 and 1.38 and the flux measurements at z/h = 1.38, were found to be enhanced by factors of, on average, 1.3 for momentum flux and 1.9 for sensible heat flux, as compared to the diffusivities calculated using the flux-gradient relationships pertaining to smoother surfaces (Dyer 1974). But the dependence of the enhancement on the stability was not monotonic (Figure 2.4).

Monin-Obukhov similarity requires that the dimensionless standard deviations of the vertical velocity component and scalar concentrations be functions of $(z-d)/L$. In the surface layer under free convection conditions (large $-(z-d)/L$), these functions have the forms

$$\sigma_w/u_* = a_w[-(z-d)/L]^{1/3} \tag{2.1}$$

$$\sigma_T/T_* = a_T[-(z-d)/L]^{-1/3} \tag{2.2}$$

$$\sigma_{\rho_v}/\rho_{v*} = a_{\rho_v}[-(z-d)/L]^{-1/3} \tag{2.3}$$

where σ_w, σ_T and σ_{ρ_v} are the standard deviations of the vertical velocity component, air temperature and water vapour density, respectively, and u_*, T_* and ρ_{v*} are the corresponding characteristic scales defined as

$$u_* = \sqrt{-\overline{u'w'}}, \qquad T_* = \overline{w'T'}/u_*, \qquad \rho_{v*} = \overline{w'\rho_v'}/u_*.$$

The values of the constants a_w, a_T and a_{ρ_v} were found to be about 1.9, 0.9 and 1.1, respectively, over rather smooth surfaces (Hogstrom and Smedman-Hogstrom 1974, Takeuchi

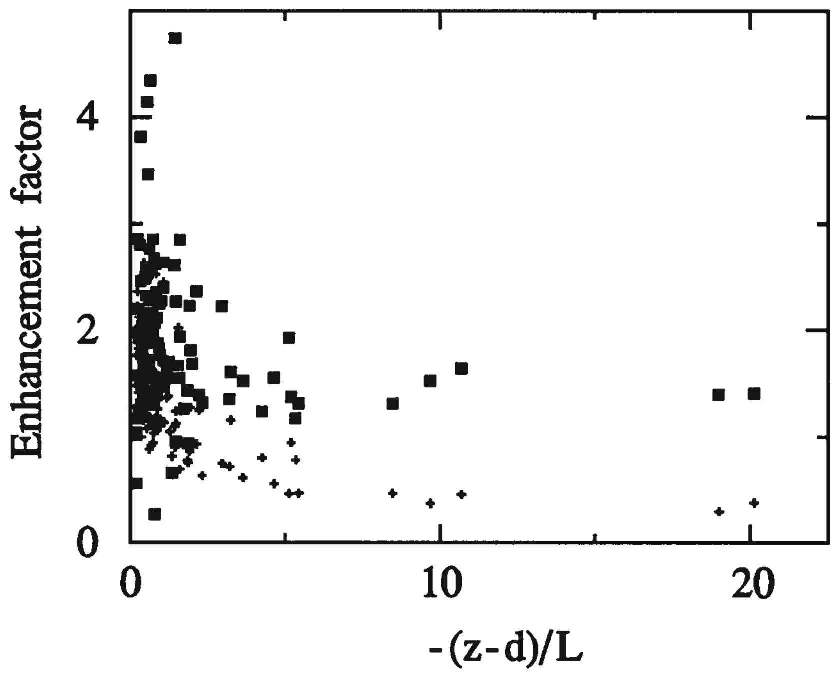

Figure 2.4: Enhancement factor (measured eddy diffusivity divided by that predicted with the flux-gradient relationships of Dyer (1974)) calculated from the profile measurements at z/h = 1.00 and 1.38 and flux measurements at z/h = 1.38 for the Douglas-fir stand at Browns River: (■), sensible heat; (+), momentum. The stability parameter $(z-d)/L$ was calculated from the flux measurements at z/h = 1.38.

et al. 1980, Wyngaard *et al.* 1971, Monji 1973, Panofsky and Tennekes 1977, Maitani and Ohtaki 1987). Ohtaki (1985) found that (2.1)–(2.3) performed well in wheat fields.

Figure 2.5 shows the dimensionless standard deviations as functions of the stability at z/h = 1.38. The value of σ_w/u_* at small $-(z-d)/L$ was about 1.16, close to 1.25, a typical value for the neutral surface layer (Panofsky and Dutton 1984). There were large uncertainties in σ_T/T_* and $\sigma_{\rho_v}/\rho_{v*}$ for small values of $-(z-d)/L$. At large $-(z-d)/L$, the trend is clear: σ_w/u_* was well approximated by the 1/3 power law, and σ_T/T_* and $\sigma_{\rho_v}/\rho_{v*}$ by the −1/3 power law. Overall the measurements and the predictions agree well for large $-(z-d)/L$, with slight differences probably caused by the rather arbitrary choice of the value of d.

Stability was found to have little effect on the statistics within the stand. In contrast, Shaw *et al.* (1988) observed that the normalized Reynolds stress and turbulence intensity at the middle of a deciduous forest showed clear decreases with the onset of stable conditions from moderately unstable conditions.

2.3.2 Means and Variances of the Velocity Components

Figure 2.6 shows the profiles of daytime cup wind speed (U) normalized against that at z/h = 1.38 and averaged over the nine days listed in Table 2.1, and longitudinal velocity component (u) normalized against that at z/h = 1.38. During the experimental period, the 30-minute average cup wind speed and the longitudinal velocity component at z/h = 1.38 varied between 0.94 and 3.28 m/s and between 0.22 and 2.60 m/s, respectively. The normalized cup wind speed decreased sharply from z/h = 1.38 to z/h = 0.60, with a minimum of 0.25 occurring at z/h = 0.60. There was a marked secondary maximum at around z/h = 0.12, the normalized value being 0.40. The existence of secondary maximum is a common feature of the wind speed profiles in forest stands having a trunk space relatively free of branches where air movement is less restricted (e.g. Allen 1968,

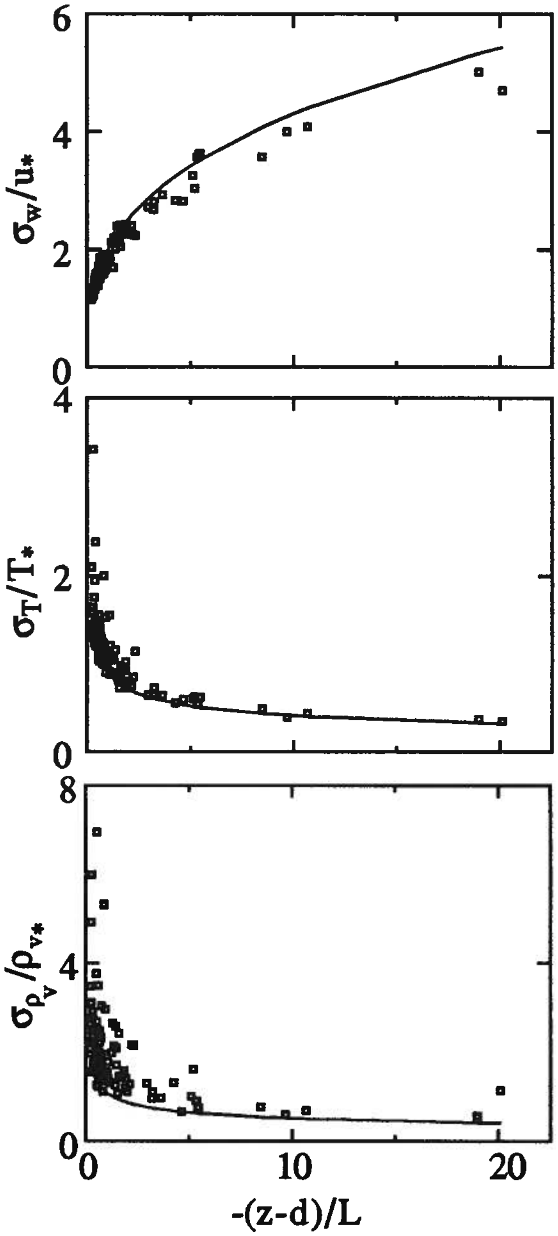

Figure 2.5: Dimensionless standard deviations of the vertical velocity component (σ_w/u_*), air temperature (σ_T/T_*) and water vapour density ($\sigma_{\rho_v}/\rho_{v*}$) as functions of the stability parameter $(z-d)/L$ at z/h = 1.38 for the Douglas-fir stand at Browns River. Squares: measured; lines: calculated from Equations (2.1–2.3).

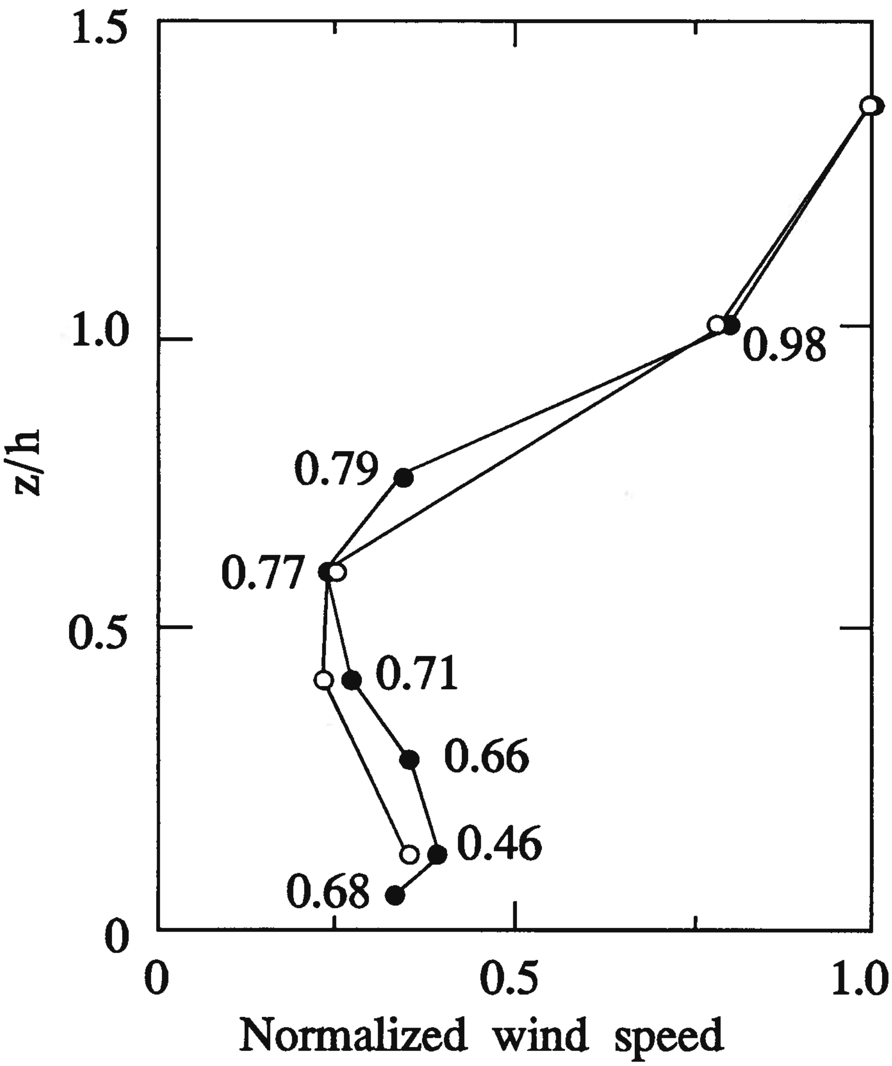

Figure 2.6: Profiles of normalized daytime wind speed in the Douglas-fir stand at Browns River: (•), wind speed measured using cup anemometers (U) and averaged over nine days, where the numbers are correlation coefficients (R) between the wind speed at the indicated heights and that at z/h = 1.38; (o), longitudinal velocity component (u) measured using one sonic anemometer located for 2–3 days at various heights and normalized against that measured by the other sonic anemometer located permanently at z/h = 1.38.

Shaw 1977, Baldocchi and Hutchison 1987, Baldocchi and Meyers 1988). The correlation coefficient between the cup wind speed at the height of the secondary maximum and that at z/h = 1.38 was lower than those between the wind speed at all other heights and that at z/h = 1.38 (Figure 2.6). This indicates that the wind at the height of the secondary maximum was least coupled to that above the stand compared to the wind at the other heights. The profile of the normalized longitudinal velocity component was similar to the profile of the normalized cup wind speed.

In the following plots of the vertical profiles of statistics in this Chapter, values at z/h = 1.38 were averaged over 31 July and 1 August, while those at lower heights were averaged over the corresponding operating periods (Table 2.1). The plots of these ensemble averages should retain the basic features of these statistics as functions of height because the atmospheric conditions were similar throughout the experimental period.

Figure 2.7 illustrates the dependence of the velocity variance on height. The variance of the vertical velocity component was smaller than the variances of the longitudinal and lateral components, a feature in agreement with the observations made in agricultural crops by Shaw *et al.* (1974), Finnigan (1979a) and Wilson *et al.* (1982), and in forests by Baldocchi and Hutchison (1987), Baldocchi and Meyers (1988), Shaw *et al.* (1988) and Amiro (1990), and decreased approximately linearly with decreasing height. But unlike most of the experimental results of those workers who showed that $\overline{u'^2}$ was larger than $\overline{v'^2}$, the profiles of $\overline{u'^2}$ and $\overline{v'^2}$ in the present study were quite similar both in magnitude and in shape. Both variances were relatively constant with height in the layer extending a few metres above the stand and decreased rapidly with depth into the stand. Both reached minima at z/h = 0.60, where their values were about equal to the value of $\overline{w'^2}$. Below this height, both increased slightly with depth.

Figure 2.8 shows the vertical profiles of turbulence intensity (velocity standard deviation divided by the average longitudinal velocity component) for the three velocity

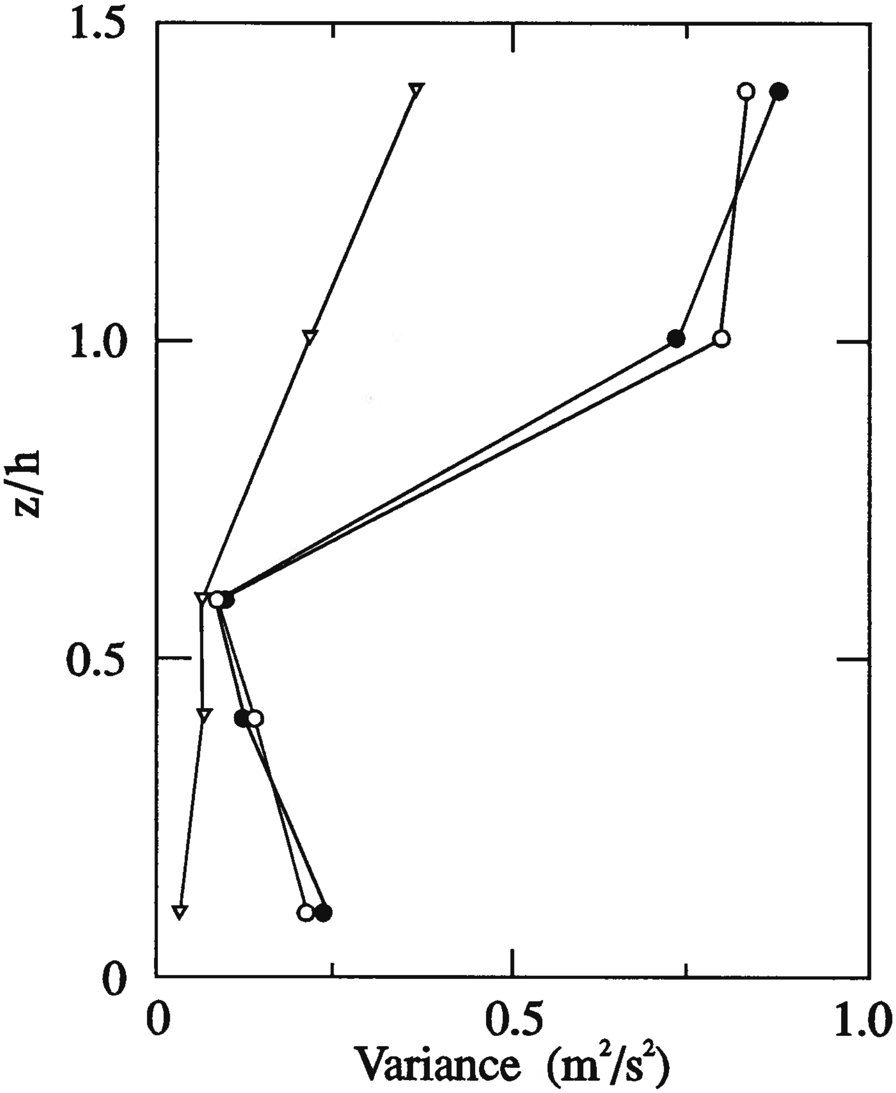

Figure 2.7: Profiles of daytime average velocity variance in the Douglas-fir stand at Browns River: (○), longitudinal component ($\overline{u'^2}$); (•), lateral component ($\overline{v'^2}$); (▽), vertical component ($\overline{w'^2}$). The average values of the standard error of the mean (SEM) for $\overline{u'^2}$ and $\overline{v'^2}$ were 0.08 m^2/s^2 on the top and above the stand and 0.01 m^2/s^2 within the stand, and the corresponding values for $\overline{w'^2}$ were 0.02 and 0.01 m^2/s^2.

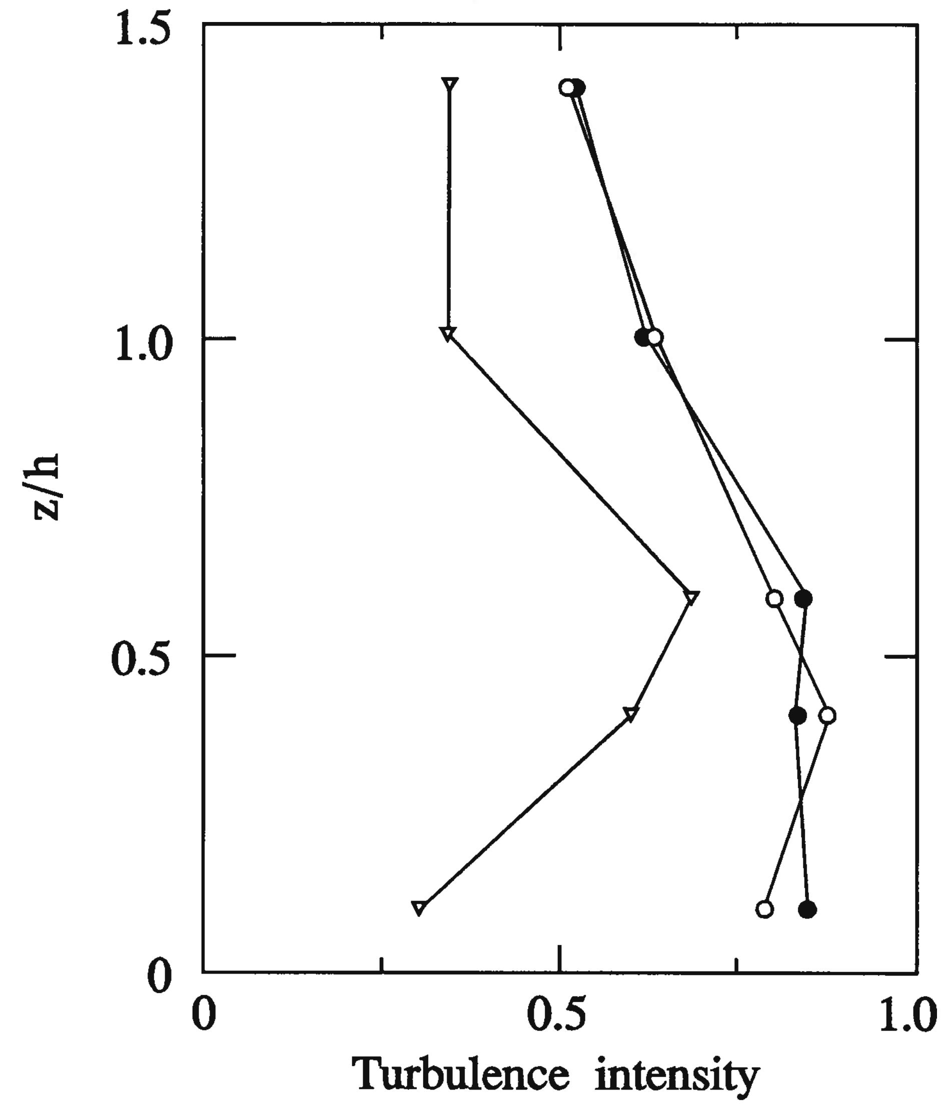

Figure 2.8: Profiles of daytime average turbulence intensity in the Douglas-fir stand at Browns River: (○), longitudinal component (i_u); (•), lateral component (i_v); ($\bigtriangledown$), vertical component (i_w). The average values of SEM were 0.04 for i_u and i_v and 0.02 for i_w.

components: longitudinal (i_u), lateral (i_v) and vertical (i_w). These profiles reflect the combined effect of the variance (Figure 2.7) and the longitudinal velocity component (Figure 2.6) profiles. On average, at z/h = 1.38, i_u and i_v had a value of 0.52. They increased gradually in magnitude with decreasing height. At z/h = 0.12, the values of i_u and i_v were 0.75 and 0.81, respectively. The profiles of i_u and i_v reported here were similar in shape and magnitude to that for the u component observed in a Japanese larch plantation (Allen 1968), but differed from those observed in a spruce forest by Amiro (1990) and in a deciduous forest by Baldocchi and Meyers (1988) in that their profiles of i_u and i_v showed marked maxima in the middle of the canopy.

The turbulence intensity of the vertical velocity component, i_w was approximately constant at 0.34 in the layer 1.00<z/h<1.38. It increased sharply with depth into the canopy. A maximum value of 0.68 occurred at z/h = 0.60, where the wind speed was lowest (Figure 2.6). Below this height, the intensity decreased with decreasing height. The value of i_w near the forest floor (z/h = 0.12) was about 0.30. A well-defined maximum in the i_w profile seems to be a common phenomenon occurring in the layer between the middle and upper third of forest stands (Amiro and Davies 1988, Baldocchi and Meyer 1988, Shaw *et al.* 1988, Bradley *et al.* reported in Wilson *et al.* (1982), Amiro 1990). In most cases, the maximum value falls in the range between 0.6 and 0.8.

2.3.3 Higher Order Moments

Skewness describes the asymmetry of a probability density distribution. The profiles of velocity skewness are presented in Figure 2.9. The average values of the skewness for the three velocity components at z/h = 1.38 were close to zero, the value for a Gaussian distribution. The values of Sk_u and Sk_v increased linearly with decreasing height until they reached maximum values of 0.73 and 0.57, respectively, at the middle of the canopy (z/h = 0.60), where the wind speed was lowest (Figure 2.6). Below this height both Sk_u

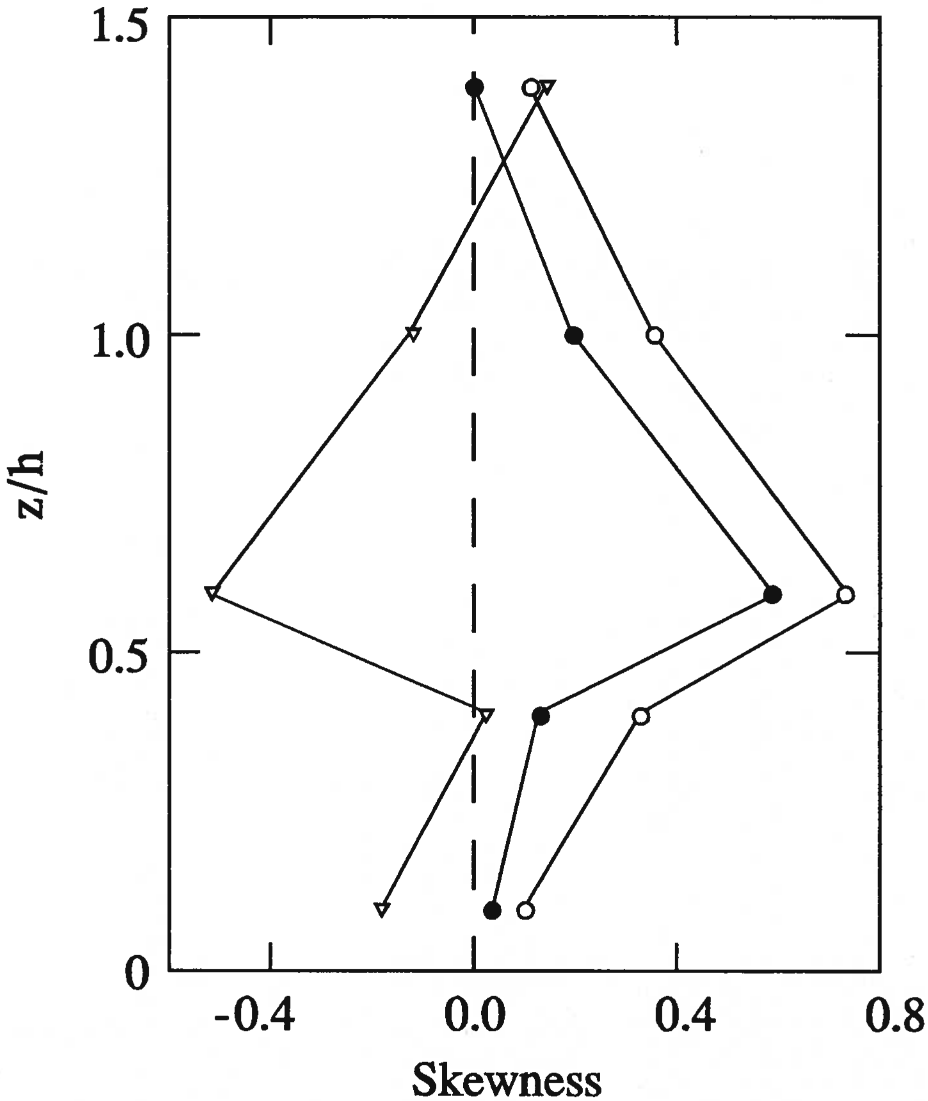

Figure 2.9: Profiles of daytime average velocity skewness in the Douglas-fir stand at Browns River: (○), longitudinal component (Sk_u); (•), lateral component (Sk_v); (∇), vertical component (Sk_w). The average values of SEM were 0.06 for Sk_u and Sk_v and 0.04 for Sk_w.

and Sk_v decreased with decreasing height. Positive values of Sk_u were consistent with the theoretical arguments of Shaw and Seginer (1987) that the penetration of occasional sweeps of fast moving air into the canopy from above should result in positive Sk_u. However, they did not expect the nonzero Sk_v as reported here.

Intense turbulent activity above a vegetation canopy is carried downward whereas in the interior of the canopy there is no source for the creation of large updrafts (Shaw and Seginer 1987). Consequently, the vertical velocity component immediately above the stand and in the canopy layer was negatively skewed. The most negative value of −0.52 for Sk_w occurred at the middle of the canopy (z/h = 0.60). The profile of Sk_w was practically a mirror image of the profiles of Sk_u and Sk_v, a pattern observed previously in several other experimental studies (Seginer *et al.* 1976, Raupach *et al.* 1986, Shaw and Seginer 1987, Amiro 1990).

Kurtosis is a measure of peakness or flatness of a probability density distribution. For a Gaussian distribution, it has a value of 3. As shown in Figure 2.10, the kurtosis values for the three velocity components above the stand in this study were not significantly different from 3. Higher values of kurtosis were observed in the canopy layer, indicating the existence of active extreme events in this layer. Like that of skewness, the magnitude of kurtosis peaked at z/h = 0.60. The peak values for Kr_u, Kr_v, Kr_w were 5.1, 5.1 and 4.1, respectively. Kurtosis was smaller in the trunk space, the values at z/h = 0.12 being 3.2, 2.9 and 3.9, respectively. This might indicate that the canopy layer above suppressed the activity of extreme events by blocking the penetration of large gusts from above the stand and imposing a thermal inversion (Chapter 3) on the trunk flow.

2.3.4 Reynolds Stress

The variation of Reynolds stress with height is presented in Figure 2.11. The ratio, $u_*/\overline{u}$, at z/h = 1.38 was 0.20 ± 0.08. A reduction of 20% in the stress occurred from the tree

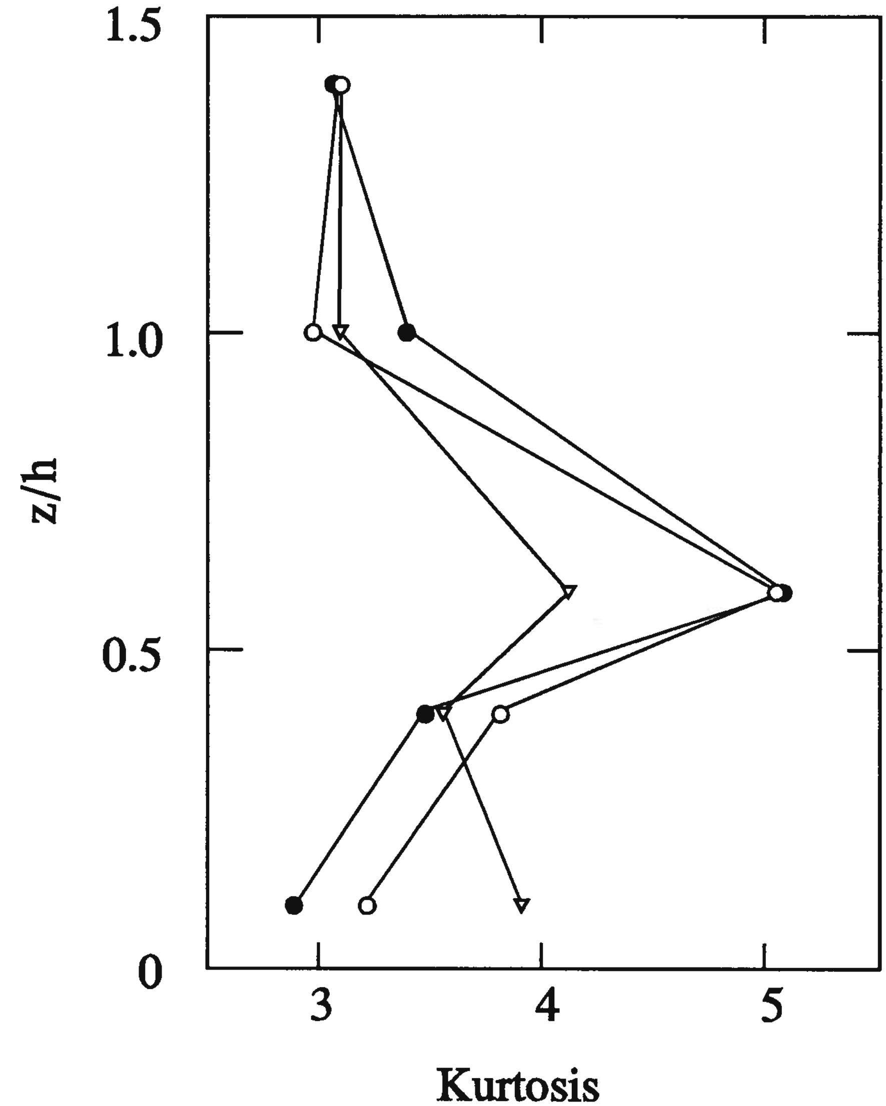

Figure 2.10: Profiles of daytime average velocity kurtosis in the Douglas-fir stand at Browns River: (∘), longitudinal component (Kr_u); (•), lateral component (Kr_v); (▽), vertical component (Kr_w). The average values of SEM were 0.13 for Kr_u and Kr_v and 0.10 for Kr_w.

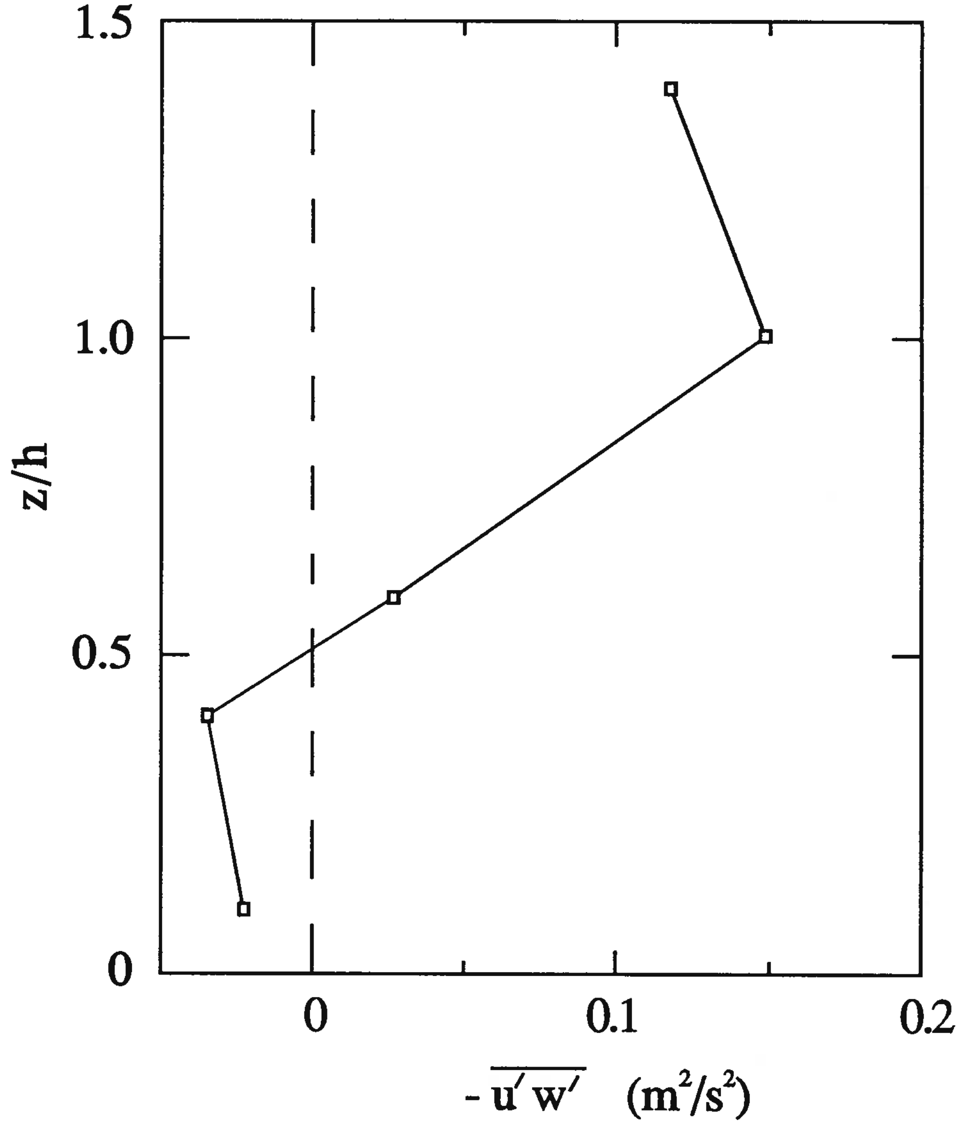

Figure 2.11: Profile of daytime average kinematic Reynolds stress in the Douglas-fir stand at Browns River. The average value of SEM were 0.014 m^2/s^2 on the top and above the stand and 0.002 m^2/s^2 within the stand.

tops to z/h = 1.38. The stress decreased sharply with depth into the canopy due to momentum absorption by the foliage. It was negative at the base of the canopy (z/h = 0.42) and in the middle of the trunk space (z/h = 0.12), with magnitudes of about 25% of that at z/h = 1.38.

Negative Reynolds stress persistently occurred at z/h = 0.12 and 0.42, with only two exceptions in a total of seventy one 30-minute runs. The most negative values were –0.052 m^2/s^2 at z/h = 0.12 and –0.058 m^2/s^2 at z/h = 0.42. An explanation for the negative values can be obtained by examining the Reynolds stress budget (Raupach *et al.* 1986)

$$\begin{aligned}
\frac{\partial}{\partial t}<\overline{u'w'}> = 0 = & -\underbrace{<\overline{w'^2}>\frac{\partial \overline{u}}{\partial z}}_{P_s} - \underbrace{<\overline{u_1'u_j'}''\frac{\partial \overline{u_3}''}{\partial x_j} + \overline{u_3'u_j'}''\frac{\partial \overline{u_1}''}{\partial x_j}>}_{P_w} \\
& -\underbrace{\frac{\partial}{\partial z}<\overline{u'w'^2}>}_{T_t} + \underbrace{\frac{1}{\rho}<\overline{p'(\frac{\partial u'}{\partial z}+\frac{\partial w'}{\partial x})}>}_{\Phi}
\end{aligned} \tag{2.4}$$

where u_i and x_i (i=1, 2, 3) are the components of velocity and position vectors, respectively, in tensor notation, (u, v, w) and (x, y, z) are velocity and position vectors in meteorological notation, t is time, p is pressure, ρ is air density; triangular brackets and double primes denote, respectively, spatial averages (horizontally) and departures therefrom; and overbar and single prime denote, respectively, temporal averages and departures therefrom. On the RHS of (2.4), P_s and P_w are shear production and wake production, respectively, representing local interactions, T_t is turbulent transport, representing interactions between layers, and Φ is the interaction between velocity and pressure fields. In (2.4) we omit small terms such as dispersive flux divergence, molecular flux divergence, molecular dissipation and pressure transport, according to the studies of Shaw (1977) and Raupach *et al.* (1986).

It is not feasible to estimate the magnitudes of the individual terms of (2.4) in the stand of the present study, but qualitative conclusions can be drawn from (2.4). By parameterizing Φ as (Wilson and Shaw 1977, Wyngaard 1981)

$$\Phi = - <\overline{u'w'}> /\tau$$

where τ is a time scale, (2.4) becomes

$$<\overline{u'w'}> /\tau = P_s + P_w + T_t \tag{2.5}$$

According to (2.5), the contribution of P_s to Reynolds stress $< -\overline{u'w'} >$ was positive above z/h = 0.60 due to the positive wind speed gradient (Figure 2.6) and negative in the layer between z/h = 0.12 and 0.60 due to the negative wind speed gradient. P_w can be neglected provided that (1) there is negligible direct dissipation of mean kinematic energy into heat by the canopy, and (2) the dispersive covariance and dispersive transport are both negligible (Raupach *et al.* 1986). If non-zero dispersive covariances exist, a little manipulation of the budget equation of $<\overline{u}''\overline{w}''>$ (Raupach and Shaw 1982) yields (see Appendix B for details)

$$P_w = - <\overline{w}''\overline{w}''> \frac{\partial <\overline{u}>}{\partial z} \tag{2.6}$$

Equation (2.6) means that P_w, if not zero, acts in a similar way as P_s in that both have the same sign and that both are linear with the local wind speed gradient, $\frac{\partial <\overline{u}>}{\partial z}$. T_t is largely driven by the gradient of Reynolds stress (Shaw 1977). Because of the small magnitude of Reynolds stress in the lower part of the stand, this driving force was probably small, and T_t might therefore be small. On the other hand, the sum of P_s and P_w in the lower part of the stand were significant because of the very negative wind speed gradient. In other words, the sum of P_s and P_w was likely to dominate over T_t at z/h = 0.12 and 0.42, and result in the negative values of Reynolds stress. In fact, Reynolds stress was found to have strong dependence on the wind speed gradient at the lower levels, the correlation coefficient being 0.70 at z/h = 0.12 for thirty seven 30-minute runs and 0.83 at z/h = 0.42 for twenty eight 30-minute runs.

It should be pointed out that, although the non-local interactions represented by T_t are likely to be small compared to the local interactions represented by P_s and P_w for the Reynolds stress budget at lower heights of a plant canopy, they are generally significant for the flux budgets of scalars such as sensible heat and water vapour. This is well demonstrated by the phenomenon of counter-gradient flux frequently observed in the lower parts of forest stands (Denmead and Bradley 1985, Amiro 1990, Leclerc 1987, Chapter 3). A comparison of the Reynolds stress budget (Raupach *et al.* 1986) and the heat flux budget (Coppin *et al.* 1986) in an artificial canopy in a wind tunnel shows that, while T_t is much smaller in magnitude than P_s in the Reynolds stress budget, T_t is in equal magnitude to P_s in the heat flux budget.

Negative Reynolds stress indicates the upward flux of momentum and has been observed at the lower heights in vegetation canopies on a few other occasions (Raupach *et al.* 1986, Baldocchi and Hutchison 1987, Maitani and Shaw 1990, Appendix E). The momentum conservation equation can be examined to shed some light on the origin of the upward momentum flux. For a stationary flow without buoyancy forces and advection, the conservation equation for momentum is

$$\frac{\partial}{\partial z} < -\overline{u'w'} > + \frac{\partial}{\partial z} < -\overline{u}''\overline{w}'' > = C_d A < \overline{u} >^2 + \frac{1}{\rho}\frac{\partial < \overline{p} >}{\partial x} \tag{2.7}$$

where C_d is the effective drag coefficient of the plant elements and A is the element area density (Raupach *et al.* 1986). Integration of (2.7) with respect to z yields

$$\begin{aligned}[< -\overline{u'w'} > + < -\overline{u}''\overline{w}'' >]_z &= \int_0^z C_d A < \overline{u} >^2 dz \\ &+ [< -\overline{u'w'} > + < -\overline{u}''\overline{w}'' >]_0 + \int_0^z \frac{1}{\rho}\frac{\partial < \overline{p} >}{\partial x} dz\end{aligned} \tag{2.8}$$

The first and second parts of the term on the LHS of (2.8) are spatially averaged Reynolds momentum flux (or Reynolds stress, assumed to equal the point measurement (Shaw 1985)) and dispersive momentum flux (or dispersive stress), respectively; the first term on the RHS of (2.8) represents momentum absorption by the plant elements, the second term momentum absorption by the ground surface, and the third term the contribution of momentum divergence due to the longitudinal pressure gradient, $\frac{\partial <\overline{p}>}{\partial x}$. The onset of the sea/upslope breeze in the daytime was associated with a negative $\frac{\partial <\overline{p}>}{\partial x}$. According to the estimates of Atkinson (1981, pp 125-127 and 217-219), the gradient due to the uneven radiative heating between land and sea was on the order of 0.2 kPa/100 km, and the gradient due to the uneven radiation heating between slope and horizontal land was on the same order of magnitude. Using a value of −0.5 kPa/100 km for $\frac{\partial <\overline{p}>}{\partial x}$, the third term on the RHS of (2.8) was estimated at −0.035 m^2/s^2 for z/h = 0.42. Momentum absorption by the ground was probably negligible. Momentum absorption by the trunks (the main elements below z/h = 0.42) was estimated at 0.010 m^2/s^2 for the height z/h = 0.42, by using the value of C_d for a cylinder in turbulent flow (0.45, p 622 Schlichting 1968). The sum of the terms on the RHS of (2.8) was thus on the order of −0.025 m^2/s^2, which was similar to the average value of −0.033 m^2/s^2 for $<-\overline{u'w'}>$ measured at z/h = 0.42. The result of this simple exercise suggests that the longitudinal pressure gradient might, to a large extent, be responsible for the upward momentum flux. It is not feasible to estimate the magnitude of the dispersive term from a point measurement, but results of earlier wind tunnel experiments suggested that this term might be negligible (Raupach *et al.* 1986, Mulhearn 1978).

2.3.5 Quadrant Representation of Reynolds Stress

Quadrant-hole analysis, a conditional-sampling technique, is useful in identifying kinds of turbulent motion which dominate the vertical transfer of momentum represented by the kinematic Reynolds stress, $-\overline{u'w'}$. It was used in the experimental investigations of momentum transfer in agricultural crops (Finnigan 1979b, Shaw *et al.* 1983), in an almond orchard (Baldocchi and Hutchison 1987), in deciduous forests (Baldocchi and Meyers 1988, Gao *et al.* 1989, Maitani and Shaw 1990), and in a wind tunnel model canopy (Raupach *et al.* 1986). These studies have shown the common features that within a vegetation canopy, a large proportion of momentum transfer occurs in a small fraction of time and that in the upper part of and immediately above the canopy, the transfer is dominated by sweeps or gusts.

The four quadrants in the $u'w'$ plane are conventionally labelled as outward interaction (i = 1; $u' > 0$, $w' > 0$), ejection (i = 2; $u' < 0$, $w' > 0$), inward interaction (i = 3; $u' < 0$, $w' < 0$), and sweep (i = 4; $u' > 0$, $w' < 0$). A stress fraction $S_{i,H}$ and a time fraction $t_{i,H}$ are defined, respectively, as

$$S_{i,H} = \frac{1}{\mid \overline{u'w'} \mid} \frac{1}{T} \int_0^T u'(t)w'(t) I_{i,H} dt$$

$$t_{i,H} = \frac{1}{T} \int_0^T I_{i,H} dt$$

where T is the averaging time interval (30 minutes in this study), and $I_{i,H}$ is a conditioning function which equals one if the point $(u'(t),\ w'(t))$ is located in the i^{th} quadrant and $\mid u'(t)w'(t) \mid$ is greater than $H \mid \overline{u'w'} \mid$ and zero otherwise. The dimensionless parameter, H, is called hole size.

One 30-minute run at each level was selected for quadrant-hole analysis (Table 2.2). As shown in Table 2.2, the stability parameter $(z-d)/L$, was similar for all runs. Figure 2.12 shows the stress fraction $S_{i,H}$ plotted against hole size H and Table 2.3 lists related information. In Table 2.3, H' is the hole size above which half of the momentum transfer occurs

$$\mid \sum_{i=1}^{4} S_{i,H'} \mid = 0.5$$

Table 2.2: Values of Reynolds stress $-\overline{u'w'}$, standard deviations of the longitudinal and vertical velocity components (σ_u and σ_w), and the mean longitudinal velocity component ($\overline{u}$) at the indicated levels for the five runs selected for quadrant-hole analysis of Reynolds stress for the Douglas-fir stand at Browns River. The stability parameter (z–d)/L was calculated from the measurements at z/h = 1.38.

Time interval PST	z/h	(z–d)/L	$-\overline{u'w'}$ m^2/s^2	σ_u m/s	σ_w m/s	$\overline{u}$ m/s
13:30–14:00 19 July	0.12	-0.26	-0.024	0.45	0.19	1.00
12:00–12:30 27 July	0.42	-0.25	-0.052	0.41	0.32	0.42
12:30–13:00 30 July	0.60	-0.35	0.036	0.34	0.33	0.50
13:30–14:00 1 Aug	1.00	-0.25	0.184	1.17	0.54	2.14
12:00–12:30 27 July	1.38	-0.25	0.354	1.16	0.75	2.19

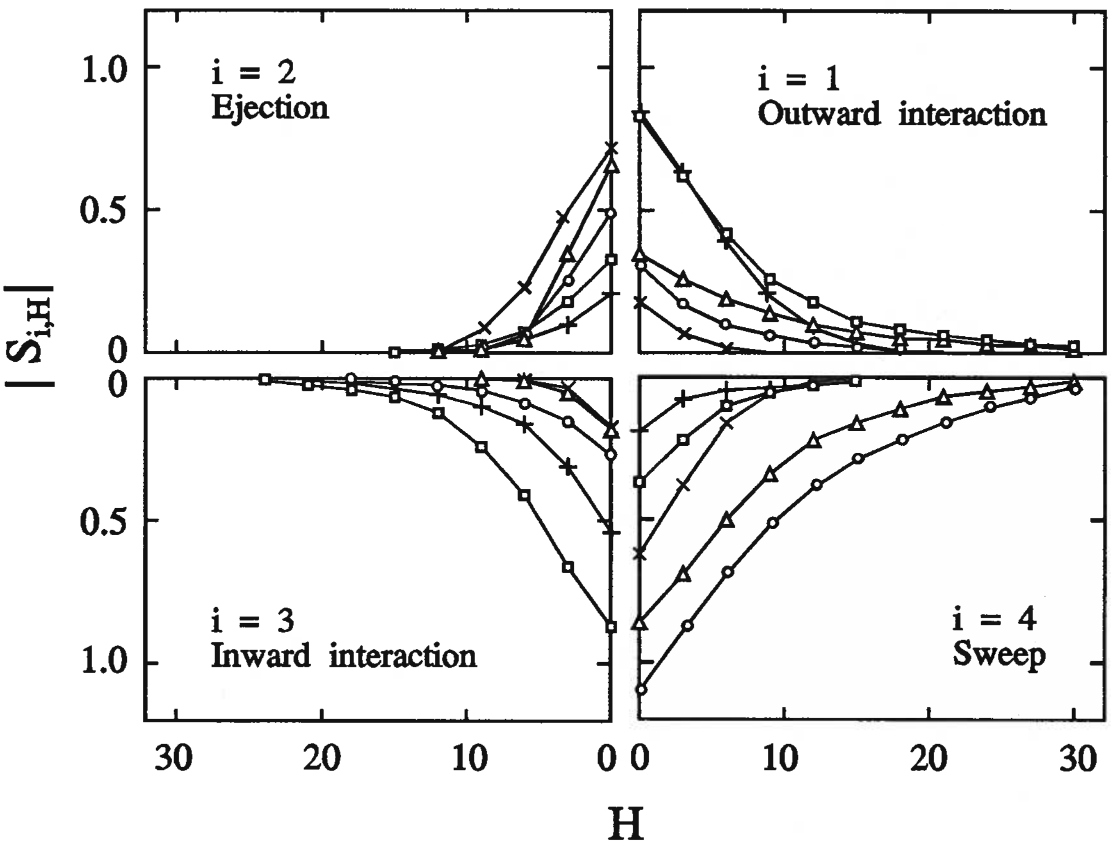

Figure 2.12: Stress fraction ($S_{i,H}$) plotted against hole size (H) for the Douglas-fir stand at Browns River for five values of z/h: 1.38 ($\times$), 1.00 ($\triangle$), 0.60 ($\circ$), 0.42 ($+$), and 0.12 ($\square$).

Table 2.3: Intermittence parameters (H' and $\sum_{i=1}^{4} t_{i,H'}$), exuberance ($\frac{S_{1,0}+S_{3,0}}{S_{2,0}+S_{4,0}}$) and the ratio of the contribution to Reynolds stress by sweeps to that by ejections ($\frac{S_{4,0}}{S_{2,0}}$) for the Douglas-fir stand at Browns River.

z/h	0.12	0.42	0.60	1.00	1.38
H'	8.0	5.6	7.5	4.8	5.0
$\sum_{i=1}^{4} t_{i,H'}$	0.064	0.084	0.064	0.125	0.096
$\frac{S_{1,0}+S_{3,0}}{S_{2,0}+S_{4,0}}$	-2.44	-3.45	-0.36	-0.39	-0.26
$\frac{S_{4,0}}{S_{2,0}}$	1.12	0.90	2.20	1.30	0.86

and $\sum_{i=1}^{4} t_{i,H'}$ is the corresponding time fraction. $\sum_{i=1}^{4} t_{i,H'}$ and H' are measures of intermittence. The intermittent nature of the momentum transfer can be readily seen: At all levels, half of the momentum flux was contributed by the events with hole size greater than 4.8–8.0 which occupied small fractions of time (6.4–12.5%).

The relative importance of the kinds of turbulent motion in momentum transfer can be examined by forming ratios of stress fractions at zero hole size. The ratio of the contributions by the interaction components ($S_{1,0} + S_{3,0}$) to the contributions by the ejection and sweep components ($S_{2,0} + S_{4,0}$), called exuberance (Shaw *et al.* 1983), varied between –0.26 and –0.39 in the layer between z/h = 0.60 and 1.38, which is consistent with the net downward momentum flux. At z/h = 1.38, ejections dominated over sweeps, the ratio $S_{4,0}/S_{2,0}$ being 0.86. But sweeps gained strength at the tree tops and in the canopy layer. The values of the ratio $S_{4,0}/S_{2,0}$ were 1.3 at z/h = 1.00 and 2.2 at z/h = 0.60. The dominance of sweeps over ejections was even greater at these two heights if only larger events were considered, as shown in Figure 2.12. These results generally agree with those of the experimental studies reviewed previously, but differ in some details. For example, the magnitudes of $S_{i,0}$ (i = 1–4) in the present work were generally less than 1, while Baldocchi and Meyers (1988) reported the magnitudes to be 1 to 3 for a deciduous forest.

At the lower heights of the stand, a different picture evolved. The interaction components played a major role in momentum transfer. The exuberance values were –2.44 at z/h = 0.12 and –3.45 at z/h = 0.42. This is consistent with the upward transfer of momentum or negative Reynolds stress at these two heights as discussed in the previous section. Baldocchi and Hutchison (1987) attributed the large contribution of the interaction components to either sloshing of the air near the forest floor or the existence of a systematic wake circulation in the lee of the tree upwind. However, it likely reflects a local interaction with the wind speed gradient: A downward/upward motion (negative/positive w') would normally result in a decrease/increase in u (negative/positive u') due to the negative wind speed gradient in the layer between z/h = 0.12 and 0.42.

2.4 Summary and Conclusions

Daytime turbulence statistics for the velocity field within and above a Douglas-fir forest on a 5° slope have been presented in this paper. The stability parameter, $(z-d)/L$ varied mainly between -0.20 and -5.0 at z/h = 1.38. Eddy diffusivities under these moderately to strongly unstable conditions, calculated from the profile measurements at z/h = 1.00 and 1.38 and the flux measurements at z/h = 1.38, were found to be enhanced by factors of, on average, 1.3 for momentum flux and 1.9 for sensible heat flux, as compared to the diffusivities calculated using the flux-gradient relationships pertaining to smoother surfaces. However, the similarity functions for the standard deviations of the vertical velocity component, air temperature and water vapour density were found to perform well at z/h = 1.38.

The vertical profiles of the turbulence statistics reflect the influence of the vertical structure of the stand. A marked secondary maximum in the wind speed profile occurred in the middle of the trunk space (around z/h = 0.12). The turbulence intensities for the longitudinal and lateral velocity components increased with decreasing height, but the intensity for the vertical velocity component had a maximum at z/h = 0.60, where the leaf area density was highest. Magnitudes of the higher order moments (skewness and kurtosis) for the three velocity components were higher in the canopy layer than in the trunk space and above the stand.

There was a 20% reduction in Reynolds stress from z/h = 1.00 to 1.38, probably a result of topographic effects and land-sea/upslope-downslope circulations. Negative

Reynolds stress persistently occurred at z/h = 0.12 and 0.42 (height of the base of the canopy). Examination of the Reynolds stress budget revealed that the negative value was associated with negative wind speed gradients at the two heights. The longitudinal pressure gradient due to the land-sea/upslope-downslope circulations was believed to be the main factor responsible for the upward momentum flux or negative Reynolds stress.

Momentum transfer was highly intermittent. Sweep and ejection events dominated the transfer process at z/h = 0.60, 1.00 and 1.38, with sweeps playing the more important role of the two at z/h = 0.60 and 1.00 and the less important role at z/h = 1.38. But interaction events were of greater magnitude than sweep and ejection events at z/h = 0.12 and 0.42.

2.5 References

Allen, L.L.: 1968, 'Turbulence and wind speed spectra within a Japanese larch plantation', *J. Appl. Meteorol.* **7,** 73-78.

Amiro, B.D.: 1990, 'Comparison of turbulence statistics within three Boreal forest canopies', *Boundary-Layer Meteorol.* **51,** 99-121.

Amiro, B.D. and Davis, P.A.: 1988, 'Statistics of atmospheric turbulence within a natural black spruce forest canopy', *Boundary-Layer Meteorol.* **44,** 267-283.

Atkinson, B.W.: 1981, *Meso-scale Atmospheric Circulations*, Academic Press, New York.

Aylor, D.E.: 1989, 'Aerobiology and atmospheric turbulence – examinig the interface' *10th Conference on Biometeorology and Aerobiology*, American Meteorological Society, Salt Lake City, UT. Preprint volume. pp 23-26.

Baldocchi, D.D. and Hutchison, B.A.: 1987, 'Turbulence in an almond orchard: Vertical variations in turbulence statistics', *Boundary-Layer Meteorol.* **40,** 127-146.

Baldocchi, D.D. and Meyers, T.P.: 1988, 'Turbulence structure in a deciduous forest', *Boundary-Layer Meteorol.* **43,** 345-364.

Chen, F. and Schwerdtfeger, P.: 1989, 'Flux-gradient relationships for momentum and heat over a rough natural surface', *Quart. J. R. Meteorol. Soc.* **115,** 335-352.

Coppin, P.A.: 1982, 'An examination of cup anemometer overspeeding', *Meteorol. Rdsch.* **35,** 1-11.

Coppin, P.A., Raupach, M.R. and Legg, B.J.: 1986, 'Experiments on scalar dispersion within a model plant canopy. Part II: An elevated plane source', *Boundary-Layer Meteorol.* **35,** 167-191.

Denmead, O.T. and Bradley, E.F.: 1985, 'Flux-gradient relationships in a forest canopy', in Hutchison, B.A. and Hicks, B.B. (eds.), *The Forest-Atmospheric Interaction*, D. Reidel Publishing Co., Dordrecht, 421-442.

Dyer, A.J.: 1974, 'A review of flux-profile relationships', *Boundary-Layer Meteorol.* **7,** 363-372.

Finnigan, J.J.: 1979a, 'Turbulence in waving wheat. Part I: Mean statistics and Honami', *Boundary-Layer Meteorol.* **16,** 181-211.

Finnigan, J.J.: 1979b, 'Turbulence in waving wheat. Part II: Structure of momentum transfer', *Boundary-Layer Meteorol.* **16,** 213-236.

Gao, W., Shaw, R.H. and Paw U, K.T.: 1989, 'Observation of organized structure in turbulent flow within and above a forest canopy', *Boundary-Layer Meteorol.* **47,** 349-377.

Garratt, J.R.: 1980, 'Surface influence upon vertical profiles in the atmospheric near-surface layer', *Quart. J. Met. Soc.* **106,** 803-819.

Garratt, J.R.: 1978, 'Transfer characteristics for a heterogeneous surface of large aerodynamic roughness', *Quart. J. R. Met. Soc.* **104,** 491-502.

Hogstrom, U., Bergstrom, H., Sedman, A.-S., Halldin, S. and Lindroth, A.: 1989, 'Turbulent exchange above a pine forest, I: Fluxes and gradients', *Boundary-Layer Meteorol.* **49,** 197-217.

Hogstrom, U. and Smedman-Hogstrom, A.S.: 1974, 'Turbulent mechanisms at an agricultural site', *Boundary-Layer Meteorol.* **7,** 373-389.

Jarvis, P.G., James, G.B. and Landsberg, J.J.: 1976, 'Coniferous forest', in Monteith, J.L. (ed.), *Vegetation and the Atmosphere II: Case Studies*, Academic Press, New York, 171-240.

Leclerc, M.Y.: 1987, 'Turbulence and turbulent diffusion inside and above vegetation', Ph.D. Thesis, University of Guelph, Guelph, Ontario.

Leclerc, M.Y., Beissner, K.C., Shaw, R.H., den Hartog, G, and Neumann, H.H: 1991, 'The influence of buoyancy on third-order turbulent velocity statistics within a deciduous forest', *Boundary-Layer Meteorol.* **55,** 109-124.

Maitani, T. and Ohtaki, E.: 1987, 'Turbulent transport processes of momentum and sensible heat in the surface layer over a paddy field', *Boundary-Layer Meteorol.* **40,** 283-293.

Maitani, T. and Shaw, R.H.: 1990, 'Joint probability analysis of momentum and heat fluxes at a deciduous forest', *Boundary-Layer Meteorol.* **52,** 283-300.

Monji, N.: 1972, 'Budgets of turbulent energy and temperature variance in the transition zone from forced to free convection', Ph.D. Thesis, University of Washington.

Mulhearn, P.J.: 1978, 'Turbulence over a periodic rough surface', *Phys. Fluids* **21,** 1113-1115.

Mulhearn, P.J. and Finnigan, J.J.: 1978, 'Turbulence over a very rough, random surface', *Boundary-Layer Meteorol.* **15,** 109-132.

Ohtaki, E.: 1985, 'On the similarity in atmospheric fluctuations of carbon dioxide, water vapor and temperature over vegetated fields', *Boundary-Layer Meteorol.* **32,** 25-37.

Panofsky, H.A. and Dutton, J.A.: 1984, *Atmospheric Turbulence: Models and Methods for Engineering Applications*, John Wiley and Sons, New York.

Panofsky, H.A. and Tennekes, H.: 1977, 'The characteristics of turbulent velocity components in the surface layer under convective conditions', *Boundary-Layer Meteorol.* **11,** 355-361.

Raupach, M.R.: 1979, 'Anomalies in flux-gradient relationships over forest', *Boundary-Layer Meteorol.* **16,** 467-486.

Raupach, M.R., Coppin, P.A. and Legg, B.J.: 1986, 'Experiments on scalar dispersion within a model plant canopy. Part I: The turbulence structure', *Boundary-Layer Meteorol.* **35,** 21-52.

Raupach, M.R. and Shaw, R.H.: 1982, 'Averaging procedures for flow within vegetation canopies', *Boundary-Layer Meteorol.* **22,** 79-90.

Raupach, M.R. and Thom, A.S.: 1981, 'Turbulence in and above plant canopies', *Ann. Rev. Mech.* **13,** 97-129.

Raupach, M.R., Thom, A.S. and Edwards, I.: 1980, 'A wind-tunnel study of turbulent flow close to regularly arrayed rough surfaces', *Boundary-Layer Meteorol.* **18,** 373-397.

Sagar, R.M., Black, T.A., Lee, X. and Chen, J.M.: 1991, 'Heat transfer relationships for deer in Douglas-fir stands', *10th Conference on Biometeorology and Aerobiology*, American Meteorological Society, Salt Lake City, UT. Preprint volume. pp 129-132.

Schlichting, H.: 1968, *Boundary-Layer Theory*, 6th Edition, McGraw-Hill Book Company, New York.

Seginer, I., Mulhearn, P.J., Bradley, E.F. and Finnigan, J.J.: 1976, 'Turbulent flow in a model plant canopy', *Boundary-Layer Meteorol.* **10,** 423-453.

Shaw, R.H.: 1985, 'On diffusive and dispersive fluxes in forest canopies', in Hutchison, B.A. and Hicks, B.B. (eds.), *The Forest-Atmospheric Interaction*, D. Reidel Publishing Co., Dordrecht, 407-419.

Shaw, R.H.: 1977, 'Secondary wind speed maxima inside plant canopies', *J. Appl. Meteorol.* **16,** 514-523.

Shaw, R.H., den Hartog, G., King, K.M. and Thurtell, G.W.: 1974, 'Measurements of mean wind flow and three-dimensional turbulence intensity within a matured corn canopy', *Agric. Meteorol.* **13,** 419-425.

Shaw, R.H., den Hartog, G. and Neumann, H.H.: 1988, 'Influence of foliar density and thermal stability on profiles of Reynolds stress and turbulence intensity in a deciduous forest', *Boundary-Layer Meteorol.* **45,** 391-409.

Shaw, R.H. and Seginer, I.: 1987, 'Calculation of velocity skewness in real and artificial plant canopies', *Boundary-Layer Meteorol.* **39,** 315-332.

Shaw, R.H., Tavangar, J. and Ward, D.P.: 1983, 'Structure of Reynolds stress in a canopy layer', *J. Climate Appl. Meteorol.* **22,** 1922-1931.

Shuttleworth, W.J.: 1989, 'Micrometeorology of temperate and tropical forest', *Phil. Trans. R. Soc. Lond.* **324B,** 299-334.

Takeuchi, K., Ohtaki, E. and Seo, T.: 1980, 'Turbulent transport of water over paddy fields', *Ber. Ohara Inst. Landw. Biol. Okayama Univ.* **18,** 1-30.

Tanner, C.B. and Thurtell, G.W.: 1969, 'Anemoclinometer measurements of Reynolds stress and heat transport in the atmospheric surface layer', Research and Development Technical Report ECOM-66-G22-F, University of Wisconsin, Madison, Wisconsin.

Tennekes, H.: 1973, 'The logarithmic wind profile', *J. Atmos. Sci.* **30,** 234-238.

Thom, A.S., Stewart, J.B., Oliver, H.R. and Gash, J.H.: 1975, 'Comparison of aerodynamic and energy budget estimates of fluxes over a pine forest', *Quart. J. R. Meteorol. Soc.* **101,** 93-105.

Wilson, R.N. and Shaw, R.H.: 1977, 'A higher order closure model for canopy flow', *J. Appl. Meteorol.* **14,** 1197-1205.

Wilson, J.D., Ward, D.P., Thurtell, G.W. and Kidd, G.E.: 1982, 'Statistics of atmospheric turbulence within and above a corn canopy', *Boundary-Layer Meteorol.* **24,** 495-519.

Wyngaard, J.C.: 1981, 'Boundary-layer modeling', in Nieuwstadt, F.T.M. and van Dop, H. (eds.), *Atmospheric Turbulence and Air Pollution Modelling*, D. Reidel Publishing Company, Dordrecht, 69-106.

Wyngaard, J.C., Cote, O.R. and Izumi, Y.: 1971, 'Local free convection, similarity, and the budgets of shear and heat flux', *J. Atmos. Sci.* **28,** 1171-1182.

Chapter 3

Eddy Fluxes of Sensible Heat and Water Vapour

3.1 Introduction

Measurements of the exchange of atmospheric scalar constituents such as heat and water vapour between forest communities and the atmosphere are needed to provide information for studies of global and regional water and CO_2 balances, deposition of atmospheric pollutants, and productivity of forest ecosystems. Most micrometeorological studies of the exchange processes in forests over the past twenty years have been conducted above the stand (Verma *et al.* 1986, Shuttleworth *et al.* 1984, McNaughton and Black 1973, Jarvis *et al.* 1976, *etc.*). There have been fewer studies performed both within and above the stand (Denmead and Bradley 1985, Gao *et al.* 1989, Maitani and Shaw 1990). Yet, a complete picture can evolve only if the physical processes in both parts are considered.

As reported in Chapter 2, an experiment to study the exchange processes within and above a coniferous forest of Douglas-fir trees was conducted on Vancouver Island during a two-week rainless period in July and August 1990. This Chapter reports the results of the analysis of eddy fluxes of sensible heat and water vapour within and above this stand. As part of the analysis, energy budget closure above the stand and beneath the overstory is examined. The big leaf model is used to calculate the canopy resistance and Omega factor of the stand for the purpose of describing the degree of coupling between the atmosphere and the stand. The implications of measured flux profiles, namely, the relationships between the flux and source distributions and the phenomenon of counter-gradient flux are addressed. Finally, the technique of quadrant-hole analysis is used to identify the kinds of motion which dominate the exchange processes.

3.2 Experimental Methods

3.2.1 Site Description

The experimental site was located on a slope with a 5° inclination angle near Browns River approximately 10 km northwest of Courtenay on Vancouver Island, 125°10′W, 49°42′N. The overstory species is Douglas-fir planted in 1962. In 1988 it was thinned to 575 stems/ha and pruned to a height of approximately 6 m. The height of the stand (h) was 16.7 m. The average trunk diameter at the height of 1.3 m was 0.20 m. The total (projected) leaf area index was 5.4. The forest floor was littered with dead branches and trunks, with a little short understory vegetation less than 0.5 m tall. A more detailed description of the site can be found in Chapter 2.

The experiment was conducted in late July and early August 1990. The most recent rainfall event prior to the experiment occurred on 6 July. The weather remained mostly clear during the experimental period. The average water content of the root zone (0-60 cm) was 0.19 on 27 July, 0.13 on 2 August and 0.11 kg/kg on 17 August on dry soil basis. During the late stage of the experiment, there was water stress of the trees as indicated by some needle yellowing.

3.2.2 Instrumentation

Primary instrumentation included two eddy correlation units mounted 1.5 m from a 25 cm open-lattice triangular tower, which measured the fluctuations in the three velocity components, air temperature and water vapour density. One unit was operated permanently at a height of 23.0 m (z/h = 1.38). The other unit was operated at the following heights (z/h in brackets): 2.0 (0.12), 7.0 (0.42), 10.0 (0.60), and 16.7 m (1.00), for 2–3 eight hour periods at each height. The two units were operated in the daytime when the wind direction was favorable. The sampling rate was 9.9 Hz. About 120 hours of data were collected for subsequent analysis.

In the early stage of the experiment, three 1-dimensional sonic anemometer/thermocouple units (Campbell Scientific Inc., Logan, UT) were operated at 2 m above the forest floor and located in the upwind direction of the main instrument tower. The main tower and the three 1-dimensional units were positioned approximately along a line with 15 m separation from each other. The signals from the three units were sampled at 10 Hz by a data logger (Campbell Scientific Inc., 21X with extended software II), which gave on-line calculations of sensible heat flux for every 30-minute period.

Net radiation flux above the stand was measured with a net radiometer (Swissteco Instruments, Oberriet, Switzerland, Model S-1) at a height of 24.0 m. Net radiation flux near the forest floor was measured at a height of 1.3 m (z/h = 0.08) with two net radiometers of the same type: one mounted on a tram and moving back and forth at a speed of 1.49 m/min along a 15.6 m pathway (Black *et al.* 1991) and the other at a height of 1.3 m at a fixed position. Only data collected with the tram system were used in the analysis of energy budget beneath the overstory. Soil heat flux was measured with two pairs of soil heat flux plates (one pair, Middleton Instruments, Australia, Model F; one pair, home-made following the design of Fuchs anf Tanner (1968)) placed at a depth of 3 cm and two nickel wire integrating thermometers to correct for the change in heat storage in the surface soil layer.

Relative humidity was measured at heights of 24.0 and 1.5 m with two hygrometers (Physical-Chemical Corp., New York, NY, Model PRC). Both sensors were calibrated against an Assmman psychrometer (Casella Ltd., London, England) in the field. Air temperature and wind speed were measured with fine wire thermocouples (25 μm welded chromel-constantan) and sensitive cup anemometers (C.W. Thornthwaite Associates, Centerton, NJ, Model 901-LED), respectively, at heights of 0.9, 2.0, 4.6, 7.0, 10.0, 12.7, 16.7 and 23.0 m.

Soil water content was measured once a week using gravimetric method. Soil water content of the root zone (0–60 cm) was measured at a 5 cm increment at two locations. Soil water content of the surface layer (0–3 cm) was measured at four locations and was used to determine the volumetrical heat capacity of this layer for the calculations of soil heat flux.

3.2.3 Theoretical Considerations

Turbulence statistics were calculated over 30-minute intervals. A two-way coordinate rotation was applied to the statistics measured at the heights of 16.7 m and 23.0 m, following the procedure of Tanner and Thurtell (1969), and a one-way coordinate rotation applied to the statistics measured within the stand, following the procedure of Baldocchi and Hutchison (1987). Corrections were made to the measurements of water vapour flux made with the krypton hygrometers to account for the effect of oxygen (Massman *et al.* 1990) and the effect of the air density due to the simultaneous transfer of heat and water vapour (Webb *et al.* 1980).

Assuming horizontal homogeneity and neglecting the energy used in photosythesis, the energy budget of the forest stand can be expressed as

$$R_n - S - G = H + \lambda E \tag{3.1}$$

where R_n is the net radiation flux above the stand, G is the soil heat flux, H is the sensible heat flux above the stand, λE is the latent heat flux above the stand, and S is the rate of heat storage per unit ground area in the layer between the 0 and 23.0 m heights, all of which have units of W/m^2.

The rate of heat storage, S was separated into the following four components:

$$S = S_s + S_l + S_{nb} + S_t$$

where S_s is the rate of sensible heat storage in the air, S_l is the rate of latent heat storage in the air, S_{nb} is the rate of heat storage in the needles and branches, and S_t is the rate of heat storage in the tree trunks. The first three components can be expressed as

$$S_s = \int_0^{23m} \rho c_p \frac{\partial T_a}{\partial t} dz \tag{3.2}$$

$$S_l = \int_0^{23m} \lambda \frac{\partial \rho_v}{\partial t} dz \tag{3.3}$$

$$S_{nb} = \int_0^{23m} m c_{nb} \frac{\partial T_{nb}}{\partial t} dz \tag{3.4}$$

where $\frac{\partial T_a}{\partial t}$, $\frac{\partial \rho_v}{\partial t}$, and $\frac{\partial T_{nb}}{\partial t}$ are the time rates of change in air temperature, water vapour density and temperature of the needles and branches; ρ is the air density, c_p is the specific heat of air at constant pressure, λ is the latent heat of vaporization of water, m is the mass of the needles and branches per unit volume of air, and c_{nb} is the specific heat of the needles and branches. Using appropriate values for ρ, c_p and λ, (3.2) and (3.3) reduce to

$$S_s = 14.2 \Delta \overline{T}_a$$

$$S_l = 31.2 \Delta \overline{\rho}_v$$

where $\Delta \overline{T}_a$ (°C) and $\Delta \overline{\rho}_v$ (g/m^3) are the changes over a 30-minute interval in air temperature and water vapour density averaged over the layer between the 0 and 23.0 m heights. $\Delta\overline{T}_a$ was calculated from the measurements of air temperature made at the eight heights, and $\Delta\overline{\rho_v}$ was approximated by the measurement of water vapour density made at the height of 24.0 m. Using the measured mass of needles and branches and a value of 2647 J/(kg °C) for c_{nb}, based on the specific heat of dry wood (Cohen *et al.* 1985) and corrected for the measured water content of the needles and branches, (3.4) reduces to

$$S_{nb} = 4.3\Delta\overline{T}_{nb}$$

where $\Delta\overline{T}_{nb}$ (°C) is the change over a 30-minute interval in the average temperature of the needles and branches, estimated to a good approximation from the change in air temperature averaged over the four heights of 7.0, 10.0, 12.7 and 16.7 m. The rate of heat storage in the trunk (S_t) was estimated, using a method similar to that used by Denmead and Bradley (1985), from a solution obtained by Herrington (1969) for radial heat flow in a semi-infinite slab with a periodic surface temperature. Using the values for bulk density, specific heat and thermal diffusivity of Douglas-fir wood (Cohen *et al.* 1985) and the average surface area of a trunk, and approximating the trunk surface temperature by air temperature in the stand (assumed to vary sinusoidally), S_t is expressed as

$$S_t = 3.5A_{T_a}\cos(\omega t - \phi + \pi/4) \tag{3.5}$$

where A_{T_a} (°C) and ϕ are the amplitude and phase angle of the diurnal course of air temperature in the stand, respectively, ω is the diurnal angular frequency which equals $\pi/12$ (rad/h), and t is the time of the day.

The bulk canopy resistance (r_c) can be obtained from the Penman-Monteith equation, i.e. the big leaf model (Monteith 1965)

$$r_c = \frac{\rho c_p D}{\gamma\lambda E} + r_a[(\beta s/\gamma) - 1] \tag{3.6}$$

where D is the saturation pressure deficit measured at the height of 24.0 m, γ is the psychrometric constant, s is the slope of the saturation vapour pressure curve at air temperature, r_a is the aerodynamic resistance to water vapour and sensible heat diffusion between the reference height (23.0 m in the present study) and their effective source heights (assumed to be the same), and β is the Bowen ratio calculated from the measured eddy fluxes. The aerodynamic resistance, r_a was approximated by the aerodynamic resistance to momentum transfer (r_m) without stability and roughness sublayer corrections

$$r_a = r_m = u/u_*^2$$

where u is the mean wind speed at the reference height, and u_* is the friction velocity. This simplification will not introduce much error in r_c since of the two terms on the RHS of (3.6), the first term is dominant.

To perform the quadrant-hole analysis of the eddy fluxes of sensible heat and water vapour, the quantity α (either air temperature or water vapour density) and the vertical velocity component w are separated into means ($\overline{\alpha}$, $\overline{w}$) and fluctuating parts (α', w'). The four quadrants in the $\alpha' w'$ plane are labelled as ejection (i = 1; $\alpha' > 0$, $w' > 0$), outward interaction (i = 2; $\alpha' < 0$, $w' > 0$), sweep (i = 3; $\alpha' < 0$, $w' < 0$), and inward interaction (i = 4; $\alpha' > 0$, $w' < 0$). A flux fraction $F_{i,H}$ and a time fraction $t_{i,H}$ with a hyperbolic exclusion zone set by the hole size H are defined as

$$F_{i,H} = \frac{1}{\mid \overline{w'\alpha'} \mid} \frac{1}{T} \int_0^T w'(t)\alpha'(t) I_{i,H} dt$$

and

$$t_{i,H} = \frac{1}{T} \int_0^T I_{i,H} dt$$

where T is the average time interval (30 minutes in this study), and $I_{i,H}$ is a conditioning function which equals one if the point ($\alpha'(t)$, $w'(t)$) is located in the ith quadrant and $\mid w'(t)\alpha'(t) \mid$ is greater than $H \mid \overline{w'\alpha'} \mid$, and zero otherwise.

3.3 Results and Discussion

3.3.1 Eddy Fluxes above the Stand

3.3.1.1 Energy Budget Closure

Figure 3.1 shows the sum of the eddy fluxes ($H + \lambda E$) measured at z/h = 1.38 plotted against the available energy flux ($R_n - S - G$). On average, $H + \lambda E$ accounted for 83% of $R_n - S - G$. The correlation coefficient was 0.85 for a total of 118 thirty-minute runs. The following sources of error contributed to the energy imbalance and the scatter in Figure 3.1. First, neglect in (3.1) of the solar energy used in photosynthesis would result in overestimating the available energy flux by 1–4% (Verma *et al.* 1986, Stewart and Thom 1973). Second, estimating the heat storage component, S with the method described above was subject to uncertainties. McCaughey (1985) showed that in a dry, mixed forest, the temporal change in biomass temperature lagged behind that in air temperature within the stand. Part of the effect of the time lag was incorporated into (3.5). But (3.5) was only a first order approximation, since the temporal course of air temperature was not perfectly sinusoidal. Third, the heat flux into the soil was characterized by large horizontal uncertainties due to the high horizontal heterogeneity of the solar irradiance on the forest floor. Consequently, two pairs of heat flux plates were insufficient to provide a good spatial average of G.

The choice of averaging time interval is important for eddy correlation measurements. McMillen (1988) suggests a time constant of 200 seconds for the running mean removal for the on-line computation of fluxes. Using the Reynolds averaging procedure, the fluxes and other statistics were first calculated over 5-minute intervals and averaged for each 30-minute period. A large flux loss occurred, with $H + \lambda E$ being only 75% of $R_n - G - S$. This was due to the effect of low frequency cut-off and indicated the importance of eddies

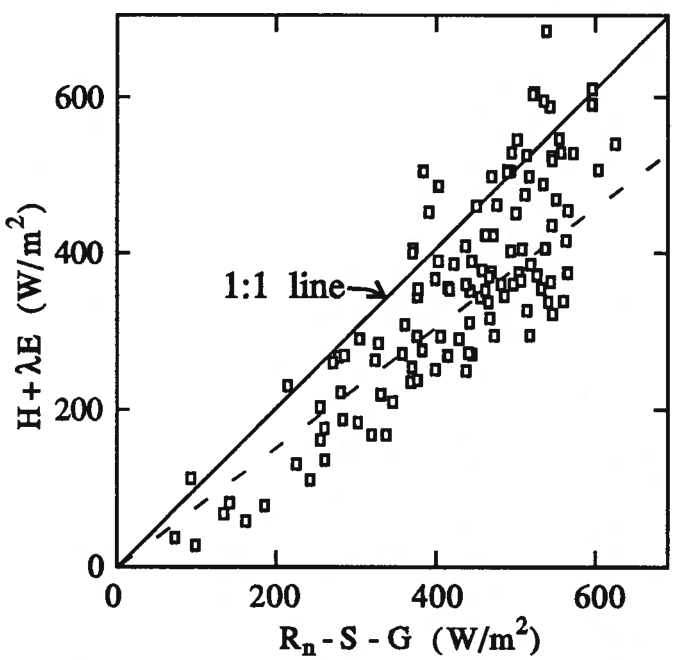

Figure 3.1: Comparison of the sum of the eddy flux densities ($H + \lambda E$) measured at z/h = 1.38 and the available energy flux density ($R_n - S - G$) for the Douglas-fir stand at Browns River during the entire experimental period in 1990. The dash line represents the linear regression forced through zero with a slope of 0.83.

with periods exceeding 5 minutes. The atmosphere was moderately to strongly unstable in the daytime during the experimental period (Chapter 2). According to the estimate of McBean (1972) for the unstable surface layer, the loss of covariance resulting from the low frequency cut-off at 0.0033 Hz, a frequency corresponding to the period of 5 minutes, is on the order of 10%. By changing the averaging time interval to 30 minutes, the energy budget closure was increased by 8% to 83%. Further increase in the averaging time interval, however, had little effect on the computation of fluxes. The averaging interval of 30 minutes therefore appears to be a good choice for the present study.

Table 3.1 lists the daytime average components of the energy budget for the stand for the nine experimental days. The sky was clear except on 26 July and 1 August, when partly cloudy conditions occurred. The average values of R_n, H and λE during the measurement periods on the nine days were 449, 231 and 115 W/m^2, respectively. On some days, energy budget closure was much better than on others. The values of the ratio, $(H + \lambda E)/(R_n - S - G)$ ranged from 0.67 (31 July) to 0.96 (20 July).

Figure 3.2 shows the daytime variation of the energy budget components on 1 August and on 28 July. On 1 August, it was partly cloudy. The fluctuations in R_n were closely followed by the fluctuations in H and λE, and good closure was obtained. The three main energy budget components of this day peaked at around 12:00 PST, the peak values of R_n, H and λE being 669, 456 and 135 W/m^2, respectively.

It was perfectly clear on 28 July, as indicated by the smoothness of the R_n record. But large fluctuations were observed in H and λE. There was a significant energy imbalance around noon. During the period between 11:30 and 13:00 PST, the average available energy flux $(R_n - S - G)$ was 524 W/m^2, while sensible and latent heat fluxes were only 244 and 107 W/m^2, respectively, with the ratio, $(H + \lambda E)/(R_n - S - G)$ being 0.66.

Table 3.1: Average values of the energy budget components, R_n, G, S, H and λE (W/m^2) during the indicated periods for the Douglas-fir stand at Browns River. Also shown are the values of the ratio, $(H + \lambda E)/(R_n - S - G)$, and the daytime Bowen ratio, β.

Date	19 July	20 July	26 July	27 July	28 July
Hour (PST)	11:30–18:00	9:30–16:00	9:00–16:30	12:00–17:30	8:30–16:00
R_n	462	533	444	460	512
G	13	21	13	8	21
S	7	23	20	15	36
H	183	286	230	241	264
λE	142	184	113	111	113
$\frac{H+\lambda E}{R_n - S - G}$	0.76	0.96	0.83	0.81	0.83
β	1.3	1.6	2.0	2.2	2.3

Date	29 July	30 July	31 July	1 August	Mean
Hour (PST)	12:00–19:00	9:00–16:30	12:30–17:30	9:00–17:00	
R_n	376	469	319	469	449
G	12	11	7	12	13
S	6	22	3	18	17
H	171	271	139	292	231
λE	88	110	69	107	115
$\frac{H+\lambda E}{R_n - S - G}$	0.73	0.87	0.67	0.91	0.83
β	1.9	2.5	2.0	2.7	2.1

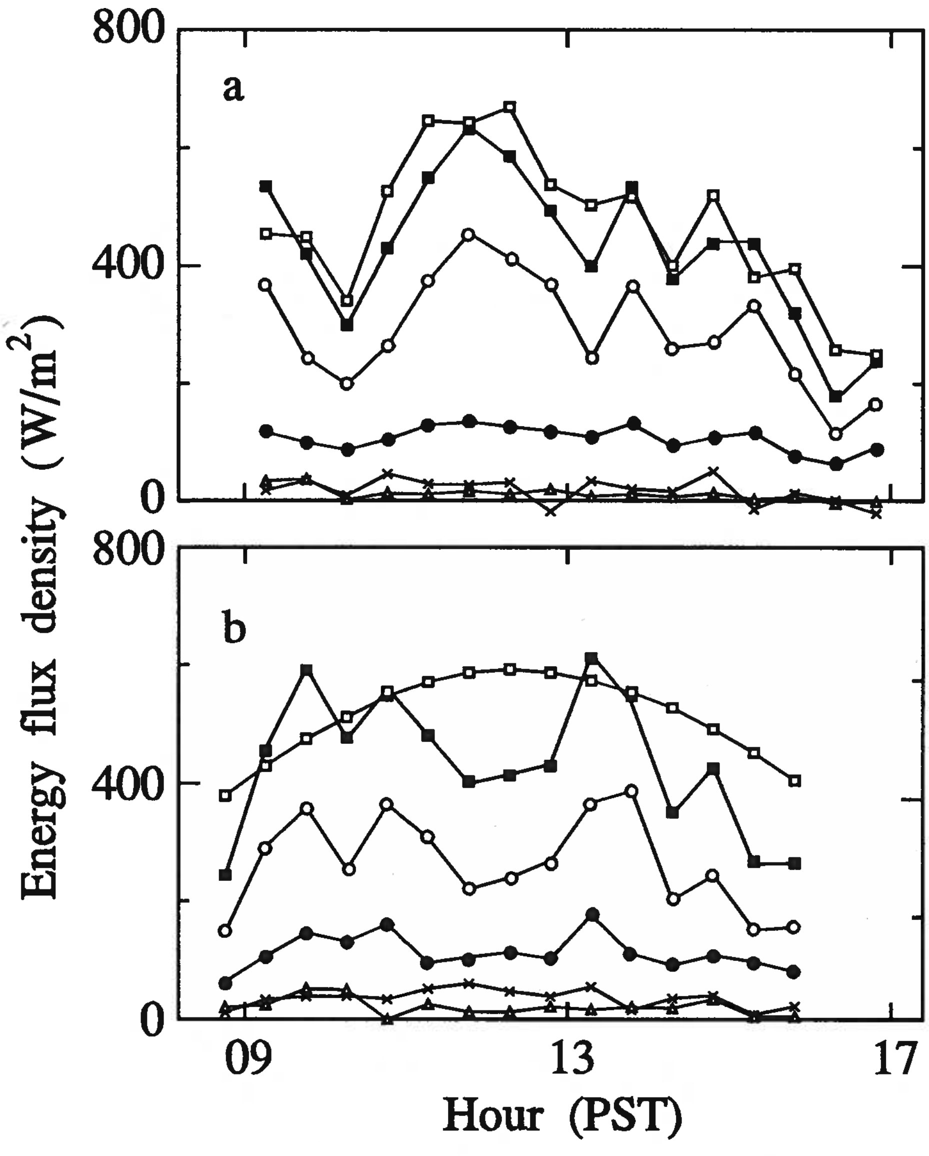

Figure 3.2: Energy budget closure as shown by the comparison of values of R_n (□) and $H + \lambda E + S + G$ (■) for the Douglas-fir stand at Browns River on (a) a partly cloudy day (1 August) and (b) a clear day (28 July 1990). Also shown are the variations of H (○), λE (•), G (△) and S (×).

The large imbalance did not appear to be related to the wind direction, since the daytime wind blew very constantly from the NE–NEE sector as a result of land-sea/upslope-downslope circulations, and cannot be fully accounted for by the sources of error discussed above. Furthermore, it was very unlikely that the imbalance was caused by instrument malfunction. This is demonstrated by the good agreement in the measurements made by the two eddy correlation units. On 31 July and 1 August, the lower eddy correlation unit was operated at z/h = 1.00. In Chapter 2, it was shown that on these two days the covariance of the vertical velocity and air temperature and the covariance of the vertical velocity and water vapour density measured at z/h = 1.00 agreed very well with those measured at z/h = 1.38. Figure 3.3 shows the daytime variation of the fluxes measured at these two heights on 31 July. The measurements at the two heights were almost identical. But, as on 28 July, there was a large energy imbalance around noon.

The energy imbalance is believed to be related to the cell-like structure of the flow under convective conditions in the planetary boundary layer (Thurtell, G.W. 1991, personal communication). In some areas there are ascending movements, which are compensated by the descending movements in the surrounding areas (Deardorff 1973, Webb 1977). The vertical velocity at a single point, even though averaged over a certain time period, is likely different from zero. Because of the non-zero vertical velocity, the eddy correlation measurement made at a single point under convective conditions will tend to underestimate the vertical fluxes of sensible and latent heat. If the convection is very active, the underestimation may be significant.

3.3.1.2 Canopy Resistance and the Omega Factor

The daytime Bowen ratio increased with time during the 9-day experimental period from 1.3 to 2.7 as the soil dried (Table 3.1). This is not surprising considering the steep water retention curve for this coarse soil (Nnyamah and Black 1977) and the shallow root zone.

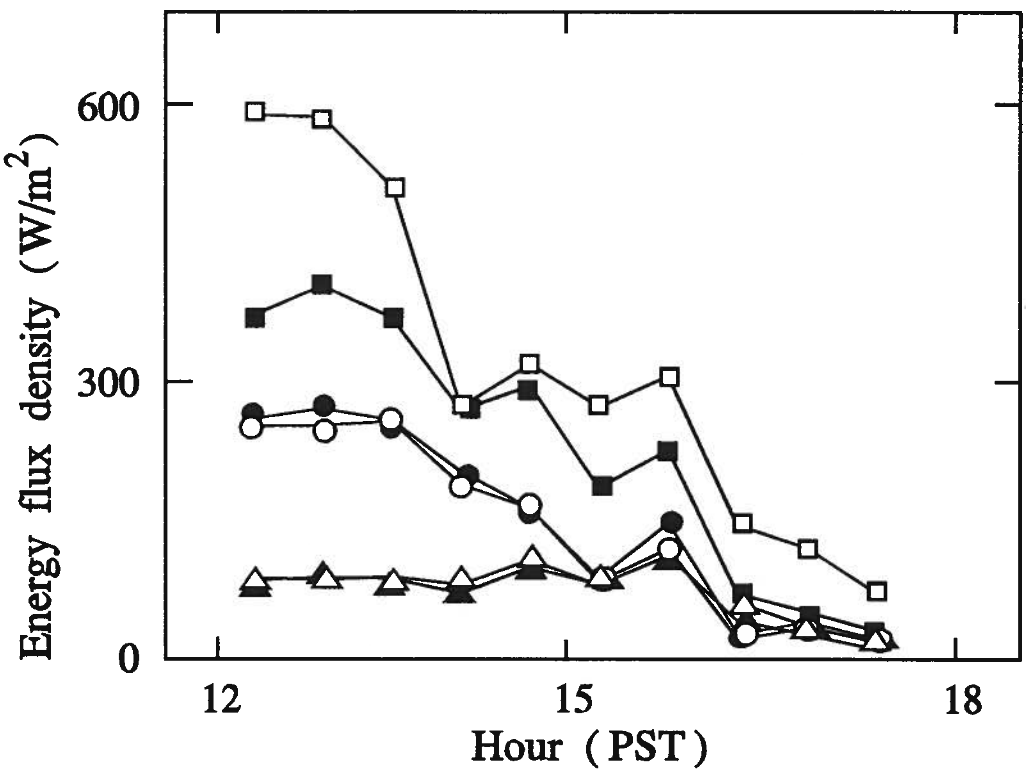

Figure 3.3: Comparison of eddy fluxes measured at z/h = 1.38 as indicated by H (•) and λE (▲) and at z/h = 1.00 as indicated by H (○) and λE (△) for the Douglas-fir stand at Browns River on 31 July, 1990. Also shown are R_n (□) above the stand and $H + \lambda E + G + S$ (■) for z/h = 1.38.

The canopy resistance of Douglas-fir stands has a strong dependence on the soil water potential and saturation deficit of the air (D). It increases as soil water potential decreases and as D increases (Tan and Black 1976). Figure 3.4 shows the daytime variation in r_c and D on 19 and 20 July. The value of r_c was about 300 s/m in the mid-morning, and tended to increase with time in the late afternoon as D increased. A similar time trend was also observed on the remaining days. The magnitude and the time trend reported here agree with those obtained with energy balance/Bowen ratio technique for coniferous stands of younger Douglas-fir trees under water stress (Price and Black 1990 and 1991, Tan and Black 1976).

Figure 3.5 shows the the courses of the daytime mean canopy resistance and saturation deficit during the experimental period. The daytime mean canopy resistance $\overline{r}_c$ was obtained by weighting the half-hourly values of r_c by D as follows (Tan and Black 1976)

$$\overline{r_c} = \overline{D}/\frac{1}{n}\sum_{i=1}^{n}(D_i/r_{ci})$$

where D_i and r_{ci} are the half-hourly values of D and r_c, and $\overline{D}$ is the arithmetic average of the daytime D. At very similar values of $\overline{D}$, $\overline{r}_c$ was higher on 29 July than on 19 and 20 July, a result of the steady decrease in soil water content during the experimental period. During the period between 26 July and 1 August, $\overline{r_c}$ was well correlated with $\overline{D}$.

McNaughton and Jarvis (1983) and Jarvis (1985) introduced the concept of coupling between vegetation communities and the atmosphere in terms of the dimensionless decoupling factor

$$\Omega = (s/\gamma + 1)/(s/\gamma + 1 + r_c/r_a)$$

where Ω has values between zero and one. They suggested Ω values of about 0.1 to 0.2 for forests (strong coupling) and about 0.8 to 0.9 for grasslands (weak coupling). Based on their analyses, transpiration from trees is expected to follow closely the saturation deficit and to be controlled by the canopy resistance. Figure 3.6 shows the daytime variation of

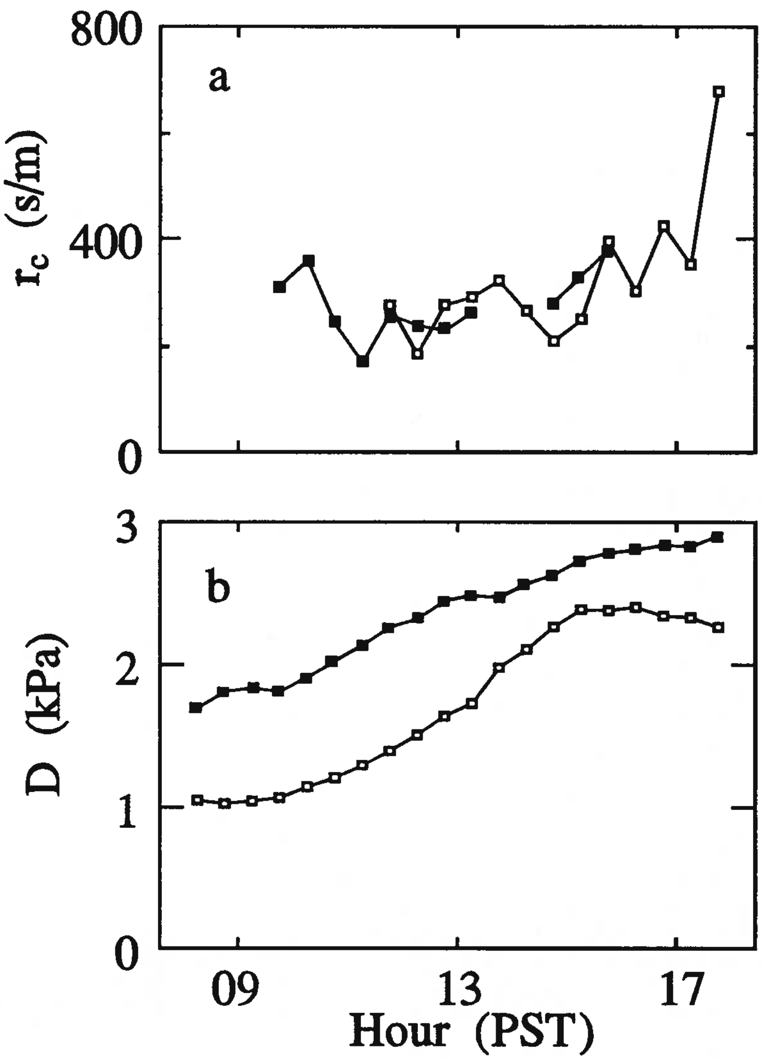

Figure 3.4: Daytime variation of (a) canopy resistance r_c, and (b) saturation deficit D for the Douglas-fir stand at Browns River on 19 July (□) and 20 July, 1990 (■).

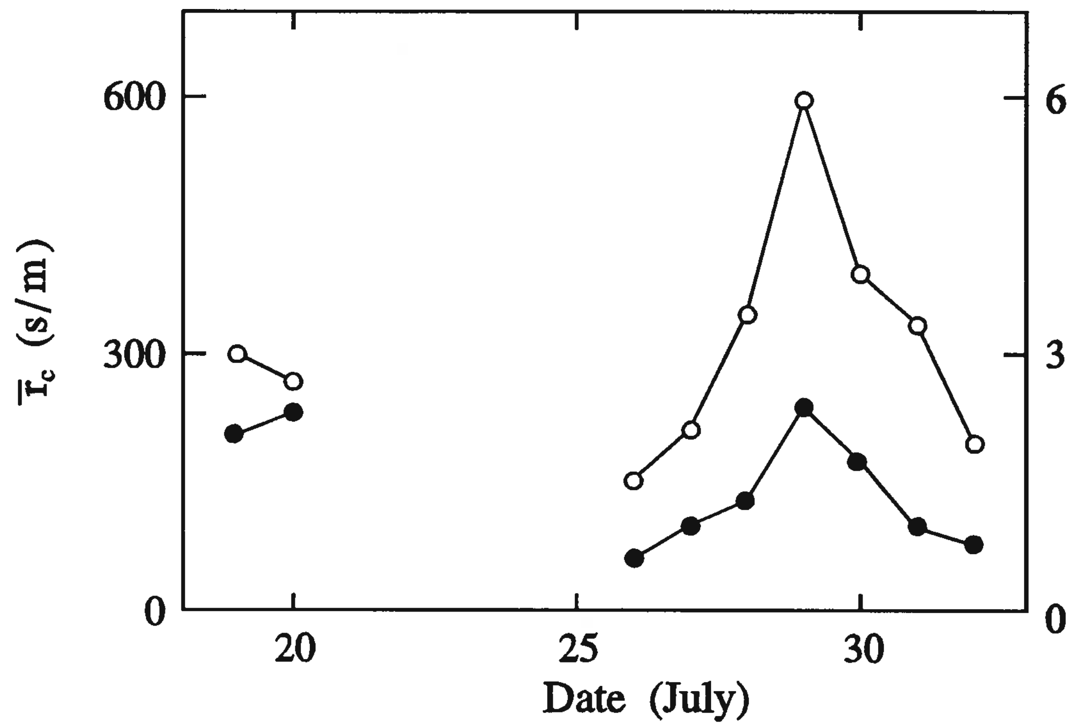

Figure 3.5: Courses of daytime mean canopy resistance $\overline{r}_c$ (∘) and mean saturation pressure deficit $\overline{D}$ (•) for the Douglas-fir stand at Browns River in 1990.

Omega factor on 19 and 20 July. The mid-day value of Ω was around 0.2, a value close to those suggested by McNaughton and Jarvis (1983) and Jarvis (1985). Similar results were obtained on the remaining days.

3.3.2 Eddy Fluxes beneath the Overstory

3.3.2.1 Energy Budget Closure

An advantage of the eddy correlation method in measuring fluxes from the forest floor and understory vegetation is that it is *in situ* so that the impact on the vegetation and the environment is minimized. It is the only technique that can measure fluxes at various heights within a forest stand. The technique is expected to give reasonable areal average values of fluxes (Raupach 1989). It was used by Baldocchi and Meyers (1991) in a study of evaporation and CO_2 efflux near the forest floor of a deciduous forest. Its reliability can be evaluated by examining the energy budget closure.

Table 3.2 lists the daytime average value of the energy budget components beneath the overstory of the stand. The rate of heat storage in the air and trunks was very small, and was neglected in the analysis. On 19, 20 and 26 July, eddy correlation measurements were made at z/h = 0.12. Later, on 27 and 28 July, measurements were made at z/h = 0.42, the approximate height of the canopy base. Divergence of the eddy fluxes between these two heights was very small (Figure 3.9). The value of the ratio of the daytime total eddy flux of sensible and latent heat ($H + \lambda E$) to the available energy flux ($R_n - G$) ranged from 0.66 to 0.88, with an average value of 0.74. The large heterogeneities in R_n and G (see below) may be one of the reasons for the energy imbalance. But overall closure was satisfactory, bearing in mind that each component of the energy budget was of small magnitude.

Although it was a small component in the energy budget of the whole stand, G was

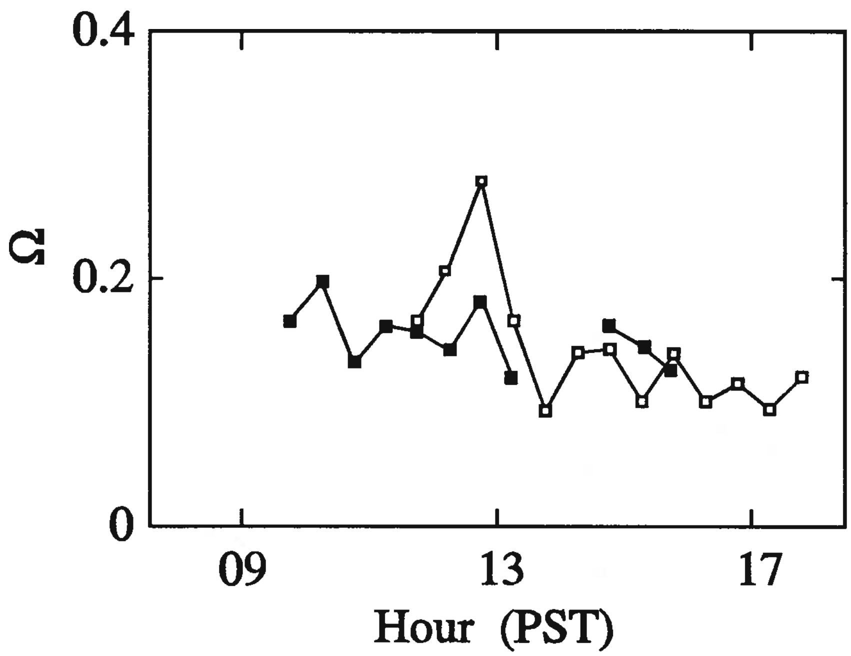

Figure 3.6: Daytime variation of Omega factor (Ω) for the Douglas-fir stand at Browns River on 19 July (□) and 20 July, 1990 (■).

Table 3.2: Daytime average values of the energy budget components, R_n, G, H and λE (W/m^2) beneath the overstory of the Douglas-fir stand at Browns River in July 1990. Also listed are the ratio, $(H+\lambda E)/(R_n-G)$, the daytime Bowen ratio, β, and the relative height (z/h) of the measurement of H and λE.

Date	19	20	26	27	28
Hour (PST)	12:00-18:00	9:30-16:30	9:00-16:30	11:00-16:30	8:30-16:00
z/h	0.12	0.12	0.12	0.42	0.42
R_n	97	157	106	113	137
G	11	21	13	10	21
H	33	47	52	48	47
λE	29	48	29	26	34
$\frac{H+\lambda E}{R_n - G}$	0.73	0.69	0.88	0.72	0.69
β	1.1	1.0	1.8	1.9	1.4

significant in the energy budget beneath the overstory. As above the stand, H was the largest output component of the energy budget, but was not as dominant. The value of β was close to one on the first two days (19 and 20 July) and greater than one on the later three days (26, 27 and 28 July), with a mean value of 1.4. The increase of β with time was a result of soil drying and was consistent with the trend of the Bowen ratio above the stand. However, the value of β beneath the overstory was smaller than that above the stand.

3.3.2.2 Temporal and Horizontal Variations in the Energy Budget Components

Figure 3.7 presents the daytime variation of the energy budget components beneath the overstory and the net radiation flux above the stand on 20 and 26 July. It was clear on 20 July and partly cloudy on 26 July. The midday values of H and λE were about 60 and 70 W/m^2 on 20 July and 90 and 40 W/m^2 on 26 July, respectively. The trends of H and λE was similar to the trend of the net radiation above the stand rather than R_n measured near the forest floor.

Considerable fluctuations occurred in R_n measured near the forest floor, even under clear sky conditions (Figure 3.7b). This means that the pathway of the tram system was not long enough to obtain a good spatially averaged value of R_n. Large fluctuations also occurred in G. To obtain more reliable measurements of R_n and G in this stand, the length of the tram pathway and the number of heat flux plates would have to be increased.

The optimal length of the pathway of the tram depends on crown closure. The same tram system has given satisfactory measurements of shortwave and longwave irradiances in an unthinned Douglas-fir stand of similar age (Black *et al.* 1991). The pathway length/tree spacing ratio in that study was about 6.3. Using this ratio as a rule of thumb,

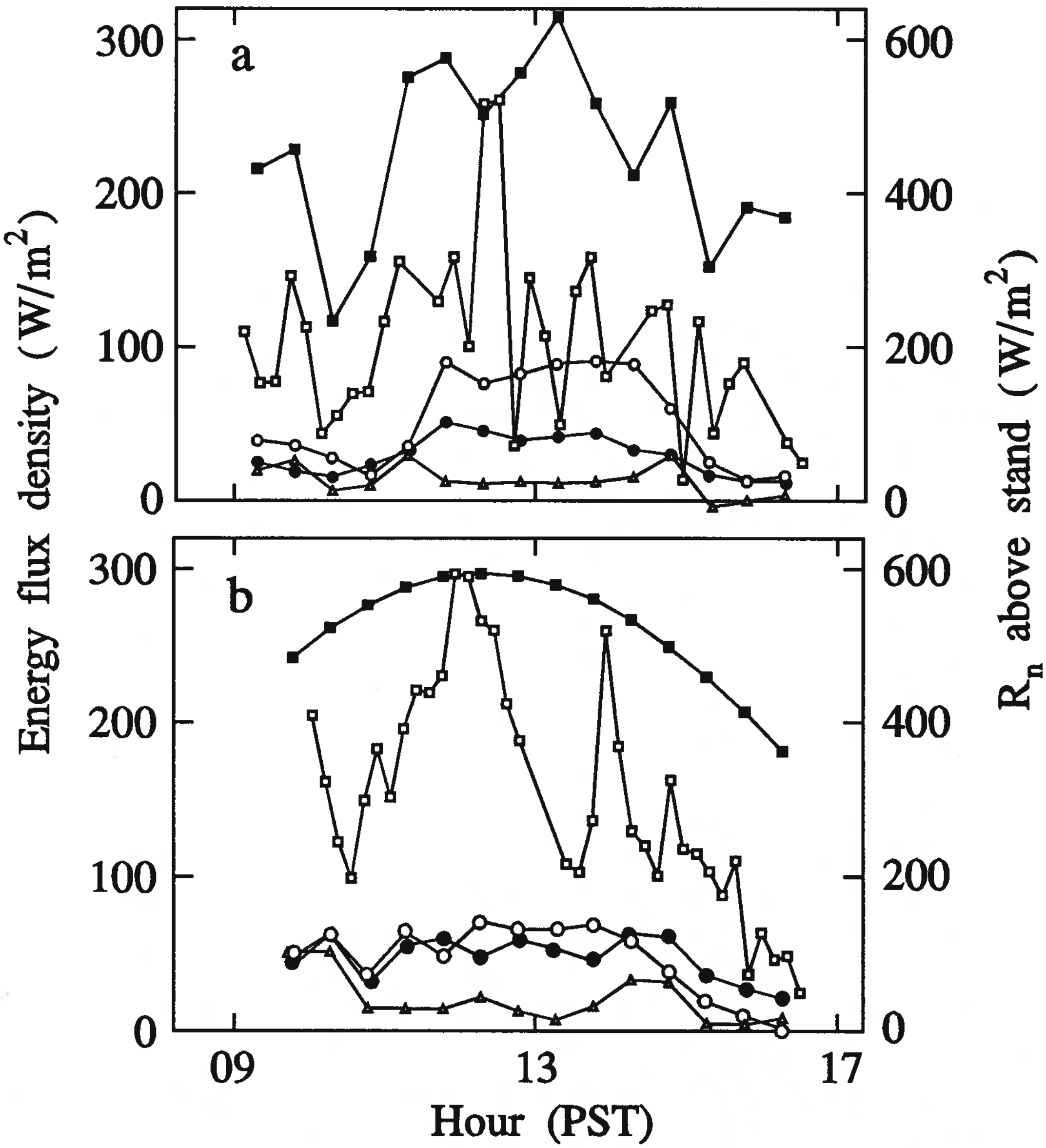

Figure 3.7: Variation of the energy budget components, R_n (□), H (○), λE (•) and G (△) beneath the overstory of the Douglas-fir stand at Browns River on (a) a partly cloudy day (26 July) and (b) a clear day (20 July, 1990). Also shown is the variation of the net radiation flux density above the stand (■).

the pathway length should have been increased to 26 m for a reliable measurement of R_n in the present study.

Figure 3.8 compares the kinematic sensible heat flux $\overline{w'T'}$ near the forest floor measured at four positions with three 1-dimensional sonic anemometer/thermocouple units and one 3-dimensional sonic anemometer/thermometer unit. Good agreement was obtained among the measurements of the three 1-dimensional units: much of the scatter fell in the range of ±15%. The flux measured with the 3-dimensional unit was slightly lower than that measured with the 1-dimensional units. The results indicate that the eddy correlation measurement made at the height of 2 m provided a good spatial average of the sensible heat flux from the forest floor and the understory in this pruned and thinned stand.

3.3.3 Profiles of Eddy Fluxes

Figure 3.9 shows the sensible heat and water vapour fluxes at various heights in the stand as fractions of the corresponding fluxes at z/h = 1.38. There appear to be two constant flux layers, one above the tree tops and the other in the trunk space. Within the canopy layer, the fluxes increased approximately linearly with height. This pattern of vertical profiles, also observed by Denmead and Bradley (1985) in a pine forest, reflects the density distributions of the sensible heat and water vapour sources. The stand in the present study had two distinct sources: the forest floor (including a little short understory vegetation) and the canopy, separated by the trunk space of approximately 6 m in height. While flux divergences in the trunk space were very small because of the negligible source density in the trunk space, the non-zero source density of the foliage resulted in large flux divergences in the canopy layer. But the divergences were not proportional to the leaf area density. For example, based on Figure 3.9, of the total flux divergence of sensible heat in the canopy layer, 54% came from the layer between z/h = 0.60 and 1.00, which

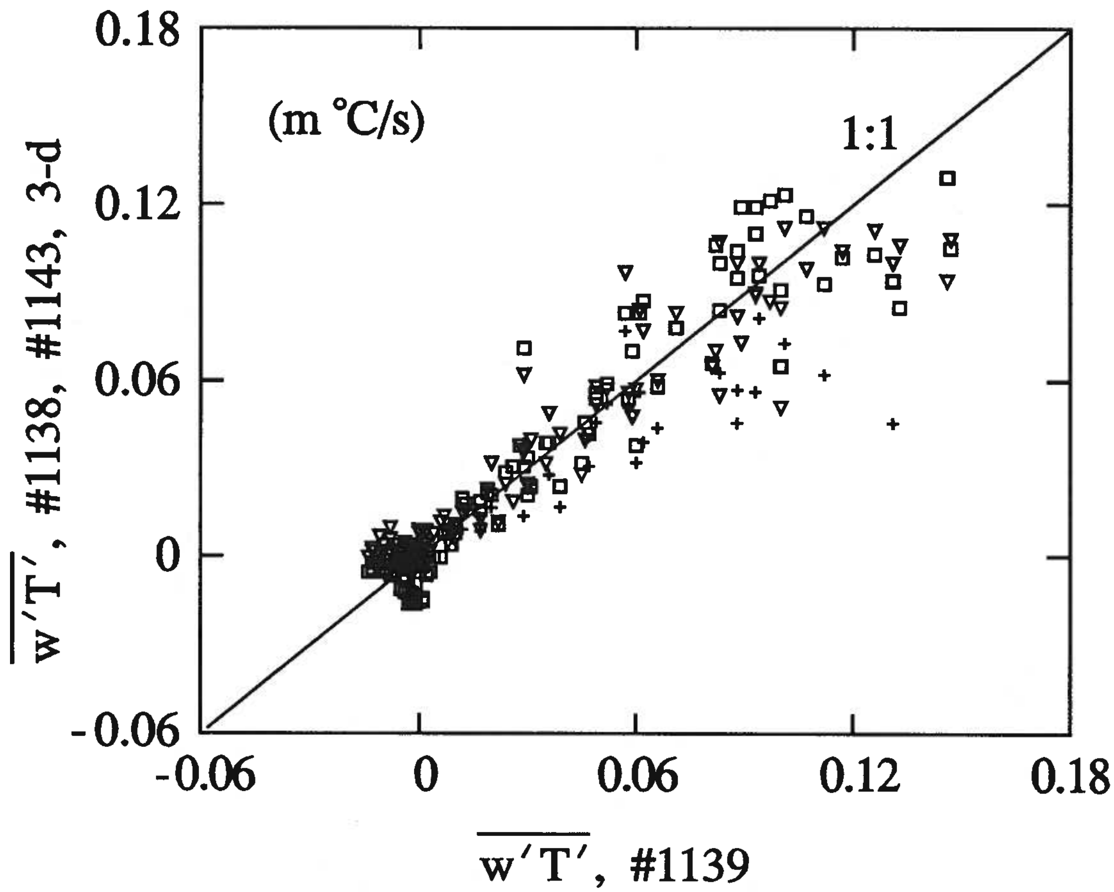

Figure 3.8: Comparison of the kinematic sensible heat flux $\overline{w'T'}$ at 2 m (z/h = 0.12) above the forest floor of the Douglas-fir stand at Browns River measured at four positions in July 1990 with three 1-dimensional sonic anemometer/thermocouple units (#1138, #1139, #1143) and one 3-dimensional sonic anemometer/thermometer unit (3-d): (□), #1138; (▽), #1143; (+), 3-d.

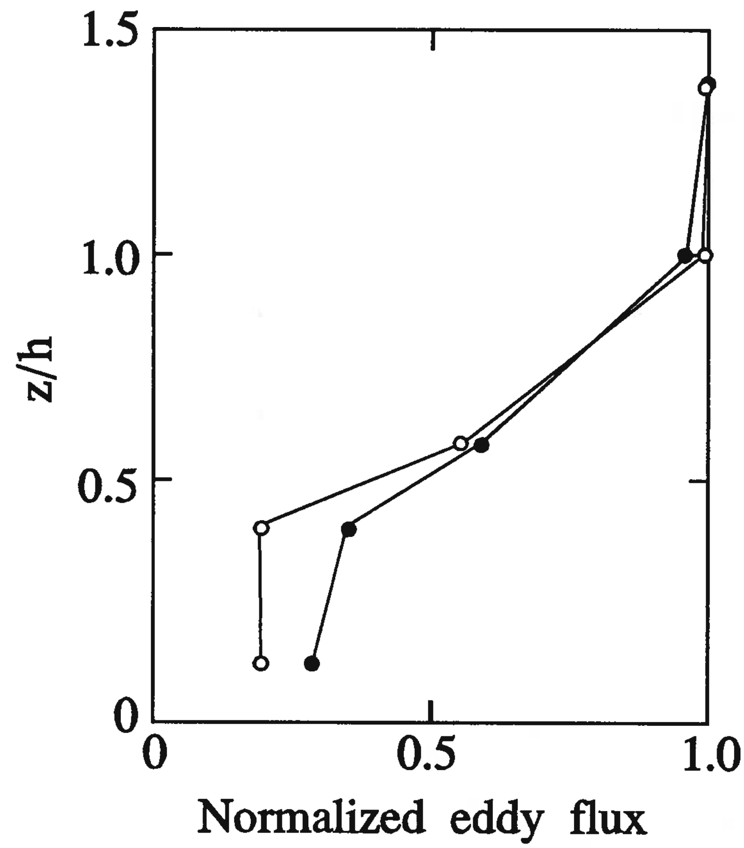

Figure 3.9: Normalized profiles of daytime averaged sensible heat flux (∘) and water vapour flux (•) in the Douglas-fir stand at Browns River in 1990. The average values of the standard error of the mean was 0.085 at z/h = 0.60 and 0.025 at all other heights.

had 40% of the canopy leaf area (Chapter 2), and 46% came from the layer below z/h = 0.60, which had 60% of the canopy leaf area. In other words, for the same amount of leaf area, the source density of sensible heat was higher in the upper canopy than in the lower canopy. This might be a result of higher radiation absorption per unit leaf area in the upper canopy than in the lower canopy.

The profiles of sensible heat and water vapour fluxes were somewhat dissimilar in that the forest floor contributed less to the total sensible heat flux from the stand (19%) than to the total water vapour flux (26%). This may imply the inequality of the effective source heights for sensible heat and water vapour. By analogy to the centre-of-pressure theorem (Thom 1971), the effective source height, d can be expressed as

$$d = \frac{\int_0^h zS(z)dz}{\int_0^h S(z)dz + F_g} \tag{3.7}$$

where $S(z)$ is the flux divergence or source density at height z and F_g is the flux from the forest floor. Physically, (3.7) defines the height of the zero-plane displacement. With the aid of the data in Figure 3.9, (3.7) gives an estimate of d = 9.6 m or d/h = 0.57 for sensible heat and d = 8.7 m or d/h = 0.52 for water vapour. The difference in d/h between sensible heat and water vapour was small compared to the large uncertainties in the ratio d/h for forests (Jarvis *et al.* 1976), and seems to support the general use of a single d for heat and water vapour (Thom 1972).

Both sensible heat and water vapour fluxes within the stand were directed upward for the majority of the runs. The numbers of the runs with upward sensible heat flux (total numbers of runs in brackets) at z/h = 0.12, 0.40 and 0.60 were 40 (42), 27 (28) and 26 (29), respectively, and the corresponding figures for water vapour flux were 41 (42), 27 (28) and 29 (29). The runs with downward fluxes occurred during the quiescent periods in the late afternoon when the upslope wind was being replaced by the downslope wind, and the fluxes were very small. Daytime air temperature characteristically exhibited a maximum near the ground and an inversion in the layer between z/h = 0.28 and 0.60 (Chapter 4). In other words, sensible heat constantly flowed against the temperature gradient in the inversion layer, a phenomenon termed counter-gradient flow that has been frequently observed in forests (Denmead and Bradley 1985, Amiro 1990, Leclerc 1987). The existence of counter-gradient flow is due in part to the sporadic penetration of transporting eddies into the canopy and their large scales (Denmead and Bradley 1985). In the context of a Lagrangian framework, it can be understood as a near-field effect of the canopy heat source (Raupach 1987). The phenomenon of counter-gradient flow at these heights invalidates K-theory. However, K-theory appears to be able to give a reasonable prediction of fluxes near the forest floor (Chapter 4).

3.3.4 Quadrant Representation of Eddy Fluxes

The technique of quadrant-hole analysis has been widely used to reveal the structure of turbulent transfer of momentum and scalars in vegetation canopies (e.g. Shaw *et al.* 1983, Finnigan 1979, Coppin *et al.* 1986, Chapter 2). In Chapter 2, it was shown that a major proportion of momentum transfer near the top of the stand and in the canopy layer occurred during intense intermittent sweep/ejection events. It was also shown that the magnitude of interaction contributions to the momentum transfer was greater than that of sweep/ejection contributions at the canopy base (z/h = 0.42) and in the middle of the trunk space (z/h = 0.12), which was consistent with the negative values of Reynolds stress at these heights.

Table 3.3 lists the set of the selected runs (same as used in Chapter 2) for performing the quadrant-hole analysis of sensible heat and water vapour fluxes. The results are summarized in Tables 3.4 and 3.5, where H' is the hole size above which half of the flux

Table 3.3: Values of the covariances of the vertical velocity component and air temperature ($\overline{w'T'}$) and the vertical velocity component and water vapour density ($\overline{w'\rho_v'}$), standard deviations of air temperature (σ_T), water vapour density (σ_{ρ_v}) and the vertical velocity component (σ_w) at the indicated heights for the five runs selected for quadrant-hole analysis of eddy fluxes of sensible heat and water vapour for the Douglas-fir stand at Browns River. The stability parameter (z – d)/L was calculated from the measurements at z/h = 1.38.

Time interval PST	z/h	(z–d)/L	$\overline{w'T'}$ m°C/s	$\overline{w'\rho_v'}$ g/(m^{2}s)	σ_T °C	σ_{ρ_v} g/m^3	σ_w m/s
13:30–14:00 19 July	0.12	-0.26	0.055	0.008	0.66	0.32	0.19
12:00–12:30 27 July	0.42	-0.25	0.112	0.015	0.75	0.15	0.32
12:30–13:00 30 July	0.60	-0.35	0.117	0.006	0.76	0.16	0.33
13:30–14:00 1 Aug	1.00	-0.25	0.217	0.017	0.77	0.12	0.54
12:00–12:30 27 July	1.38	-0.25	0.335	0.033	0.78	0.17	0.75

occurs

$$|\sum_{i=1}^{4} F_{i,H'}| = 0.5$$

and $\sum_{i=1}^{4} t_{i,H'}$ is the corresponding time fraction. H' and $\sum_{i=1}^{4} t_{i,H'}$ are measures of intermittency. The intermittent nature of the turbulent transport is obvious at all levels: Half of the sensible heat flux was accounted for by events with a hole size larger than 5.7–3.5, which occupied a small fraction of time (6–11%), while for water vapour flux the values of H' and $\sum_{i=1}^{4} t_{i,H'}$ were 34.6–5.2 and 1–10%, respectively.

The relative importance of the kinds of turbulent motion in the transport of scalars can be examined by calculating the ratios of the flux fractions at zero hole size. The variation of the ratio, $F_{3,0}/F_{1,0}$ with height was related to the source distributions. For sensible heat flux, it had values less than one at the tree tops (z/h = 1.00) and above the stand (z/h = 1.38), indicating that the ejection contribution to sensible heat flux exceeded the sweep contribution. The sweep contribution exceeded the ejection contribution in the middle and at the base of the canopy (z/h = 0.60 and 0.42), with the ratio $F_{3,0}/F_{1,0}$ greater than one. Close to the ground, at z/h = 0.12, the ejection contribution again exceeded the sweep contribution. For water vapour flux, the ejection and sweep contributions were of about equal magnitude at z/h = 1.38 and 1.00. At z/h = 0.60 and 0.42, the sweep contribution was greater than the ejection contribution, but the ejection contribution exceeded the sweep contribution at z/h = 0.12.

The ratio of the contribution of the interactions to that of the sweeps/ejections, $(F_{2,0} + F_{4,0})/(F_{1,0} + F_{3,0})$, varied between –0.23 and –0.13 for sensible heat flux and between –0.67 and –0.30 for water vapour flux (Tables 3.4 and 3.5). In Chapter 2, it was shown that the magnitude of this ratio for momentum flux exceeded one at z/h = 0.42 and 0.12. This was not the case for sensible heat and water vapour fluxes. At z/h = 0.42, where the air temperature inversion occurred, the magnitude of the ratio was smaller than

Table 3.4: Summary of the results of quadrant-hole analysis for sensible heat flux of the five runs in Table 3.3.

z/h	0.12	0.42	0.60	1.00	1.38
H'	5.7	5.2	4.6	3.5	3.7
$\sum_{i=1}^{4} t_{i,H'}$	0.064	0.067	0.080	0.107	0.110
$\frac{F_{2,0}+F_{4,0}}{F_{1,0}+F_{3,0}}$	-0.21	-0.23	-0.19	-0.13	-0.16
$\frac{F_{3,0}}{F_{1,0}}$	0.81	1.20	1.39	0.82	0.75

Table 3.5: Summary of the results of quadrant-hole analysis for water vapour flux of the five runs in Table 3.3.

z/h	0.12	0.42	0.60	1.00	1.38
H'	17.4	8.2	34.6	5.0	5.2
$\sum_{i=1}^{4} t_{i,H'}$	0.047	0.050	0.009	0.102	0.101
$\frac{F_{2,0}+F_{4,0}}{F_{1,0}+F_{3,0}}$	−0.67	−0.37	−0.71	−0.30	−0.30
$\frac{F_{3,0}}{F_{1,0}}$	0.87	1.15	1.50	1.09	1.03

one (0.23). This indicates that the transport of sensible heat at this height was of large scale and was no longer driven by the local temperature gradient.

Figure 3.10 shows the sensible heat flux fraction at different heights plotted against the hole size. Unlike the case for momentum flux, there was very little contribution from the interactions beyond $H = 6$. For example, $(F_{2,6} + F_{4,6})/(F_{1,6} + F_{3,6})$, the ratio of the contribution of the interactions to that of sweeps/ejections at $H = 6$, was –0.003 at z/h = 0.60 for sensible heat flux, while the corresponding ratio for momentum flux was much more negative, with a value of –0.124. This difference, together with the difference in the magnitude of the ratio $(F_{2,0}+F_{4,0})/(F_{1,0}+F_{3,0})$, indicates that the transfers of momentum and sensible heat are dissimilar due to different mechanisms and source distributions.

These results agree broadly with the observations made in other experimental studies in and immediately above vegetation canopies (Coppin *et al.* 1986, Gao *et al.* 1989, Maitani and Shaw 1990, Bergstrom and Hogstrom 1989), with some differences in the fine details. For example, the sweep dominated region for sensible heat flux for the stand in the present study was confined below the tree tops, while the sweep dominated region for a mixed deciduous forest reached as high as z/h = 1.9 (Maitani and Shaw 1990).

3.4 Summary and Conclusions

Results have been presented of the analysis of the daytime eddy fluxes of sensible heat and water vapour within and above a Douglas-fir stand under low soil water conditions. The sum of sensible and latent heat fluxes above the stand accounted for, on average, 83% of the available energy flux. But on some days, energy budget closure was far better than on others. The occurrences of large energy imbalance on several occasions are believed to be associated with the possible non-zero value of the vertical velocity measured at a single point and averaged over a short time interval under convective conditions.

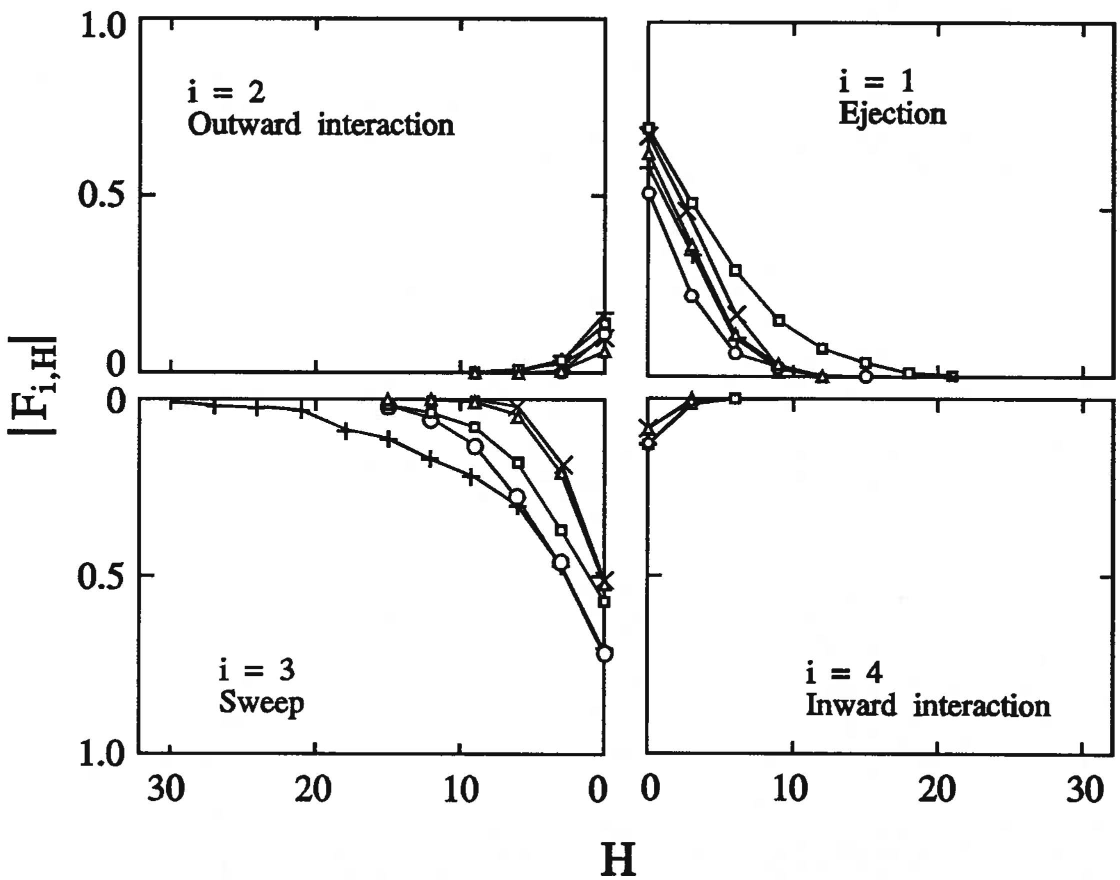

Figure 3.10: Flux fraction $F_{i,H}$ plotted against hole size H for sensible heat flux at z/h = 1.38 (×), 1.00 (△), 0.60 (o), 0.42 (+), and 0.12 (□).

The sum of sensible and latent heat fluxes beneath the overstory accounted for 74% of the available energy flux. One of the reasons for the energy imbalance was that the small number of soil heat flux plates and the short radiometer pathway of the tram system was unable to account for the large horizontal heterogeneity in the available energy flux beneath the overstory. The eddy flux of sensible heat, on the other hand, exhibited very little horizontal variation. Good agreement was obtained among the measurements of sensible heat flux made at $z/h = 0.12$ at four positions 15 m apart.

Sensible heat flux was the main output component of the energy budget both above and beneath the overstory. The average Bowen ratio had a value of 2.1 above the stand and 1.4 beneath the overstory. The mid-morning value of the canopy resistance was about 300 s/m in the early stage of the experiment and mid-day value of the Omega factor was about 0.20. The daytime mean canopy resistance showed a strong dependence on the mean vapour saturation deficit during the two-week experimental period.

The profiles of the eddy fluxes reflect source distributions. There was a constant flux layer in the trunk space, a large flux divergence in the canopy layer, and a constant flux layer above the stand. Counter-gradient flux of sensible heat constantly occurred at the base of the canopy ($z/h = 0.42$).

The transfer of sensible heat and water vapour was dominated by intermittent sweep and ejection events at all levels. The ratio of the sweep contribution to the ejection contribution was influenced to a large degree by the source distributions. For sensible heat flux, the ratio was greater than one in the canopy layer and less than one above the stand and near the forest floor.

3.5 References

Amiro, B.D.: 1990, 'Comparison of turbulence statistics within three Boreal forest canopies', *Boundary-Layer Meteorol.* **51,** 99-121.

Baldocchi, D.D. and Hutchison, B.A.: 1987, 'Turbulence in an almond orchard: Vertical variations in turbulence statistics', *Boundary-Layer Meteorol.* **40,** 127-146.

Baldocchi, D.D. and Meyers, T.P.: 1991, 'Trace gas exchange above the floor of a deciduous forest. I: Evaporation and CO_2 efflux', *J. Geophys. Res.* **96(D4),** 7271-7286.

Bergstrom, H. and Hogstrom, U.: 1989, 'Turbulent exchange above a pine forest. II: Organized structure', *Boundary-Layer Meteorol.* **49,** 231-264.

Black, A.T., Chen, J.M., Lee, X. and Sagar, R.M.: 1991, 'Characteristics of shortwave and longwave irradiances under a Douglas-fir stand', *Can. J. For. Res.* **21,** 1020-1028.

Cohen, Y., Kelliher, F.M. and Black, T.A.: 1985, 'Determination of sap flow in Douglas-fir trees using the heat pulse technique', *Can. J. For. Res.* **15,** 422-428.

Coppin, P.A., Raupach, M.R. and Legg, B.J.: 1986, 'Experiments on scalar dispersion within a model plant canopy. Part II: An elevated plane source', *Boundary-Layer Meteorol.* **35,** 167-191.

Deardorff, J.W.: 1973, 'Three-dimensional numerical modeling of the planetary boundary layer', in Haugen, D.A. (ed.), *Workshop on Micrometeorology*, American Meteorological Society, 271-311.

Denmead, O.T. and Bradley, E.F.: 1985, 'Flux-gradient relationships in a forest canopy', in Hutchison, B.A. and Hicks, B.B. (eds.), *The Forest-Atmospheric Interaction*, D. Reidel Publishing Co., Dordrecht, 421-442.

Finnigan, J.J.: 1979, 'Turbulence in waving wheat. Part II: Structure of momentum transfer', *Boundary-Layer Meteorol.* **16,** 213-236.

Fuchs, M. and Tanner, C.B.: 1968, ' Calibration and field test of soil heat flux plates', *Soil Sci. Soc. Am. Proc.* **32**, 326-328.

Gao, W., Shaw, R.H. and Paw U, K.T.: 1989, 'Observation of organized structure in turbulent flow within and above a forest canopy', *Boundary-Layer Meteorol.* **47,** 349-377.

Herrington, L.P.: 1969, 'On temperature and heat flow in tree stems', School of Forestry Bulletin No.73, Yale University.

Jarvis, P.G.: 1985, 'Transpiration and assimilation of tree and agricultural crops: The 'Omega factor", in Cannell, M.G.R. and Jackson, J.E. (eds.), *Attributes of Trees as Crop Plants*, I.T.E. (NERC), Monkswood Experimental Station, Abbots Ripton, Huntinghon, England, 460-480.

Jarvis, P.G., James, G.B. and Landsberg, J.J.: 1976, 'Coniferous forest', in Monteith, J.L. (ed.), *Vegetation and the Atmosphere II: Case Studies*, Academic Press, New York, 171-240.

Leclerc, M.Y.: 1987, 'Turbulence and turbulent diffusion inside and above vegetation', Ph.D. Thesis, University of Guelph, Guelph, Ontario.

Maitani, T. and Shaw, R.H.: 1990, 'Joint probability analysis of momentum and heat fluxes at a deciduous forest', *Boundary-Layer Meteorol.* **52,** 283-300.

Massman W J, Fox, D.G., Zeller, K.F. and Lukens, D.: 1990, 'Verifying eddy correlation measurements of dry deposition: A study of energy balance components of the

Pawnee Grasslands', USDA Forest Service, Research Paper RM-288, Fort Collins, U.S.A, 14pp.

McBean, G.A.: 1972, 'Instrument requirements for eddy correlation measurements', *J. Appl. Meteorol.* **11,** 1078-1084.

McCaughey, J.H.: 1985, 'Energy balance storage terms in a mixed forest at Petawawa, Ontario: A case study', *Boundary-Layer Meteorol.* **32,** 1-24.

McMillen, R.T.: 1988, 'An eddy correlation technique with extended applicability to non-simple terrain', *Boundary-Layer Meteorol.* **43,** 231-245.

McNaughton, K.G. and Black, T.A.: 1973, 'A study of evapotranspiration from a Douglas-fir forest using the energy balance approach', *Water Res. Res.* **9,** 1579-1590.

McNaughton, K.G. and Jarvis, P.G.: 1983, 'Predicting the effects of vegetation changes on transpiration and evaporation', in Kozlowski, T.T. (ed.), *Water Deficits and Plant Growth*, Academic Press, New York, 1-47.

Monteith, J.L.: 1965, 'Evaporation and environment', in Fogg, G.E. (ed.), *The State and Movement of Water in Living Organisms*, Academic Press, New York, 1-47.

Nnyamah, J. U. and Black, T.A.: 1990, 'Rate and patterns of water uptake in a Douglas-fir stand', *Soil Sci. Am. J.* **41,** 972-979.

Price, D.T. and Black, T.A.: 1991, 'Effects of summertime changes in weather and root-zone soil water storage on canopy CO_2 flux and evapotranspiration of two juvenile Douglas-fir stands', *Agric. For. Meteorol.* **53,** 303-323.

Price, D.T. and Black, T.A.: 1990, 'Effects of short-term variation in weather on diurnal canopy CO_2 flux and evapotranspiration of juvenile Douglas-fir stand', *Agric. For. Meteorol.* **50,** 139-158.

Raupach, M.R.: 1989, 'Stand overstory processes', *Phil. Trans. R. Soc. Lond.* **B324,** 175-190.

Raupach, M.R.: 1987, 'A Lagrangian analysis of scalar transfer in vegetation canopies', *Quart. J. R. Meteorol. Soc.* **113,** 107-120.

Shaw, R.H., Tavangar, J. and Ward, D.P.: 1983, 'Structure of Reynolds stress in a canopy layer', *J. Climate Appl. Meteorol.* **22,** 1922-1931.

Shuttleworth, W.J., Gash, J.H.C., LLoyd, C.R., Moore, C.J., Roberts, J., Filho, A.D.O.M., Fuchs, G., Filho, V.D.P.S., Molin, L.C.B., Abreu Sa, L.D.D., Nobre, J.C.A., Cabral, O.M.R., Patel, S.R. and Moraes, J.C.D.: 1984, 'Eddy correlation measurements of energy partition for Amazonian forest', *Quart. J. R. Meteorol. Soc.* **110,** 1143-1162.

Stewart, J.B. and Thom, A.S.: 1973, 'Energy budgets in pine forest', *Quart. J. R. Meteorol. Soc.* **99,** 154-170.

Tan, C.S. and Black, T.A.: 1976, 'Factors affecting the canopy resistance of a Douglas-fir forest', *Boundary-Layer Meteorol.* **10,** 475-488.

Tanner, C.B. and Thurtell, G.W.: 1969, 'Anemoclinometer measurements of Reynolds stress and heat transport in the atmospheric surface layer', Research and Development Technical Report ECOM-66-G22-F, University of Wisconsin, Madison, Wisconsin.

Thom, A.S.: 1972, 'Momentum, mass, and heat exchange of vegetation', *Quart. J. Roy. Meteorol. Soc.* **98**, 124-134.

Thom, A.S.: 1971, 'Momentum absorption by vegetation', *Quart. J. Roy. Meteorol. Soc.* **97**, 414-428.

Verma, S.B., Baldocchi, D.D., Anderson, D.D., Matt, D.R. and Clement, R. J.: 1986, 'Eddy fluxes of CO_2, water vapor, and sensible heat over a deciduous forest', *Boundary-Layer Meteorol.* **36**, 71-91.

Webb, E.K.: 1977, 'Convection mechanisms of atmospheric heat transfer from surface to global scales', in Bilger, R.W. (ed), *Second Australian Conference on Heat and Mass Transfer*, The University of Sydney, 523-539.

Webb, E.K., Pearman, G.I. and Leuning, R.: 1980, 'Correction of flux measurements for density effects due to heat and water vapour transfer', *Quart. J. R. Meteorol. Soc.* **106**, 85-100.

Chapter 4

Observation and Lagrangian Simulation of Air Temperature Profiles

4.1 Introduction

Many problems in agricultural and forest research require an understanding of the dispersion of atmospheric scalar constituents such as heat, water vapour, CO_2, trace gases, spores, pollen and other aerosols in vegetation canopies (e.g. Raupach *et al.* 1989a, Aylor 1989, Di-Giovanni and Kevan 1991). It is well known that K-theory is not adequate to describe the dispersion process in the canopy. In the search for alternatives, much attention has been focused on the simulation in a Lagrangian framework. Using the expression of Taylor (1921) for the second moments of concentration distribution in homogeneous turbulence, Raupach (1987) demonstrated the near-field effect of the canopy source on the concentration profiles of scalar quantities in a plant canopy and explained phenomena such as counter-gradient flux. Later, Raupach (1989b) developed a localized near-field theory which expresses the mean scalar concentration as the sum of diffusive far-field and non-diffusive near-field contributions. While these analytical models are relatively easy to use, the assumptions involved in the model development may limit their applications. Random flight models, on the other hand, can incorporate the inhomogeneity characteristic of the turbulent motion in the canopy environment. In these models, an ensemble of particle trajectories is constructed numerically from one or a set of stochastic differential equations which determine the evolution of the Lagrangian velocity of a marked fluid particle. Random flight models have been used for the dispersion of scalars in canopy environments from elevated line sources (Legg *et al.* 1986, Leclerc *et al.* 1988), from hypothetical elevated plane sources (Wilson *et al.* 1981b, Wilson *et al.* 1983) and from hypothetical canopy sources (Raupach 1989b). However, there have been fewer studies performed to simulate the dispersion processes related to outdoor extensive canopy sources/sinks.

An experiment to study the exchange processes within and above an extensive coniferous stand of Douglas-fir trees was described in Chapters 2 and 3. The experiment provides a data set for testing and further development of the Lagrangian theory of scalar dispersion in the canopy environment. Accordingly, the specific objectives of this chapter are (1) to examine the profiles of air temperature in relation to the sensible heat source/sink distributions in the stand, (2) to simulate the profile of air temperature using a random flight model, and (3) to discuss the applicability of K-theory near the forest floor.

4.2 Experimental Methods

Details of the experimental methods can be found in Chapter 2 and Chapter 3. The following is a brief summary of the information relevant to this Chapter.

4.2.1 Site Description

The experimental site was located near Browns River approximately 10 km northwest of Courtenay on Vancouver Island, 125°10′W, 49°42′N. The overstory species is Douglas-fir, planted in 1962. In 1988, it was thinned to a density of 575 stems/ha and pruned uniformly to a height of approximately 6 m. The height of the stand was 16.7 m, and the total (projected) leaf area was 5.4. The forest floor was littered with dead branches and trunks, with a sparse understory vegetation less than 0.5 m tall.

The experiment was conducted in late July and early August 1990. The weather remained mostly clear during the experimental period. There was water stress of the trees as indicated by yellowing of the needles. Sensible heat flux was the main output component of the energy budget, with daytime average values of 230 W/m^2 above the stand and 45 W/m^2 beneath the overstory, and the daytime Bowen ratio of the stand varied from 1.3 to 2.7 during the course of the experiment (Chapter 3).

4.2.2 Instrumentation

Eddy flux of sensible heat and other turbulence statistics were measured in the daytime with two eddy correlation units mounted on an open lattice 25 cm wide triangular tower. One unit was operated permanently at a height of 23.0 m (z/h = 1.38), and the other unit at various heights within the stand, with 2-3 eight hour periods at each height. Air temperature and wind speed was measured continuously during the experimental period with fine wire thermocouples and sensitive cup anemometers, respectively, at heights of (z/h in brackets) 0.9 (0.05), 2.0 (0.12), 4.6 (0.28), 7.0 (0.42), 10.0 (0.60), 12.7 (0.76), 16.7 (1.00), and 23.0 m (1.38). This Chapter focuses on the measurements made on 19, 20 and 26 July, when the lower eddy correlation unit was operated at a height of 2.0 m (z/h = 0.12).

4.3 The Model

4.3.1 Construction of Trajectories

The dispersion of sensible heat can be represented by the random walk of 'hot' fluid particles. Consider the dispersion in only the vertical direction, with w_n representing the Lagrangian vertical velocity of a marked 'hot' particle at time t_n. Horizontally, the particle moves at the Eulerian streamwise velocity u. Neglecting dispersion in the horizontal direction will cause only a small error (Raupach 1989b). The particle position evolves according to the following equations

$$\left.\begin{aligned} z_{n+1} &= z_n + w_n \Delta t_n \\ x_{n+1} &= x_n + u(z_n)\Delta t_n \end{aligned}\right\} \qquad n = 1, 2, ... \tag{4.1}$$

where Δt_n is the time step at time t_n, and x_n and z_n are the horizontal and vertical components of the position vector at time t_n, with (x_1, z_1) being the position of the particle at release. The sequence $\{w_n\}$ is Markovian, and can be formed as

$$w_{n+1} = a w_n + b \sigma_w(z_n) \xi_{n+1} + c \qquad n = 1, 2, ... \tag{4.2}$$

where ξ_n is a random number from a Gaussian distribution with zero mean and unit variance, $\sigma_w(z_n)$ is the square root of the variance of the Lagrangian vertical velocity at height z_n, and a, b, and c are coefficients specified as

$$\left.\begin{aligned} a &= e^{-\Delta t_n / T_L(z_n)} \\ b &= (1 - a^2)^{1/2} \\ c &= f(z_n) T_L(z_n)(1 - a) \end{aligned}\right\} \tag{4.3}$$

with $f(z_n)$ being the gradient of the variance of the Eulerian vertical velocity at height z_n

$$f(z_n) = \frac{\partial \overline{w_E'^2}}{\partial z}\Big|_{z=z_n}$$

and $T_L(z_n)$ being the Lagrangian integral time scale at height z_n (Legg and Raupach 1982). The third term on the RHS of (4.2) accounts for the effect of the mean force on the marked particle due to the action of the mean pressure gradient. In the neutral surface layer, it is negligible. But it cannot be neglected in the vegetation canopy where there is always a significant vertical gradient in $\overline{w_E'^2}$. A positive mean vertical velocity of the particle, called biased velocity (Wilson *et al.* 1981b) or drift velocity (Legg and Raupach 1982), arises from this term. For the special case of constant T_L and f, an analytical solution has been derived, based on the differential form of (4.2), for air temperature and vertical sensible heat flux from an elementary point source (Appendix D), which can then be superposed to obtain the solutions for the plane and canopy sources. In general, however, air temperature and vertical heat flux can only be obtained using the random flight technique.

Before the construction of the particle trajectory, a set of 2000 Gaussian pseudo-random numbers with zero mean and unit variance are generated using

$$\xi_i = (-2 \ln u_i)^{1/2} \cos(2\pi u_{2i}) \qquad i = 1\text{–}2000$$

where $\{u_i\}$ is a set of uniform pseudo-random numbers in the range 0 to 1 (Abramowitz and Stegun 1964, pp 949-953). For each step of the flight, a Gaussian number is randomly drawn from the set $\{\xi_i\}$. The initial vertical velocity is given by

$$w_1 = \sigma_w(z_1)\xi_1$$

As a common practice, the Lagrangian velocity variance, σ_w^2 is assumed to be equal to the Eulerian velocity variance, $\overline{w_E'^2}$ at all positions (e.g. Wilson *et al.* 1981a). The time step is chosen as

$$\Delta t_n = 0.2 T_L(z_n)$$

The ground surface is treated as being reflective.

4.3.2 Simulation of Air Temperature and Vertical Sensible Heat Flux

For steady state conditions in an extensive horizontally homogeneous canopy (advection-free) specified by a sensible heat source density $S(z)$ with dimensions of W/m^3, the conservation of sensible heat requires (Raupach 1989b)

$$dH(z)/dz = S(z) \tag{4.4}$$

where H is the vertical sensible heat flux (with dimensions of W/m^2). Integration of (4.4) with respect to z gives

$$H(z) = H_g + \int_0^z S(z')dz' \tag{4.5}$$

where H_g is the sensible heat flux from the ground-level source. Equations of the form of (4.4) and (4.5) also apply to scalars other than sensible heat. For an extensive forest stand with a trunk space relatively free of branches and needles, or sources/sinks, the flux profiles of scalars typically exhibit a constant flux layer in the trunk space, a large flux divergence in the canopy layer and a constant flux layer above the stand (Chapter 3, Denmead and Bradley 1985, Denmead and Bradley 1989). This feature is consistent with (4.5). The total flux above the stand or the total source density of the stand can be expressed as

$$H_T = H_g + \int_0^h S(z')dz' \tag{4.6}$$

where h is the height of the stand (h = 16.7 m in the present study).

Potential air temperature, θ is separated into two parts, the contribution from the canopy source (θ_c) and the contribution from the ground-level source (θ_g), as

$$\theta(z) = \theta_c(z) + \theta_g(z)$$

The simulation technique for θ_c is that of Raupach (1989b). In the simulation, M particles (M = 2000 in the present study) are released at the leading edge ($x = 0$) of the canopy source. The initial height, z_1 of particle m is chosen from a distribution with the shape of $S(z)$. The particle moves according to (4.1) and (4.2) until it reaches the streamwise position $x = x_p$ ('horizontal fetch'). It can be shown that the potential temperature and the vertical heat flux at $x = x_p$ are

$$\theta_c(z) = \frac{H_T - H_g}{\rho c_p u(z)} \frac{1}{M\Delta z} \sum_{m=1}^{M} < X_m > (z, z + \Delta z)$$

and

$$H'(z) = H_g + (H_T - H_g)\frac{M\mathrm{cross}(z)}{M}$$

respectively, where $< X_m > (z, z + \Delta z)$ is the total streamwise distance traversed by particle m while it lies between height z and $z + \Delta z$ and $M_{\mathrm{cross}}(z)$ is the net number of particles that cross height z between $x = 0$ and $x = x_p$. As the fetch x_p increases, H'(z) converges to $H(z)$.

The simulation technique for θ_g is based on the assumption that the dispersion from the ground-level source is basically diffusive (Hunt and Weber 1979, Raupach 1983), thus

$$H_g = -\rho c_p K_f \frac{\partial \theta_g(z)}{\partial z} \tag{4.7}$$

where K_f is a far-field eddy diffusivity expressed as (Raupach 1989b)

$$K_f = \sigma_w^2(z) T_L(z) \tag{4.8}$$

Integrating (4.7) and using (4.8), θ_g is found to be

$$\theta_g(z) - \theta_g(z_r) = \int_z^{z_r} \frac{H_g}{\rho c_p \sigma_w^2(z') T_L(z')} dz'$$

where z_r is a reference height (z_r = 23.0 m in the present study).

The source density of sensible heat in the canopy, S was estimated from the measured profiles of leaf area density and sensible heat flux. According to the measurements reported in Chapter 3, of the total source density of the canopy, 54% was from the layer between z/h = 0.60 and 1.00 and 46% was from the layer below z/h = 0.60. These percentages were further partitioned into values as a function of height assuming that the source density was proportional to the measured leaf area density. The S profile obtained in this manner is well represented by a beta function as follows

$$S(z) = \begin{cases} 6.9(\frac{z-5.5}{h-5.5})^{0.80}(1-\frac{z-5.5}{h-5.5})^{1.44} & 5.5 \le z \le h \\ \\ 0 & z < 5.5 \quad \text{and} \quad z > h \end{cases} \tag{4.9}$$

where z is in metres and the height of the stand is h = 16.7 m.

The velocity field is specified by

$$u(z)/u(z_r) = \begin{cases} \ln\dfrac{z-11.7}{0.21} \Big/ \ln\dfrac{z_r-11.7}{0.21} & z > h \\ \\ 0.8\sinh(3.5\dfrac{z}{h})/\sinh 3.5 + 1.7(\dfrac{z}{h})^{0.5}(1-\dfrac{z}{h})^{3.6} & z \leq h \end{cases} \tag{4.10}$$

$$\sigma_w(z)/\sigma_w(z_r) = \begin{cases} 1 & z > h \\ \\ (\dfrac{z}{h})^{0.5} & z \leq h \end{cases} \tag{4.11}$$

and

$$T_L(z) = \begin{cases} 0.43\dfrac{z}{\sigma_w(z_r)} & z > h \\ \\ 0.43\dfrac{h}{\sigma_w(z_r)} & 0 < z \leq h \end{cases} \tag{4.12}$$

where the reference height z_r was 23.0 m. Equation (4.10) fits well with the measured wind speed profile in the Douglas-fir stand presented in Chapter 2. Equation (4.11) is based on the fact that the variance of the vertical velocity component was approximately linear with height (Chapter 2). The Lagrangian time scale has the same form as that used by Leclerc *et al.* (1988), with the value of the constant adjusted slightly to obtain good predictions for sensible heat flux from the forest floor. Experimental evidence appears to support the use of constant T_L within the stand (Legg *et al.* 1986, Leclerc *et al.* 1988). It follows from (4.11) and (4.12) that K_f increases linearly with height. Figure 4.1 shows the plots of (4.9–4.12).

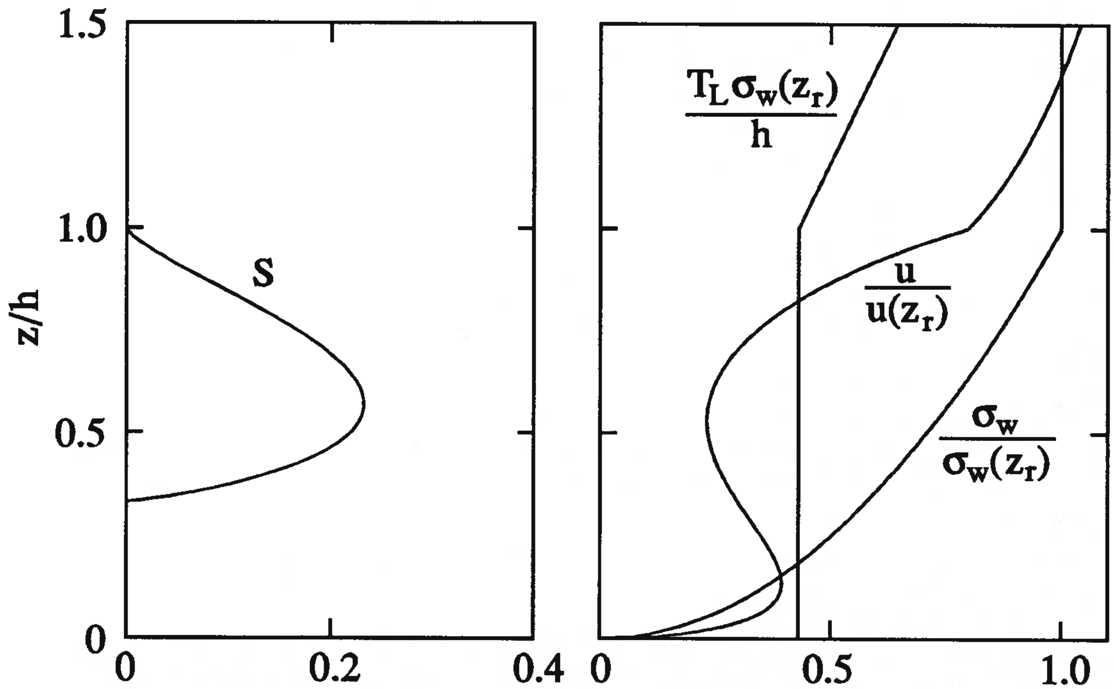

Figure 4.1: Profiles of $S(z)$, $u(z)$, $\sigma_w(z)$ and $T_L(z)$ used as model inputs. See Equations (4.9–4.12) for analytical forms.

4.4 Results and Discussion

4.4.1 Observation of Air Temperature Profiles

4.4.1.1 Diurnal Changes in the Air Temperature Profile

In the context of Lagrangian theories, potential temperature θ in a vegetation canopy is determined by the combination of the sensible heat source/sink density distribution S and the statistics of the velocity field. The effect of S on θ can be examined qualitatively without the precise knowledge of the velocity field. The stand in the present study consisted of two distinct sensible heat sources/sinks separated by a trunk space of approximately 6 m in height: the ground-level forest floor source/sink (including some sparse short understory) and the elevated canopy source/sink. At night, the canopy was a sensible heat sink due to the radiative cooling of the foliage, and the forest floor was either a sensible heat source or sink depending on whether or not the heat flux from the soil exceeded the net radiation flux from the forest floor. In the daytime, both the canopy and the forest floor were sensible heat sources.

Figure 4.2 shows the diurnal change in the θ profile observed on 26 July. Before sunrise, the net radiation flux at z/h = 1.38 was very small in magnitude, with an average value of -5 W/m^2 for the period between 00:00 and 05:00 PST. This was because there was complete cloud cover during this period. Consequently, the magnitude of S was small, and so θ at 00:00 and 03:00 PST showed only a little change with height. The ground was probably acting as a heat source during this period, resulting in a small negative θ gradient near the forest floor.

After sunrise, both the canopy and the forest floor acted as sensible heat sources. The daytime θ profile during the experimental period always exhibited a negative gradient in the layer between z/h = 0.05 and 0.28, a positive gradient (inversion) in the layer

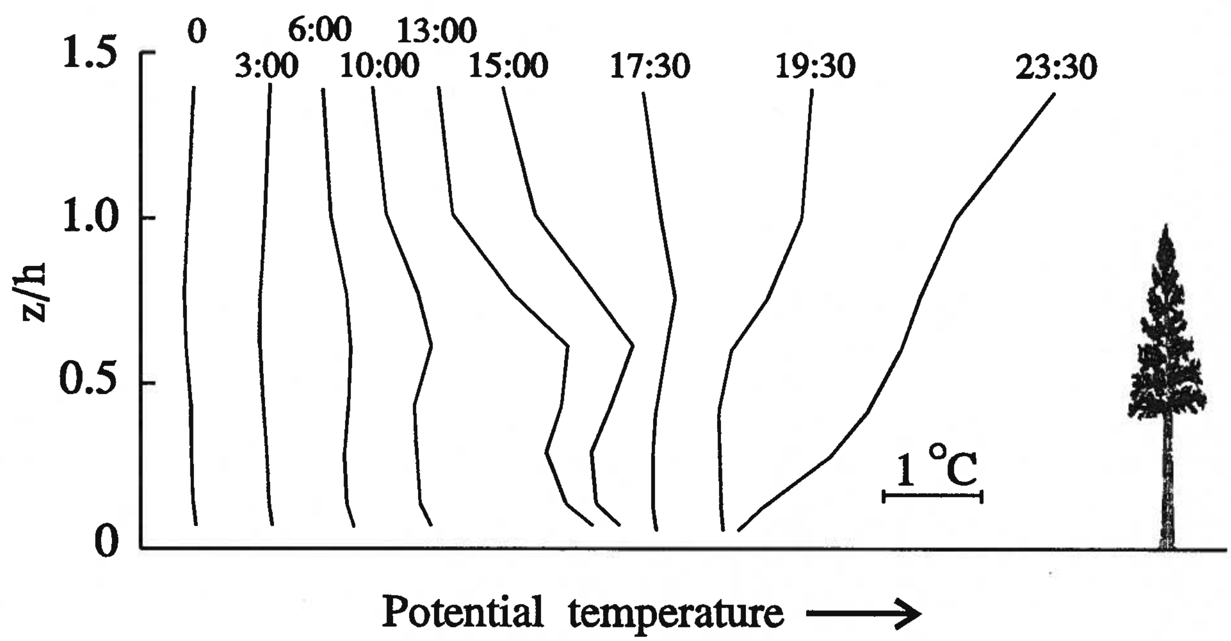

Figure 4.2: Diurnal change in the profile of the 30-minute averaged potential temperature observed in the Douglas-fir stand at Browns River on 26 July 1990. The time shown above the profiles marks the end of each 30-minute run.

between z/h = 0.28 and 0.60, and a peak at z/h = 0.60 where the leaf area density was highest (Chapter 2). The peak of the potential temperature can be viewed as a result of the near-field effect of the canopy sensible heat source. On 26 July, the inversion was strongest between 12:30 and 15:00 PST.

The sky was clear in the evening of 26 July, with an average value of -65 W/m^2 for the net radiation flux at z/h = 1.38 for the period between 20:00 and 24:00 PST. The intensive radiative cooling caused the canopy as well as the forest floor to be strong sensible heat sinks. The θ profile at 23:30 PST showed the typical features under clear sky conditions at night: θ decreasing rapidly and monotonically with depth into the stand.

4.4.1.2 Normalization of Air Temperature Profiles

The measured sensible heat flux can be used to reveal further the effect of the source density distribution on the θ profile. There were simultaneous measurements of H_g (at z/h = 0.12) and H_T (at z/h = 1.38) in the daytime of 19, 20 and 26 July. According to (4.6), the ratio H_g/H_T, hereafter called relative source density, is the density of the ground-level source normalized against the total source density of the stand, while $(1 - H_g/H_T)$ is the relative density of the canopy source. It has been found that the potential temperature difference, $\Delta\theta(z) = \theta(z) - \theta(z_r)$, where $\theta(z_r)$ is the potential temperature at height z_r, can be normalized by a characteristic potential temperature θ_* defined as

$$\theta_* = \frac{H_T}{\rho c_p \sigma_w(z_r)}$$

Figure 4.3 plots $\Delta\theta/\theta_*$ against H_g/H_T for three measurement levels, two in the trunk space (z/h= 0.05 and 0.28) and one in the canopy layer (z/h= 0.60). It can be seen that most of the variation in $\Delta\theta/\theta_*$ resulted from the variation in H_g/H_T, with the correlation coefficient of 0.63 at z/h = 0.60, 0.82 at z/h = 0.28 and 0.83 at z/h = 0.05, for 36 runs.

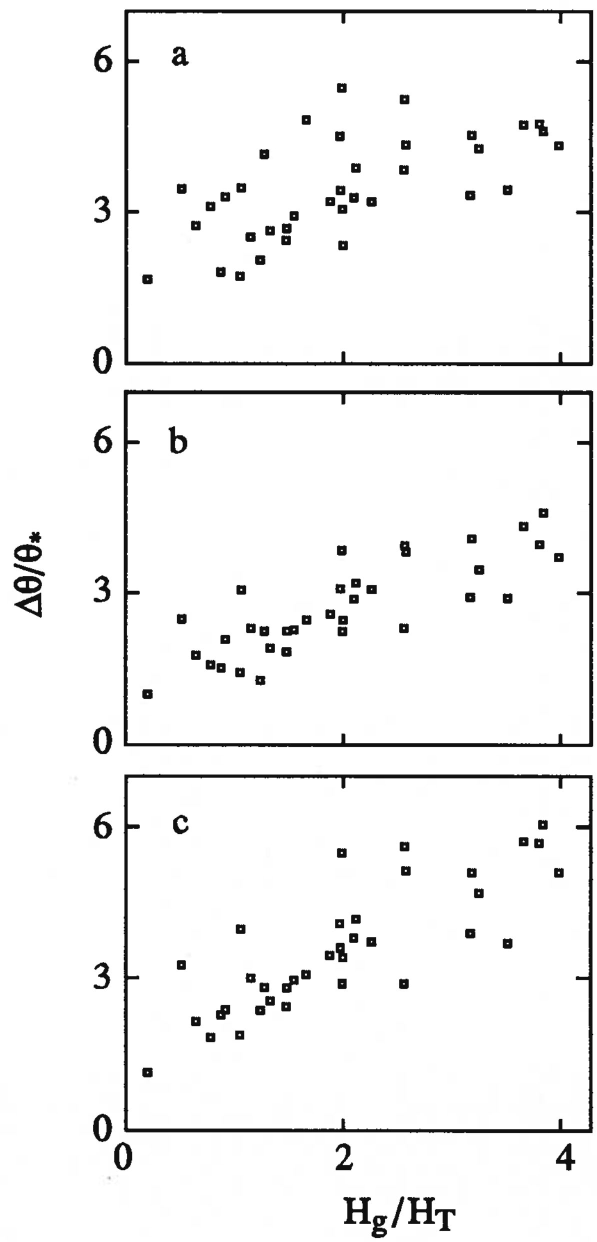

Figure 4.3: Dimensionless daytime potential temperature, $\Delta\theta/\theta_*$ versus relative source density, H_g/H_T in the Douglas-fir stand at Browns River measured on 19, 20 and 26 July 1990: (a), z/h = 0.60; (b), z/h = 0.28; (c), z/h = 0.05.

Good correlations also existed at other heights within the stand. The variation in $\Delta\theta/\theta_*$ for the runs of similar H_g/H_T can be interpreted as the result of the difference in the velocity field among the runs. But this variation was much smaller than the variation due to the change in the relative source density. In other words, the source density distribution was the primary factor influencing the potential temperature profile, while the statistics of the velocity field were secondary factors. Figure 4.3 also shows that θ_* was a temperature scale that collapsed the temperature profiles of similar relative source density reasonably well onto a single line.

Figure 4.4 shows the profiles of $\Delta\theta/\theta_*$ averaged for four ranges of H_g/H_T. The four profiles share some common features, namely a peak at z/h = 0.60 and an inversion in the layer between z/h = 0.28 and 0.60. The profile shifted to higher values of $\Delta\theta/\theta_*$ as H_g/H_T increased, which is most evident below z/h = 0.60. It can also be seen that the gradient in $\Delta\theta/\theta_*$ in the trunk space increased with increasing H_g/H_T. Daytime sensible heat flux was directed upward at all heights within the stand, indicating occurrence of counter-gradient flux in the inversion layer (Chapter 3).

4.4.2 Simulation Results

4.4.2.1 Validation of the Numerical Scheme

To test the numerical scheme of the random flight technique, air temperature and vertical sensible heat flux were simulated for the downwind edge of a 100 m long elevated plane source placed in homogeneous turbulence and were compared with those obtained by superposing the exact solutions of Taylor (1921) for a large number of elementary line sources. The velocity field was specified as

$$u = 1\,\mathrm{m/s}$$

$$\sigma_w = 0.25\,\mathrm{m/s}$$

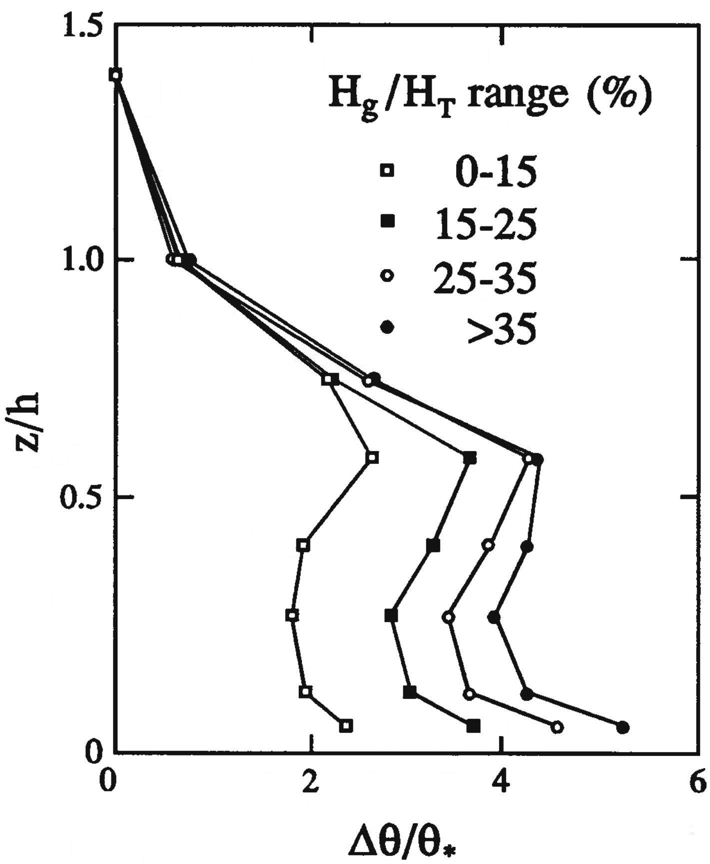

Figure 4.4: Profiles of the dimensionless daytime potential temperature, $\Delta\theta/\theta_*$ averaged over the four ranges of relative source density, H_g/H_T in the Douglas-fir stand at Browns River. The measurements were made on 19, 20 and 26 July 1990.

and

$$T_L = 1 \text{ s}$$

The kinematic heat flux from the plane source was specified as

$$\frac{H_T}{\rho c_p} = 1 \text{ °C m/s}$$

The agreement between the numerical scheme and the analytical solutions is excellent, both for the temperature and the vertical sensible heat flux (Figure 4.5).

4.4.2.2 Simulation of the Potential Temperature in the Stand

Figure 4.6 shows the comparison of the profile of the potential temperature simulated for $H_g/H_T = 0.2$ with the observed profile averaged over the runs with $0.15 < H_g/H_T < 0.25$. In the simulation, the wind speed and the square root of the vertical velocity variance at the reference height were $u(z_r) = 2.0$ m/s and $\sigma_w(z_r) = 0.6$ m/s, corresponding to the measured values averaged over the above runs. The fetch was $x_p = 960$ m. There was some random noise in the simulated profile, but overall the agreement between the simulated and the measured profiles was satisfactory. The simulated vertical flux was very close to that calculated from (4.5) and (4.9) for advection-free conditions (Figure 4.7), indicating that a fetch of 960 m was sufficient to minimize the effect of horizontal advection. There was a sharp decrease in θ_c with height near the ground. This shows the wall effect: Once a particle wanders into the layer very close to the ground, it has the tendency to stay there because of the very small velocity variance. The accumulation of 'hot' fluid particles in this layer resulted in the high air temperature. A similar pattern was also reported by Wilson *et al.* (1983) for a hypothetical plane source placed at the top of a corn canopy. Unlike their study, the wall effect in the present study was confined to a very thin layer of approximately 0.5 m or 0.03h.

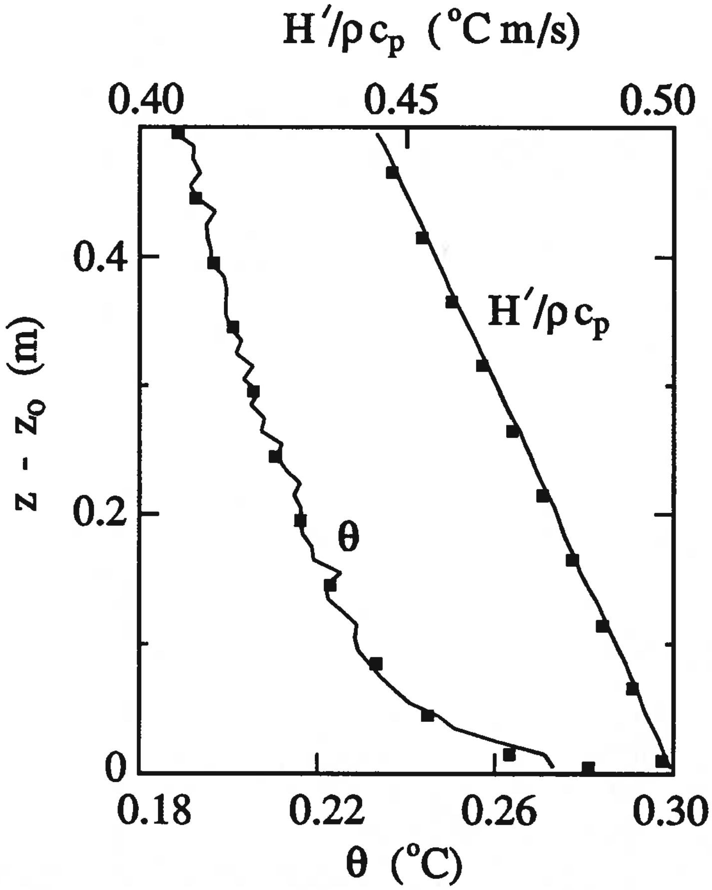

Figure 4.5: Comparison of air temperature, θ and vertical kinematic heat flux, $H'/\rho c_p$ simulated using the random flight technique (lines) with those obtained from the analytical solutions of Taylor (1921) (squares) at the downwind edge of a 100 m long plane source placed at height z_o in homogeneous turbulence.

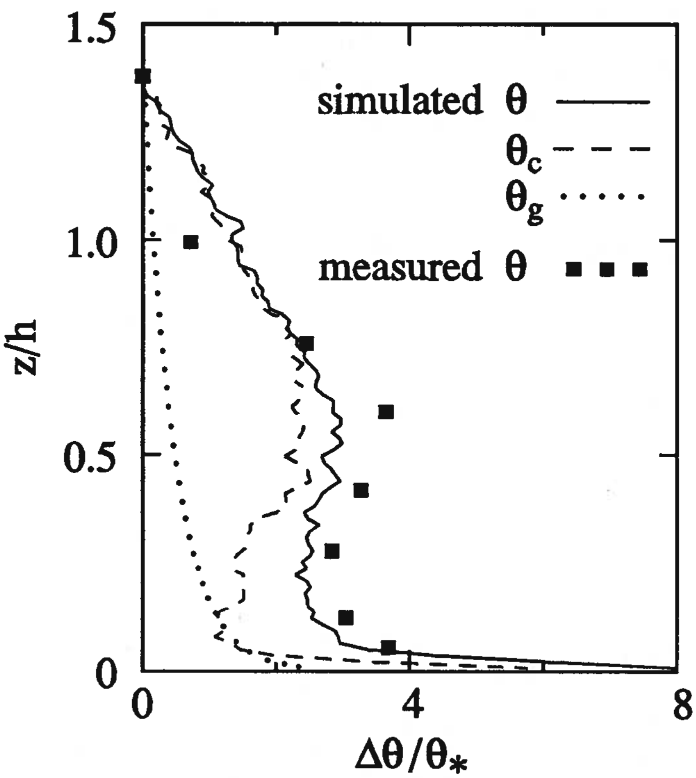

Figure 4.6: Comparison of the profile of the potential temperature simulated for $H_g/H_T = 0.2$ with the observed profile averaged over the the runs with H_g/H_T in the range 0.15–0.25 in the Douglas-fir stand at Browns River.

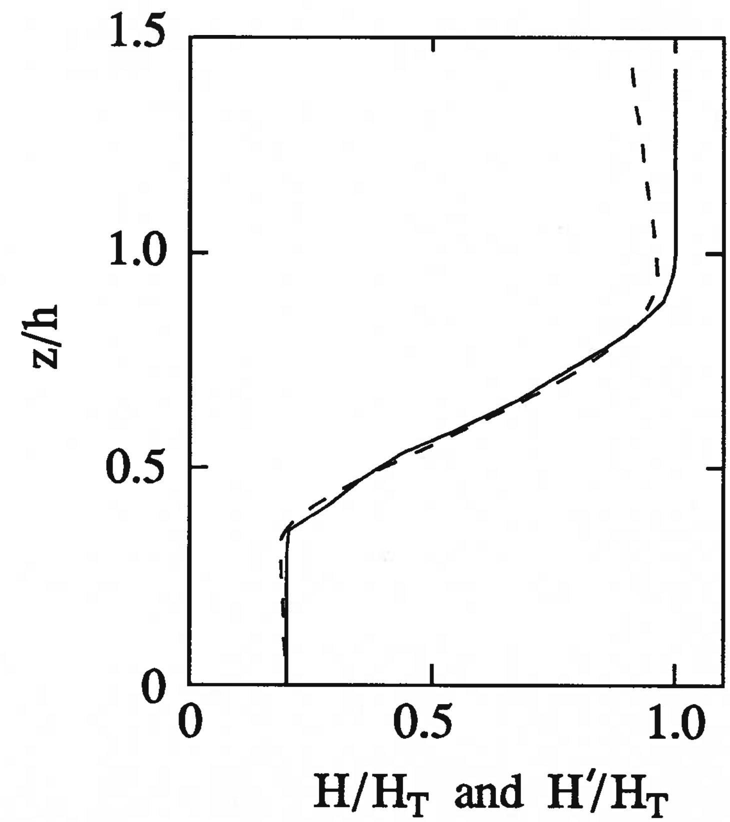

Figure 4.7: Comparison of normalized vertical heat flux simulated using the random flight technique with a fetch $x_p = 960$ m (H'/H_T, dash line) with that calculated from Equations (4.5) and (4.9) for advection-free conditions (H/H_T, solid line).

It is a common practice to treat sensible heat as a passive scalar in random flight simulations of sensible heat dispersion. In other words, it is assumed that the dispersion of sensible heat does not modify the velocity field. For an isolated line source, this is true. For an extensive plane or canopy source, however, sensible heat is not a completely passive scalar, since the extensive source will result in the stratification of air temperature. The stratification, in turn, will affect the movement of the air (including the marked fluid particles). It is possible that the results of the simulation can be improved by taking into account the effect of the source-induced buoyancy.

4.4.2.3 Test of the Effect of the Wind Speed Profile

In a forest stand with a trunk space relatively free of branches and needles, wind speed typically exhibits a maximum in the trunk space and a minimum in the canopy layer (e.g. Shaw 1977, Chapter 2). In contrast, wind speed in agricultural plant canopies or artificial canopies in wind tunnels usually decreases monotonically with depth (e.g. Wilson *et al.* 1982, Seginer *et al.* 1976). Numerical tests suggest that velocity skewness has only a small effect on the dispersion of passive scalars (Legg 1983, Raupach 1989b). Yet it is unclear how sensitive simulated results are to the wind speed profile. To test the effect of the wind speed profile, simulations were performed using the profile within the stand described by (4.10) as well as the profile described by

$$u(z)/u(z_r) = 0.8z/h \qquad z \leq h \tag{4.13}$$

which satisfies the boundary conditions but does not accurately match the actual profile. Other input parameters remained the same as in the previous section.

Figure 4.8 shows the comparison of the simulated results for three fetches. It can be seen that the two sets of profiles are similar in magnitude and in shape, with slight differences in the layer $0.05 < z/h < 0.35$, where the actual wind speed was much higher

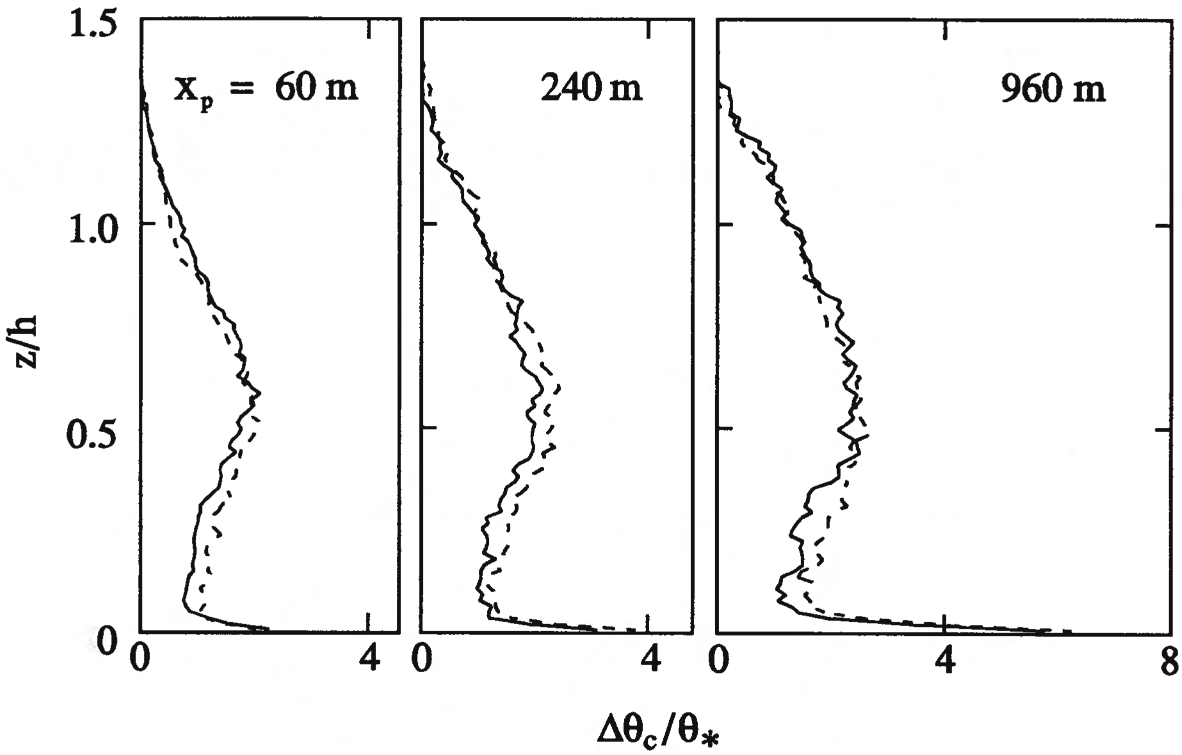

Figure 4.8: The effect of the wind speed profile on the simulation of potential temperature resulting from the canopy sensible heat source for three fetches (x_p): (—) wind speed within the stand defined by Equation (4.10); (- - - -) wind speed within the stand defined by Equation (4.13). Other parameters are the same as in Figure 4.6

than that described by (4.13) because of the existence of the secondary maximum. This suggests that the wind speed profile is not critical in the simulation. For the purpose of Lagrangian simulation, efforts should therefore be directed toward a better understanding of the velocity variance and Lagrangian time scale of the velocity field.

4.4.2.4 Flux-Gradient Relationships near the Forest Floor

Theoretically, the ground-level flux (including the contribution from the short understory vegetation) can be calculated from K-theory expressed by (4.7) and (4.8). In reality, however, only θ instead of θ_g can be measured. If the separation between the overstory canopy and the ground is large, as in the present study, it may be hypothesized that the gradient in θ_g in the layer close to the ground is well approximated by the gradient in θ or that the overstory canopy does not contribute much to the gradient in θ. If this were the case, this simple model, which requires only the measurements of θ and σ_w near the ground and an estimate of T_L as the inputs, would be applicable. Furthermore, this hypothesis would support the application of the aerodynamic approach, although not valid at higher levels in a forest stand, to the exchange between the forest floor (with its understory) and the adjacent air layer (Black and Kelliher 1989, Raupach 1989a).

Figure 4.9 shows the comparison of H_g calculated using (4.7) and (4.8), with θ substituted for θ_g, and H_g measured at z/h = 0.12. In the calculation, the potential temperature measured at z/h = 0.05 and 0.28 was used to compute $\partial\theta/\partial z$. Although some random noise is evident in the simulated profile of θ_c (Figure 4.6), it appears that θ_c does not vary much with height in the layer $0.05 < z/h < 0.28$. This suggests that $\partial\theta/\partial z$ is a good approximation for $\partial\theta_g/\partial z$ in this layer. The vertical velocity variance was measured at z/h = 0.12. The estimate of the Lagrangian time scale, T_L was based on (4.12), using the measurements of the vertical velocity variance at the reference height z_r (z/h = 1.38). Although the model for T_L was rather primitive, the modelled and the measured fluxes

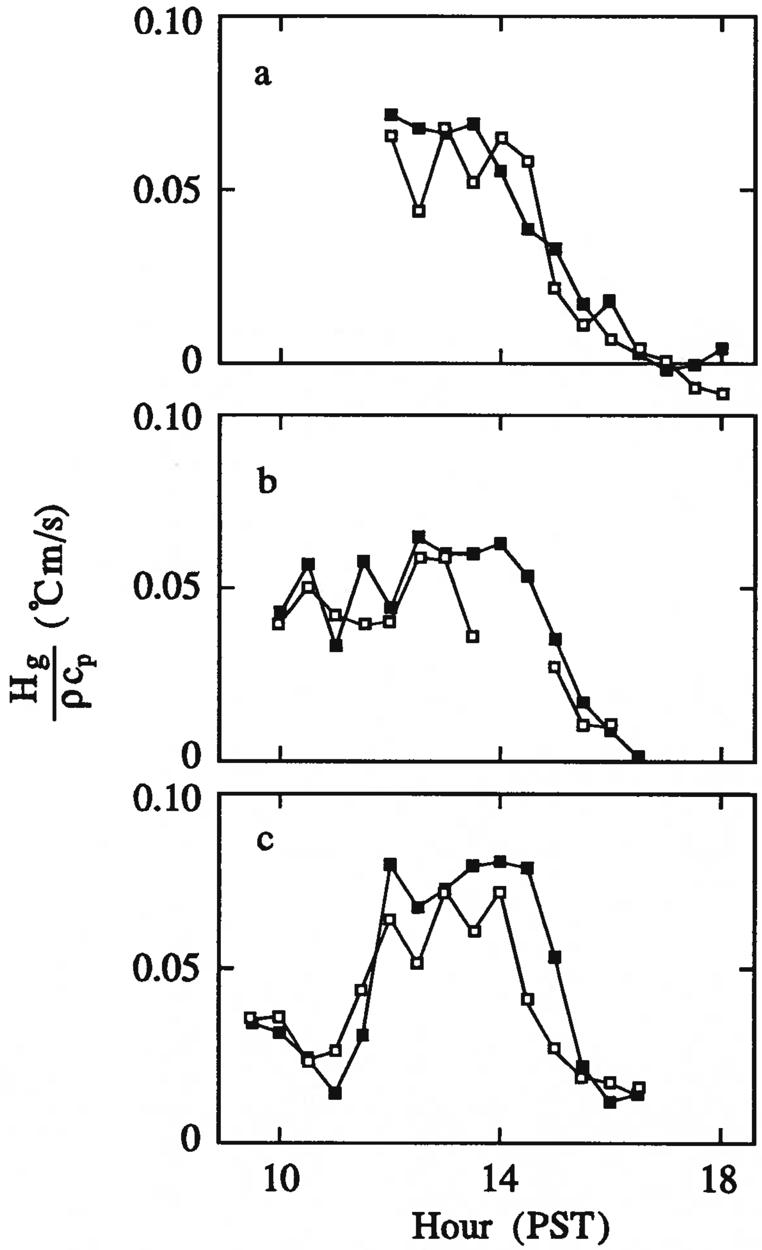

Figure 4.9: Comparison of modelled (□) kinematic sensible heat flux, $H_g/(\rho c_p)$ with that measured (■) at z/h = 0.12 in the Douglas-fir stand at Browns River on (a) 19, (b) 20, and (c) 26 July 1990.

showed good agreement.

4.5 Summary and Conclusions

The profile of potential temperature in the Douglas-fir stand was influenced to a great extent by the distribution of sensible heat source/sink density. The daytime profile always exhibited an inversion in the layer between the middle of the trunk space (z/h = 0.28) and the middle of the canopy (z/h = 0.60), and a peak in the middle of the canopy as a result of the near-field effect of the canopy sensible heat source. The daytime profiles of the dimensionless potential temperature, $\Delta\theta/\theta_*$ were found to be well stratified by the relative source density, H_g/H_T. As H_g/H_T increased, the profile of $\Delta\theta/\theta_*$ shifted to higher values.

The daytime profile of $\Delta\theta/\theta_*$ was simulated by adding the contribution from the canopy source, calculated using the random flight technique, and that from the ground-level source, calculated from gradient-diffusion theory with a far-field eddy diffusivity. The simulated profile appeared to agree reasonably well with the measured one. The simulated results suggested that the profile of $\Delta\theta/\theta_*$ was not sensitive to the shape of the wind speed profile. There was good agreement between the sensible heat flux from the forest floor calculated using the gradient-diffusion theory and that measured near the ground (z/h = 0.12). This supports the application of the aerodynamic approach to the exchange process between the forest floor and the adjacent air layer.

4.6 References

Abramowitz, M. and Stegun, I.A.: 1964, *Handbook of Mathematical Functions with Formulas, Graphs, and Mathematical Tables*, United States Department of Commerce, U.S. Government Printing Office, Washington, D.C.

Aylor, D.E.: 1989, 'Aerial spore dispersal close to a focus of disease', *Agric. Forest Meteorol.* **47,** 109-122.

Black, T.A. and Kelliher, F.M.: 1989, 'Processes controlling understory evapotranspiration', *Phil. Trans. R. Soc. Lond.* **B324,** 207-231.

Denmead, O.T. and Bradley, E.F.: 1985, 'Flux-gradient relationships in a forest canopy', in Hutchison, B.A. and Hicks, B.B. (eds.), *The Forest-Atmospheric Interaction*, D. Reidel Publishing Co., Dordrecht, 421-442.

Denmead, O.T. and Bradley E. F.: 1989, 'Eddy-correlation measurement of the CO_2 flux in plant canopies', in *Heat and Mass Transfer '90, Fourth Australian Conference on Heat and Mass Transfer*, University of Canterbury, Christchurch, New Zealand, 183-191.

Di-Giovanni, F. and Kevan, P.G.: 1991, 'Factors affecting pollen dynamics and its importance to pollen contamination: a review', *Can. J. For. Res.* **21,** 1155-1170.

Hunt, J.C.R. and Weber, A.H.: 1979, 'A Lagrangian statistical analysis of diffusion from a ground-level source in a turbulent boundary layer', *Q. J. R. Meteorol. Soc.* **105,** 423-443.

Leclerc, M.Y., Thurtell, G.W. and Kidd, G.E.: 1988, 'Measurements and Langevin simulations of mean tracer concentration fields downwind from a circular line source inside an alfalfa canopy', *Boundary-Layer Meteorol.* **43,** 287-308.

Legg, B.J. and Raupach, M.R.: 1982, 'Markov-chain simulation of particle dispersion in inhomogeneous flows: The mean drift velocity induced by a gradient in Eulerian velocity variance', *Boundary-Layer Meteorol.* **24,** 3-13.

Legg, B.J., Raupach, M.R. and Coppin, P.A.: 1986, 'Experiments on scalar dispersion within a plant canopy. Part III: An elevated line source', *Boundary-Layer Meteorol.* **35,** 277-302.

Raupach, M.R.: 1989a, 'Stand overstory processes', *Phil. Trans. R. Soc. Lond.* **B324,** 175-190.

Raupach, M.R.: 1989b, 'A practical Lagrangian method for relating scalar concentrations to source distributions in vegetation canopies', *Q. J. R. Meteorol. Soc.* **115,** 609-632.

Raupach, M.R.: 1987, 'A Lagrangian analysis of scalar transfer in vegetation canopies', *Quart. J. R. Meteorol. Soc.* **113,** 107-120.

Raupach, M.R.: 1983, 'Near field diffusion from instantaneous sources in the surface layer', *Boundary-Layer Meteorol.* **27,** 105-113.

Seginer, I., Mulhearn, P.J., Bradley, E.F. and Finnigan, J.J.: 1976, 'Turbulent flow in a model plant canopy', *Boundary-Layer Meteorol.* **10,** 423-453.

Shaw, R.H.: 1977, 'Secondary wind speed maxima inside plant canopies', *J. Appl. Meteorol.* **16,** 514-523.

Taylor, G.I.: 1921, 'Diffusion by continuous movements', *Proc. Lond. Math. Soc.* **A20,** 196-211.

Wilson, J.D., Legg, B.J. and Thomson, D.J.: 1983, 'Calculation of particle trajectories in the presence of a gradient in turbulent-velocity variance', *Boundary-Layer Meteorol.* **27,** 163-170.

Wilson, J.D., Thurtell, G.W. and Kidd, G.E.: 1981a, 'Numerical simulation of particle trajectories in inhomogeneous turbulence. I: Systems with constant turbulent velocity scale.', *Boundary-Layer Meteorol.* **21**, 295-313.

Wilson, J.D., Thurtell, G.W. and Kidd, G.E.: 1981b, 'Numerical simulation of particle trajectories in inhomogeneous turbulence. II: Systems with variable turbulent velocity scale', *Boundary-Layer Meteorol.* **21**, 423-442.

Wilson, J.D., Ward, D.P., Thurtell, G.W. and Kidd, G.E.: 1982, 'Statistics of atmospheric turbulence within and above a corn canopy', *Boundary-Layer Meteorol.* **24**, 495-519.

Chapter 5

Conclusions

Results have been presented of the analysis of the daytime velocity statistics, air temperature, sensible and latent heat fluxes based on the measurements within and above the thinned and pruned Douglas-fir stand, and of the random flight simulations of air temperature profiles. The most important findings are summarized as follows:

(1) The vertical structure of the stand affected, to a great extent, the vertical distributions of the velocity statistics (wind speed, variance, turbulence intensity, Reynolds stress, skewness and kurtosis), air temperature, sensible and latent heat fluxes. The profile of wind speed showed a minimum in the canopy layer and a marked maximum at the middle of the trunk space. The profile of potential temperature always exhibited an inversion between the middle of the trunk space and the middle of the canopy and a maximum in the middle of the canopy. The profiles of daytime sensible and latent heat fluxes in the stand showed the features as described by the scalar conservation equation under advection free conditions: constant flux layers in the trunk space and above the stand and large flux divergences in the canopy layer. The effect of the stand structure was also evident in the quadrant representation of the fluxes of momentum, sensible heat and water vapour.

(2) Negative Reynolds stress, or upward transport of momentum, persistently occurred at the lower heights of the stand, the magnitude being 0.03 m^2/s^2. The examination of the Reynolds stress budget revealed that the negative values are likely associated with the negative velocity gradients at these heights. It is believed that the longitudinal

pressure gradient due to land-sea/upslope-downslope circulations was the main factor responsible for the upward transport of the momentum.

(3) Energy budget was examined above and beneath the overstory of the stand. The sum of the sensible and latent heat fluxes above the stand accounted for, on average, 83% of the available energy flux. Beneath the overstory, the corresponding figure was 74%. On some days, energy budget closure was much better than on others. The measured sensible heat flux near the forest floor showed very little horizontal variations. The daytime Bowen ratio of the stand increased from 1.3 to 2.7 during the experimental period as the soil dried. The daytime mean canopy resistance showed strong dependence on the mean saturation deficit. The mid-day value of the Omega factor of the stand was about 0.2, indicating a strong coupling between this stand and the atmosphere as expected for forests.

(4) Counter-gradient flux of sensible heat constantly occurred at the canopy base, invalidating the conventional gradient-diffusion model or K-theory at this height. However, K-theory with a far-field eddy diffusivity appeared to be valid near the ground. The sensible heat flux from the forest floor calculated using this modified K-theory agreed reasonably well with the measured one. This supports the application of the aerodynamic approach to the exchange process between the forest floor and the adjacent air layer.

(5) The daytime profiles of the dimensionless potential temperature, $\Delta\theta/\theta_*$, where $\Delta\theta$ is the difference in potential temperature between the height of interest and the reference height, and θ_* was a characteristic temperature defined as the ratio of the kinematic sensible heat flux to the square root of the vertical velocity variance, both measured above the stand, were found to be well stratified by H_g/H_T, the ratio of the sensible heat flux measured near the forest floor to that measured above the stand (the relative sensible heat source density). As H_g/H_T increased, the profile of $\Delta\theta/\theta_*$ shifted to higher values.

(6) The daytime profile of $\Delta\theta/\theta_*$, simulated by combining the random flight technique for the dispersion of sensible heat from the elevated canopy source and the gradient-diffusion relationship (K-theory) with a far-field diffusivity for the dispersion from the ground-level source, agreed reasonably well with the measured one. The simulation results suggested that the profile of $\Delta\theta/\theta_*$ was not sensitive to the shape of the wind speed profile. This, together with the simulation results of other studies, indicates that for the purpose of Lagrangian simulation of the dispersion in canopies, efforts should be directed toward a better understanding of the velocity variance and Lagrangian time scale of the velocity field.

Appendix A

Photographs of the Site and Instrumentation

Figure A.1: Eddy correlation unit operated permanently at the height of 23.0 m (z/h = 1.38) in the Douglas-fir stand at Browns River. It consisted of one 3-dimensional sonic anemometer, one krypton hygrometer and one fine wire thermocouple and was pointed in the NNE direction. The daytime wind direction was NE to NNE.

Figure A.3: Main instrument tower used in the Browns River experiment.

Figure A.2: Eddy correlation unit operated at various heights in the Douglas-fir stand at Browns River. It consisted of one 3-dimensional sonic anemometer/thermometer and one krypton hygrometer. The photograph was taken when it was mounted at a height of 10.0 m (z/h = 0.60).

Figure A.4: Forest floor and trunk space of the Douglas-fir stand at Browns River.

Appendix B

Wake Production in the Reynolds Stress Budget

From the TKE budget equation in the canopy, Raupach and Shaw (1982) derived the budget equation for $< \overline{u}_i''\overline{u}_i'' >$, the dispersive kinetic energy. By replacing one of the two subscripts i with k, we transform the budget equation for $< \overline{u}_i''\overline{u}_i'' >$ to the budget equation for $< \overline{u}_i''\overline{u}_k'' >$, the dispersive stress, thus

$$
\begin{aligned}
\left(\frac{\partial}{\partial t} + <\overline{u}_j> \frac{\partial}{\partial x_j}\right) < \overline{u}_i''\overline{u}_k'' > \\
= 0 = \\
- < \overline{u}_i''\overline{u}_j'' > \frac{\partial <\overline{u}_k>}{\partial x_j} - < \overline{u}_k''\overline{u}_j'' > \frac{\partial <\overline{u}_i>}{\partial x_j} \\
(1) \\
+ < \overline{u_i'u_j'}'' \frac{\partial \overline{u}_k''}{\partial x_j} > + < \overline{u_k'u_j'}'' \frac{\partial \overline{u}_i''}{\partial x_j} > \\
(2) \\
- \frac{\partial}{\partial x_j}\left(< \overline{u}_i''\overline{u_k'u_j'}'' > + < \overline{u}_k''\overline{u_i'u_j'}'' >\right) \\
(3) \\
- \frac{\partial}{\partial x_j}\left(< \overline{u}_i''\overline{u}_j''\overline{u}_k'' > + 2\frac{< \overline{p}''\overline{u}_j'' >}{\rho}\right) \\
(4) \\
+\nu < \overline{u}_i'' \nabla^2 \overline{u}_k'' > + \nu < \overline{u}_k'' \nabla^2 \overline{u}_i'' > \\
(5) \\
+\frac{1}{\rho} <\overline{u}_i>< \frac{\partial \overline{p}''}{\partial x_k} > + \frac{1}{\rho} <\overline{u}_k>< \frac{\partial \overline{p}''}{\partial x_i} > \\
(6)
\end{aligned}
\tag{B.1}
$$

where u_i and x_i are velocity and position vectors, t is time, p is pressure, ν is the kinematic viscosity; triangular brackets and double primes denote, respectively, horizontal averages and departures therefrom; and overbar and single prime denote, respectively, temporal averages and departures therefrom. The six groups of the terms on the RHS of (B.1) are

(1) production of the dispersive stress due to wind shear

(2) wake production of Reynolds stress. When $i = 1$ and $k = 3$, this term becomes $-P_w$ in Equation (2.4).

(3) & (4) transport terms, assumed to be negligible. Physically this assumption means that the dispersive stress (or TKE if $i = k$) arising from work against drag on elements within an averaging volume is produced within the same averaging volume.

(5) viscous terms accounting for direct dissipation of the dispersive stress. They can be further separated into two parts as

$$\begin{aligned}(5) &= \nu < \overline{u}_i \nabla^2 \overline{u}_k'' > + \nu < \overline{u}_k \nabla^2 \overline{u}_i'' > \\ &\quad -\nu < \overline{u}_i >< \nabla^2 \overline{u}_k'' > -\nu < \overline{u}_k >< \nabla^2 \overline{u}_i'' > \end{aligned} \tag{B.2}$$

Provided that there is negligible direct viscous dissipation by the canopy of the dispersive stress without prior conversion to wake turbulence, and using $f_{Vi} = -\nu < \nabla^2 \overline{u}_i'' >$, where f_{Vi} is the viscous drag force vector exterted on a unit mass of air, (B.2) reduces to

$$(5) = < \overline{u}_i > f_{Vk} + < \overline{u}_k > f_{Vi} \tag{B.3}$$

(6) wake production of the dispersive stress due to the form drag. It can be re-written as

$$(6) = < \overline{u}_i > f_{Fk} + < \overline{u}_k > f_{Fi} \tag{B.4}$$

where f_{Fi} is the form drag vector exerted on a unit mass of air.

We replace the tensor notation by the meteorological notation, writing $x_i = (x, y, z)$

and $u_i = (u, v, w)$ with the x-coordinate in the mean streamwise direction and the z-coordinate normal to the ground surface. To an excellent approximation, horizontally averaged flow properties within the canopy are functions of z only. Substituting 1 for subscript i and 3 for subscript k into (B.1) and making use of the above simplifications give

$$\begin{aligned} P_w &= -<\overline{w}''\overline{w}''> \frac{\partial <\overline{u}>}{\partial z} + <\overline{u}> (f_{Vz} + f_{Fz}) \\ &= -<\overline{w}''\overline{w}''> \frac{\partial <\overline{u}>}{\partial z} \end{aligned} \tag{B.5}$$

where we have used the fact that $(f_{Vz} + f_{Fz})$ (vertical drag) is negligible.

Appendix C

Comparison of the Two Eddy Correlation Units over a Bare Field

Upon the completion of Chapters 2–4 of this dissertation, concern was expressed about the aerodynamic shadow effect of the rings of the 3-dimensional sonic anemometer (Applied Technologies Inc., Model SWS-211/3V) used in the Browns River Experiment on the measurements of the two horizontal velocity components. Wind tunnel tests showed that this effect might result in an underestimation of mean wind speed by 20% (G.A. Zimmerman 1991, Applied Tecnologies Inc., personal communication). By applying to the Browns River data the algorithms obtained in laminar flow in a wind tunnel to correct the shadow effect, it was found that the wind speed measured with this sonic anemometer was about 22% higher than the wind speed measured with the cup anemometers. Furthermore, the streamwise velocity measured with this sonic anemometer at the tree tops was about 13% higher than that measured with another 3-dimensional sonic anemometer (Applied technologies Inc., Model BH-478B/3, probe without rings) 6.33 m above the tree tops. It is clear that the algorithms obtained in laminar flow can not be applied directly to turbulent flow.

In order to assess the shadow effect in outdoor turbulent environments, an experiment was performed over a bare field on level ground on George Reynolds' farm in Delta, British Columbia on 3 and 5 October 1991 with the two eddy correlation units used in the Browns River Experiment: unit 1 (called the upper unit in Chapters 2 and 3, with Model BH-478B/3 sonic anemometer) and unit 2 (called the lower unit in Chapters 2 and 3, with Model SWS-211/3V sonic anemometer). The field had been laser levelled and harrowed to improve drainage. The potato crop of the previous season had been completely incorporated into the soil and no crop residue remained at the surface. Only one krypton hygrometer (Campbell Scientific Inc., Model K20, 1.021 cm path length) was available for this experiment and was used as part of unit 1. The two units were oriented toward the northwest, the direction of the daytime sea breeze. They were mounted at the same height of 2.25 m. The horizontal separation between the two units was approximately 1.2 m. For comparison, a sensitive cup anemometer (Thornthwaite Associates, Model 901-LED) was also mounted at the height of 2.25 m. Net radiation flux, R_n was measured using a net radiometer (Swissteco Instruments, Model S-1) at a height of 1.5 m. Heat flux into the soil, G was measured with a heat flux plate (Middleton Instruments, Model F) buried at a depth of 1.5 mm. The fetch was at least 600 m. The weather was mostly clear. The stability parameter, z/L, where L is Monin-Obukhov length calculated from the measurements of unit 2, had values in the range –4.42 to 0.011.

Statistics were calculated over 30-minute intervals. A two-way coordinate rotation was performed in the same manner as discussed in Chapter 2. Only runs after the onset of the sea breeze were used in the data analysis.

C.1 Comparison of Velocities

Figure C.1 compares the streamwise velocity and the equivalent cup wind speed defined in Chapter 2. Unit 2 appeared to underestimate both variables by about 4%. On the whole, the agreement was very good.

Figure C.2 compares the vertical velocity variance, $\overline{w'^2}$ for the two units. Unit 2 appeared to overestimate $\overline{w'^2}$ by about 11%.

Figure C.3 compares the equivalent cup wind speed measured with the 3-dimensional

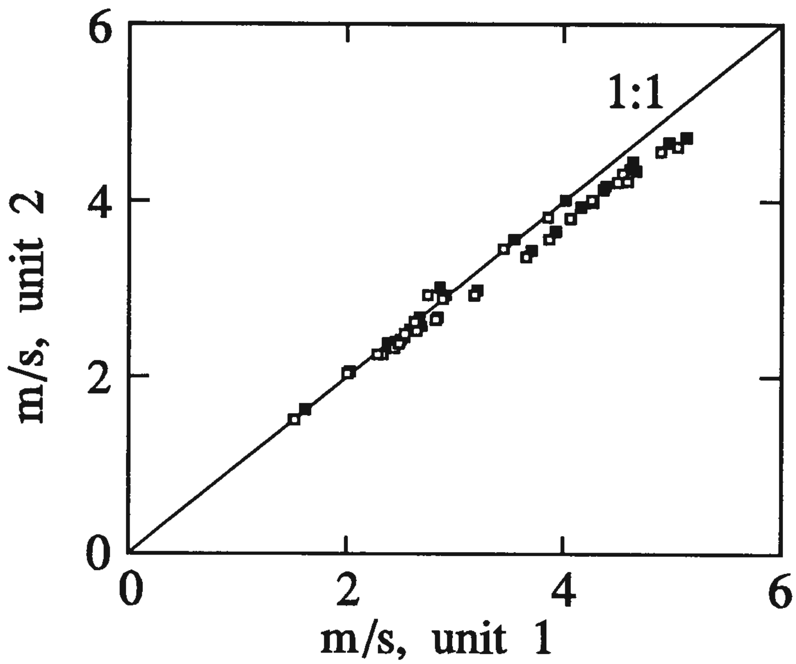

Figure C.1: Streamwise velocity (□) and equivalent cup wind speed (■) measured with unit 2 versus those measured with unit 1 over the bare field in Delta on 3 and 5 October 1991.

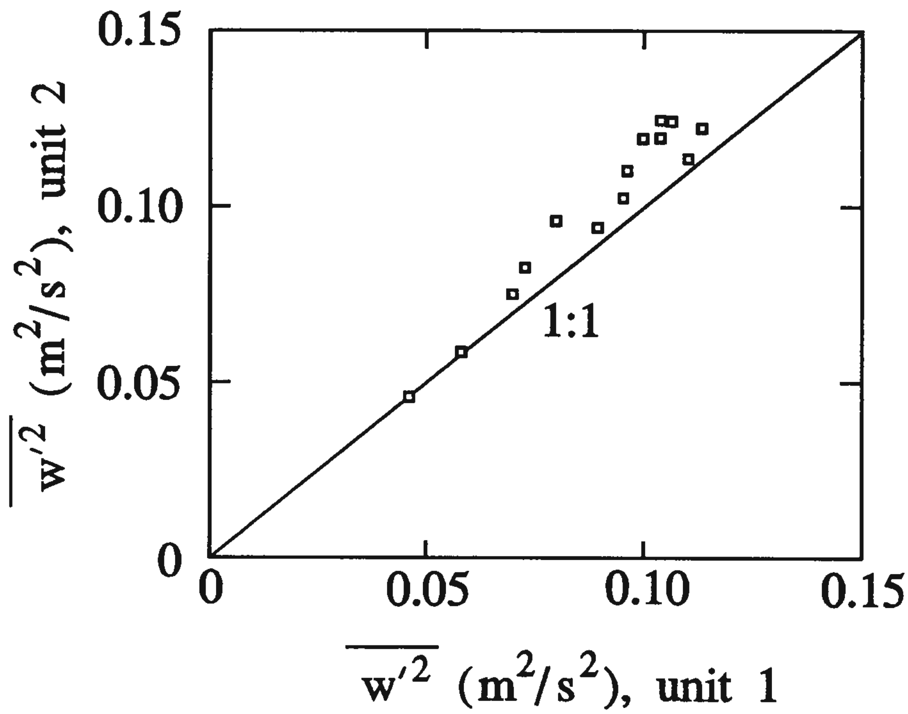

Figure C.2: Vertical velocity variance, $\overline{w'^2}$ measured with unit 2 versus that measured with unit 1 over the bare field in Delta on 3 October 1991.

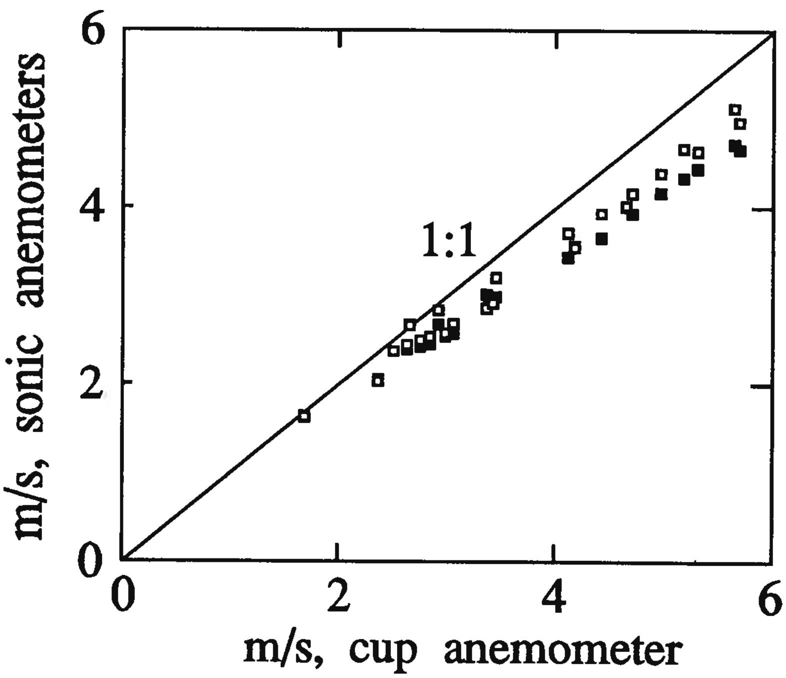

Figure C.3: Equivalent cup wind speed measured with the 3-dimensional sonic anemometers versus wind speed measured with the cup anemometer over the bare field in Delta on 3 and 5 October 1991: unit 1 (□); unit 2 (■).

sonic anemometers with the wind speed measured with the cup anemometer. There was a good correlation between the sonic and cup anemometer measurements, but the cup anemometer tended to overestimate the wind speed by about 15%, probably resulting from the overspeeding of cup anemometers in turbulent environments (Coppin 1982). The results shown in Figure C.3 were similar to those obtained within and above the Douglas-fir stand at Browns River (Chapter 2).

C.2 Comparison of Momentum Flux

Figure C.4 compares the kinematic momentum flux, $-\overline{u'w'}$. It appears that the ring-induced shadow effect of the 3-dimensional sonic anemometer in unit 2 resulted in a systematic underestimation of the magnitude of the kinematic momentum flux. The average value of the ratio of $-\overline{u'w'}$ measured with unit 2 to $-\overline{u'w'}$ measured with unit 1 was 0.80. However, there existed a good correlation between the two measurements, the correlation coefficient being 0.966 for 14 runs.

Despite this difference, some derived aerodynamic quantities from the measurements of the two units were rather similar. For example, the average value of the ratio, σ_w/u_*, where σ_w is the square root of the vertical velocity variance and u_* is the friction velocity, was 1.28 from the measurements of unit 2 for the runs with $|z/L| < 0.09$. The corresponding value for unit 1 was 1.25. Both ratios were very similar to the commonly observed value of 1.25±0.03 in the neutral surface layer (Panofsky and Dutton 1984). Figure C.5 shows $-\overline{u'w'}$ as a function of $\overline{u}^2$, where $\overline{u}$ is the mean streamwise velocity component. The correlation coefficient was 0.956 for unit 1 for 14 runs and 0.957 for unit 2 for 26 runs. The scatter in the plot for the runs with the same $\overline{u}$ was mostly a result of varying stability among the runs. The average drag coefficients (defined as the ratio of kinematic Reynolds stress to the square of the horizontal velocity component)

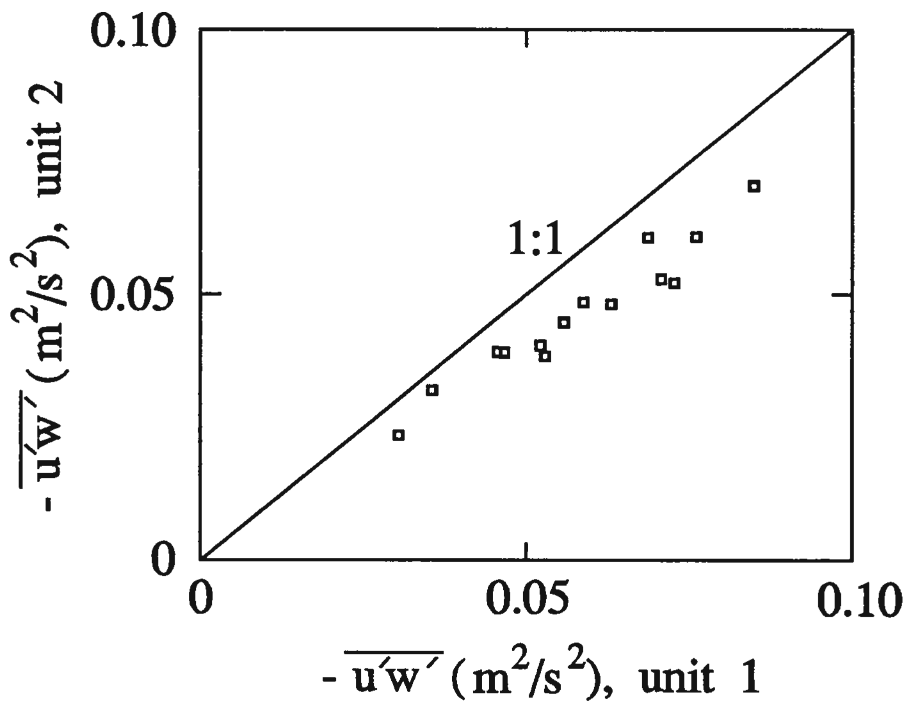

Figure C.4: Kinematic momentum flux, $-\overline{u'w'}$ measured with unit 2 versus that measured with unit 1 over the bare field in Delta on 3 October 1991.

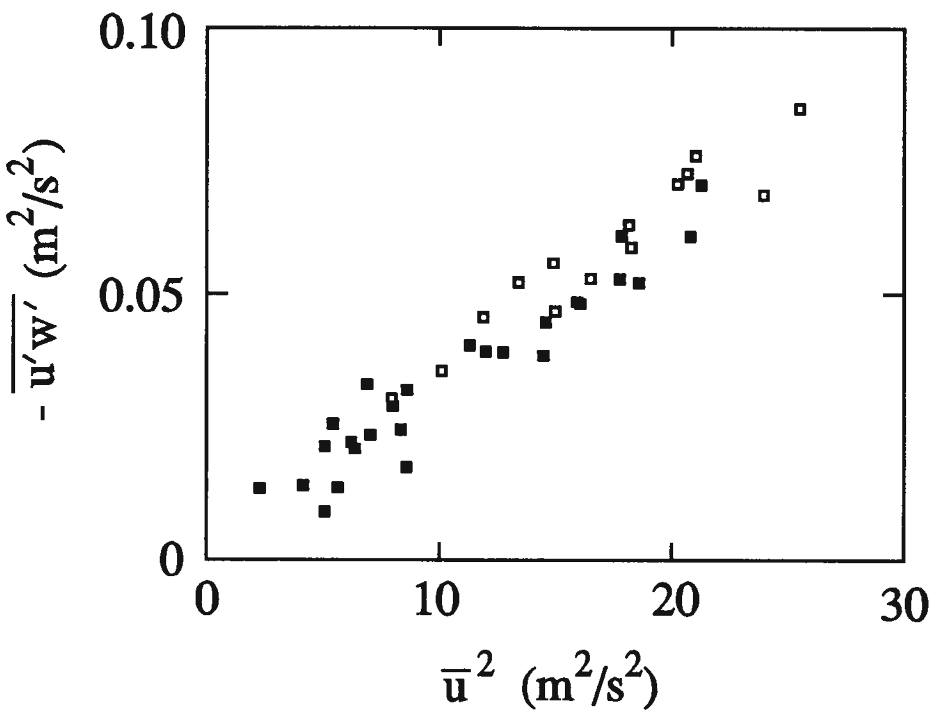

Figure C.5: Kinematic momentum flux, $-\overline{u'w'}$ as a function of the square of the average streamwise velocity component, $\overline{u}^2$ for unit 1 (□) and unit 2 (■) over the bare field in Delta on 3 and 5 October 1991.

at 2.25 m were 0.0035 and 0.0033, for units 1 and 2, respectively. The roughness length of the field was estimated to be 2.7 mm from the measurements of unit 2 and 3.0 mm from the measurements of unit 1, both values being about 1/10 of the mean height of the roughness elements.

C.3 Comparison of Scalar Fluxes

On 3 October, the output signal from the amplifier used to amplify the thermocouple voltage of unit 1 was severely contaminated by the noise created by a nearby AC voltage source. The resulting temperature variance was unrealistically high, the magnitude being 3 °C^2. Because of the noise, the plot of kinematic sensible heat flux, $\overline{w'T'}$ showed some scatter, but overall the agreement between the two units was very good (Figure C.6).

In order to compare the two units further in regard to scalar flux measurements, $\overline{w_1'T_2'}$, the covariance between the vertical velocity component measured with unit 1 (w_1) and air temperature measured with unit 2 (T_2), was calculated for each 30 minute run and was compared with $(\overline{w'T'})_2$, the kinematic sensible heat flux measured with unit 2. An excellent correlation existed between $\overline{w_1'T_2'}$ and $(\overline{w'T'})_2$, with $R^2 = 0.997$. The regression equation was

$$\overline{w_1'T_2'} = 0.75(\overline{w'T'})_2 \qquad (R^2 = 0.997, n = 16) \tag{C.1}$$

Because some of the flux contribution from eddies of small wave-length was lost due to the horizontal separation between the two units, the regression coefficient was smaller than unity. A similar result was obtained for water vapour flux, as shown by the following regression equation

$$\overline{w_2'\rho_{v1}'} = 0.77(\overline{w'\rho_v'})_1 \qquad (R^2 = 0.990, n = 16) \tag{C.2}$$

where $\overline{w_2'\rho_{v1}'}$ is the covariance between the vertical velocity component measured with unit 2 (w_2) and water vapour density measured with unit 1 (ρ_{v1}) and $(\overline{w'\rho_v'})_1$ is the

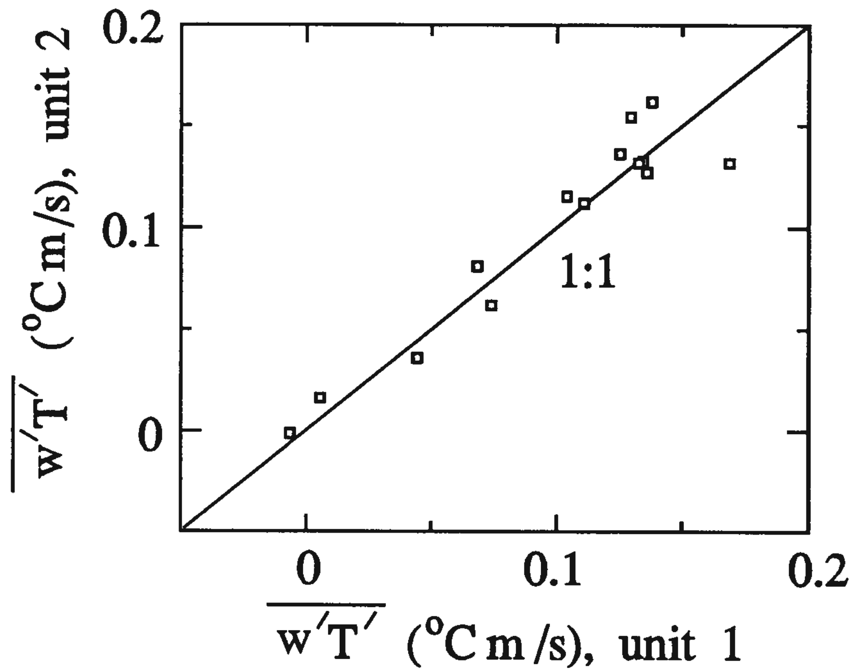

Figure C.6: Kinematic sensible heat flux, $\overline{w'T'}$ measured with unit 2 versus that measured with unit 1 over the bare field on 3 October 1991.

water vapour flux measured with unit 1. The fact that the values of the coefficient in the regression equations (C.1) and (C.2) are almost identical is another indication of the consistency between the two units in measuring scalar fluxes.

On 5 October, the noise of the amplifier was eliminated by grounding the amplifier properly and removing the AC power source. However, the electronics for the vertical velocity component of unit 1 failed. Although there was no comparison available for $\overline{w'T'}$ on this day, there was a comparison for air temperature variance, $\overline{T'^2}$ (Figure C.7). The two units measured the fluctuation in air temperature in very different ways: Unit 1 measured it directly with a fine wire thermocouple (chromel-constantan, 13 μm in diameter), while unit 2 measured it indirectly using the sonic signal of the vertical velocity component. There was excellent agreement between the two measurements of $\overline{T'^2}$.

The consistency check can also be done by examining the energy budget closure. Figure C.8 shows the comparison of the sum of turbulent fluxes, $H + \lambda E$ with the available energy flux, $R_n - G$. Sensible heat flux, H was measured with unit 2 on both days. Latent heat flux, λE was measured with unit 1 on 3 October and was estimated from $\overline{w'_2\rho'_{v1}}$ using (C.2) on 5 October. Figure C.8 shows that very good energy budget closure was achieved during the experimental period.

C.4 Summary

The rings of the sonic anemometer probe of unit 2 had little effect on the measurements of scalar fluxes. The ring-induced shadow effect resulted in an underestimation of mean wind speed by about 4%, much smaller than the value observed in laminar flow in a wind tunnel. The effect on the measurement of momentum flux was more noticeable. On average, unit 2 underestimated the magnitude of momentum flux by 20%.

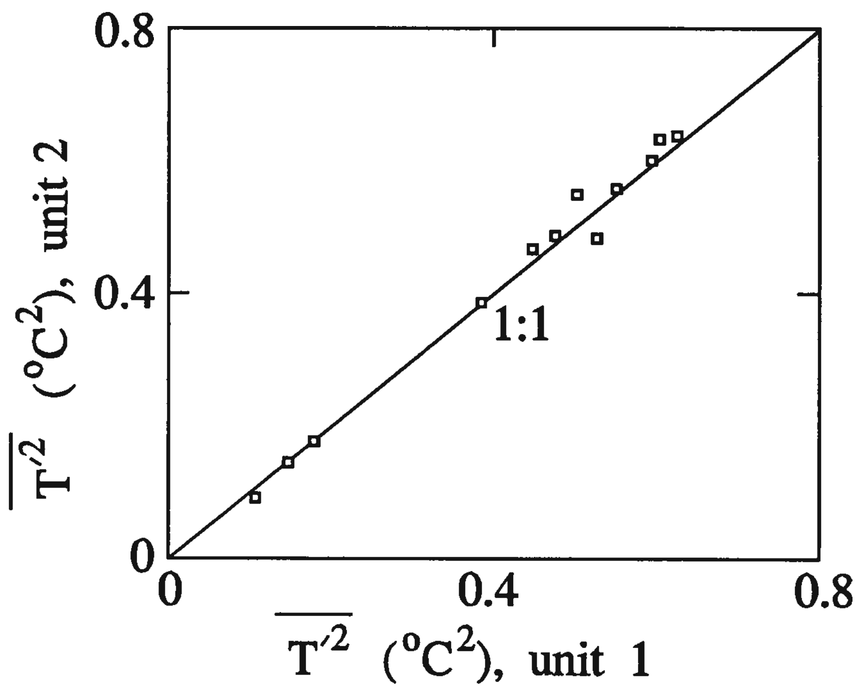

Figure C.7: Air temperature variance, $\overline{T'^2}$ measured with unit 2 (sonic signal) versus that measured with unit 1 (thermocouple signal) over the bare field in Delta on 5 October 1991.

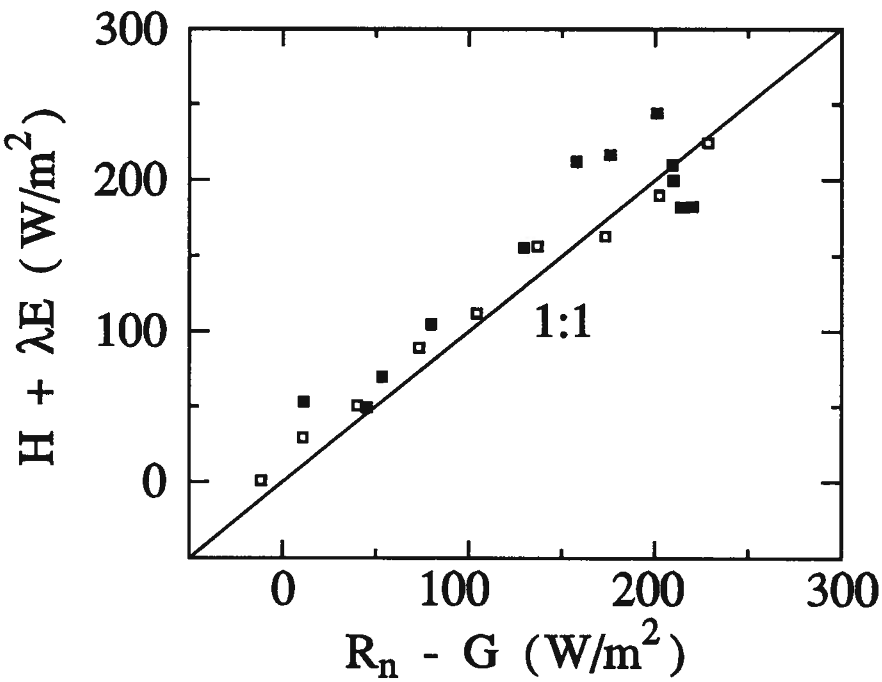

Figure C.8: The sum of the turbulent heat fluxes, $H + \lambda E$ versus the available energy flux, $R_n - G$ over the bare field in Delta on 3 (□) and 5 (■) October 1991.

It should be pointed out that the probe of the sonic anemometer in unit 2 was designed primarily for turbulence measurements in crop and forest canopies where the wind speed is very low and wind direction highly unpredictable. According to Kaimal (Kaimal, J.C., 1991, personal communication), occasional sweeps by the wakes across an acoustic path that result from the constantly changing wind speed and direction in a plant canopy, will have minimal shadow effect on the measurement. The wind direction during this experimental period, on the other hand, was rather steady and was mainly directed along the central axis of the probe (the worst-case scenario, Kaimal 1991). No attempt was made to correct the data obtained in the Browns River Experiment for the ring-induced shadow effect. But even with the correction based on these worst-case scenario results, the conclusions made in previous chapters will not be altered.

References

Coppin, P.A.: 1982, 'An examination of cup anemometer overspeeding', *Meteorol. Rdsch.* **35**, 1-11.

Panofsky, H.A. and Dutton, J.A.: 1984, *Atmospheric Turbulence: Models and Methods for Engineering Applications*, John Wiley and Sons, New York.

Appendix D

An Analytical Expression for Legg and Raupach's Model

D.1 A Modified Langevin Equation for the Canopy Environment

Consider dispersion in only the vertical direction, writing $Z(z_o, t)$ for the position and $w(z_o, t) = \partial Z(z_o, t)/\partial t$ for the Lagrangian velocity of a marked fluid particle, where t is time and z_o is the height of the source. Legg and Raupach (1982) expressed w as a Markovian process which obeys a modified Langevin equation

$$\frac{\partial w(z_o, t)}{\partial t} = -\alpha w(z_o, t) + \lambda \xi(t) + f \tag{D.1}$$

where α, λ and f are coefficients to be specified below, and ξ is a Gaussian white noise which has the properties

$$\overline{\xi(t)} = 0, \qquad \overline{\xi(s)\xi(t)} = \delta(s - t) \tag{D.2}$$

where the overbar denotes ensemble averaging. The first term on the RHS of (D.1) represents a retarding force per unit mass, the second term is a random acceleration, and the third term is a mean force per unit mass on the marked particle due to the mean pressure gradient. In a steady, horizontally homogeneous flow over a level surface, Legg and Raupach (1982) showed that

$$f = \partial \overline{w_E'^2} / \partial z \tag{D.3}$$

where $\overline{w_E'^2}$ is the variance of the Eulerian vertical velocity.

The solution of (D.1) has been found by Legg and Raupach (1982) to be

$$w(z_o,t) = w(z_o,0)e^{-\alpha t} + \lambda \int_0^t e^{\alpha(s-t)}\xi(s)ds + f\alpha^{-1}(1-e^{-\alpha t}) \tag{D.4}$$

which represents a random process with mean (called mean vertical drift velocity),

$$\overline{w}(z_o,t) = \overline{w}(z_o,0) + f\alpha^{-1}(1-e^{-\alpha t}) \tag{D.5}$$

variance,

$$\overline{[w'(z_o,t)]^2} = \overline{[w'(z_o,0)]^2}e^{-2\alpha t} + \frac{\lambda^2}{2\alpha}(1-e^{-2\alpha t}) \tag{D.6}$$

and covariance,

$$\overline{w'(z_o,0)w'(z_o,t)} = \overline{[w'(z_o,0)]^2}e^{-\alpha t} \tag{D.7}$$

It is apparent from (D.7) that

$$\alpha = 1/T_L$$

where

$$T_L = \frac{1}{\overline{[w'(z_o,0)]^2}} \int_0^\infty \overline{w'(z_o,0)w'(z_o,t)}dt$$

is the Lagrangian integral time scale.

In their derivation, Legg and Raupach (1982) assumed that w was a stationary process. From this assumption they simplified the form of $\overline{w}$ and fixed the coefficient λ. They used the above equations to perform a random flight simulation for scalar dispersion in canopies. It turns out that for the special case of constant f (corresponding to the case of $\beta_1 = 1/2$ in the simulations of Raupach (1989) for scalar concentration in the canopy and to the case of the simulation of Legg and Raupach (1982) for the evolution of scalar profiles in the canopy) and constant T_L within the canopy (Leclerc *et al.* 1988, Legg *et al.* 1986), an analytical solution can be derived for the single particle transition probability based on these equations.

We begin the derivation with two more simplifications. First, the initial statistics of the Lagrangian and the Eulerian velocities are thought to be identical (Raupach 1983), i.e.

$$\overline{w}(z_o, 0) = \overline{w}_E(z_o) = 0 \tag{D.8}$$

$$\overline{[w'(z_o, 0)]^2} = \overline{[w'_E(z_o)]^2}$$

We further assume that the Lagrangian velocity variance is not a function of time. This simplification fixes λ from (D.6) as

$$\lambda = \sigma_w(z_o)\sqrt{\frac{2}{T_L}} \tag{D.9}$$

where

$$\sigma_w(z_o) = \sqrt{\overline{[w'(z_o, 0)]^2}} = \sqrt{\overline{[w'(z_o, t)]^2}}$$

Using (D.8), (D.5) reduces to

$$\overline{w}(z_o, t) = fT_L(1 - e^{-t/T_L}) \tag{D.10}$$

It is interesting that $\overline{w}$ in (D.10) has an asymptotic behavior similar to that of the vertical drift velocity of a tracer particle released from an elevated source in the neutral surface layer (Raupach 1983). In the near field where $t << T_L$, $\overline{w}$ approximately equals zero, while at $t >> T_L$, $\overline{w}$ approaches its far field limit of fT_L. A visual inspection of the $\overline{w_E'^2}$ profile generalized from the experimental studies in a variety of plant canopies (Raupach 1989) gives

$$f \simeq 1.4u_*^2/h \tag{D.11}$$

where u_* is the friction velocity measured above the canopy and h is the height of the canopy. Furthermore, if T_L is related to u_* and h in the form (Legg *et al.* 1986)

$$T_L = 0.3h/u_* \tag{D.12}$$

then it follows from (D.11) and (D.12) that

$$fT_L \simeq 0.42u_* \tag{D.13}$$

which is remarkably close to ku_*, the far field vertical drift velocity for a marked particle in the surface layer or in the layer above the canopy (Hunt and Webber 1979, Raupach 1983), where $k = 0.4$ is the von Karman constant.

D.2 Single Particle Transition Probability

The height of the marked particle is

$$Z(z_o, t) = z_o + \int_0^t w(z_o, s)ds \tag{D.14}$$

From (D.10) and (D.14), the mean height can be shown to be

$$\overline{Z}(z_o, t) = z_o + fT_L t - fT_L^2(1 - e^{-t/T_L}) \tag{D.15}$$

To find $\sigma_Z(z_o, t) = \sqrt{\overline{(Z - \overline{Z})^2}}$, the mean depth of plume or the square root of the variance of particle position, we use (D.14), (D.4) and (D.5), thus

$$\begin{aligned}
[\sigma_Z(z_o,t)]^2 &= \overline{\{[\int_0^t w(z_o,t_1)dt_1 + z_o] - [\int_0^t \overline{w}(z_o,t_1)dt_1 + z_o]\}^2} \\
&= \int_0^t \int_0^t \overline{[w(z_o,t_1) - \overline{w}(z_o,t_1)][w(z_o,t_2) - \overline{w}(z_o,t_2)]}dt_1\, dt_2 \\
&= \underbrace{\int_0^t \int_0^t \overline{[w'(z_o,0)]^2}e^{-\alpha(t_1+t_2)}dt_1\, dt_2}_{\mathrm{I}} \\
&\quad \underbrace{+2\lambda \int_0^t \int_0^t e^{-\alpha t_1}dt_1\, dt_2 \overline{[w'(z_o,0) \int_0^t e^{\alpha(u-t_2)}\xi(u)du]}}_{\mathrm{II}} \\
&\quad \underbrace{+\lambda^2 \int_0^t dt_1 \int_0^t dt_2 \int_0^{t_1} e^{\alpha(s-t_1)}ds \int_0^{t_2} e^{\alpha(u-t_2)}\overline{\xi(s)\xi(u)}du}_{\mathrm{III}}
\end{aligned} \tag{D.16}$$

Term I can be evaluated easily as

$$\begin{aligned}\text{Term I} &= \overline{[w'(z_o,0)]^2}(1-e^{-\alpha t})^2/\alpha^2 \\ &= \sigma_w^2(z_o)T_L^2(1-e^{-t/T_L})^2 \end{aligned} \tag{D.17}$$

Using the fact that ξ is uncorrelated with w, Term II reduces to

$$\text{Term II} = 0 \tag{D.18}$$

Term III can be evaluated, using (D.2) and (D.9), as follows

$$\begin{aligned}\text{Term III} &= \lambda^2 \int_0^t dt_1 \int_0^t dt_2 \int_0^{t_1} e^{\alpha(s-t_1)}ds \int_0^{t_2} e^{\alpha(u-t_2)}\delta(s-u)du \\ &= \lambda^2 \int_0^t dt_1 \int_0^{t_1} e^{\alpha(s-t_1)}ds \\ &\quad \{\int_0^s dt_2 \int_0^{t_2} e^{\alpha(u-t_2)}\delta(s-u)du + \int_s^t dt_2 \int_0^{t_2} e^{\alpha(u-t_2)}\delta(s-u)du\} \\ &= \lambda^2 \int_0^t dt_1 \int_0^{t_1} e^{\alpha(s-t_1)}ds\{0 + \int_s^t e^{\alpha(s-t_2)}dt_2\} \\ &= \frac{\lambda^2}{\alpha^3}(\alpha t - 1 + e^{-\alpha t}) - \frac{\lambda^2}{2\alpha^3}(1-e^{-\alpha t})^2 \\ &= 2\sigma_w^2(z_o)T_L^2(t/T_L - 1 + e^{-t/T_L}) - \sigma_w^2(z_o)T_L^2(1-e^{-t/T_L})^2 \end{aligned} \tag{D.19}$$

where the following property of the δ function has been used

$$\int_0^b y(u)\delta(x-u)du = \begin{cases} 0 & b < x \\ y(x) & b > x \end{cases}$$

(with $x > 0$ and $b > 0$). Substitution of (D.17)–(D.19) into (D.16) reduces (D.16) to

$$\sigma_Z^2(z_o,t) = 2\sigma_w^2(z_o)T_L^2(t/T_L - 1 + e^{-t/T_L}) \tag{D.20}$$

The mean depth specified by (D.20) has the same form as that of a plume in homogeneous turbulence (Taylor 1921).

Because ξ is Gaussian and (D.1) is linear, w is also Gaussian (Durbin 1983). By the same argument, Z is also Gaussian because it is linear with w according to (D.14). Hence the single particle transition probability density is

$$P(z,t;z_o,0) = \frac{1}{\sqrt{2\pi}\sigma_Z}\exp[-\frac{(z-\overline{Z})^2}{2\sigma_Z^2}] \tag{D.21}$$

where $\overline{Z}$ and σ_Z are given in (D.15) and (D.20), respectively. $P(z,t;z_o,0)$ is a conditional probability density that $Z(z_o,t) = z$, given $Z(z_o,0) = z_o$.

For a point source of instantaneous release of unit mass of scalar at height z_o and time 0, the ensemble averaged scalar concentration at height z and time t is (Batchelor 1964)

$$C_e(z,t;z_o,0) = P(z,t;z_o,0) \tag{D.22}$$

where the subscript e stands for this special elementary source. For the special case of $f = 0$ or $\overline{Z}(t) \equiv z_o$, (D.21) reduces to the single particle transition probability density in homogeneous turbulence, and C_e satisfies phenomenologically the diffusion equation (Batchelor 1964)

$$\frac{\partial C_e}{\partial t} = \frac{\partial}{\partial t}\{K(z_o,t)\frac{\partial C_e}{\partial z}\} \tag{D.23}$$

with the diffusivity K given by

$$K(z_o,t) = \frac{1}{2}\frac{d\sigma_Z^2}{dt} \tag{D.24}$$

and the vertical flux F_e given explicitly by

$$F_e(z,t;z_o,0) = -K\frac{\partial C_e}{\partial z} \tag{D.25}$$

For the general case of non-zero f, however, no form of K can be found to make C_e satisfy the diffusion equation (D.23). To find F_e for the general case, we use the scalar conservation equation for the elementary source

$$\frac{\partial C_e}{\partial t} = -\frac{\partial F_e}{\partial z} \tag{D.26}$$

Equation (D.26) can be integrated with respect to z as follows

$$F_e(z,t;z_o,0) = -\int_{-\infty}^{z} \frac{\partial C_e(y,t;z_o,0)}{\partial t} dy \tag{D.27}$$

Figure D.1 shows the comparison of the concentration profiles from an elementary source calculated using (D.21-D.22) and those simulated using the random flight technique. One gram of mass was released at time zero into the velocity field specified by

$$\sigma_w(z_o) = 0.4 \ \ \mathrm{m/s}$$

$$f = 0.012 \ \ \mathrm{m/s^2}$$

and

$$T_L = 12 \ \ \mathrm{s}$$

In the random flight simulation, a total of 20,000 particles were released and the time step was $\Delta t = 0.2T_L$. It can be seen that the agreement is excellent.

D.3 Profiles of Concentration and Flux for a Plane Source

The analytical solution obtained for the elementary source can be superposed for more complicated sources. As an example, consider a horizontal plane source located at height $z = z_o$ with flux density S (with dimensions of unit mass per unit surface area per unit time) and the horizontal position of the leading edge at $x = x_f$. The observation is made at horizontal position $x = 0$ and height z. For simplicity, we assume the horizontal wind speed u to be constant with height. Using Taylor's hypothesis of frozen turbulence, the particles released at position (x, z_o) always have a migration time of $t = x/u$ when they reach the observing position $(0, z)$. The contribution to the mean concentration at $(0, z)$ from the portion of the source located between x and $x + dx$ is (Wilson *et al.* 1981)

$$SC_e(z,t;z_o,0)\frac{dx}{u}$$

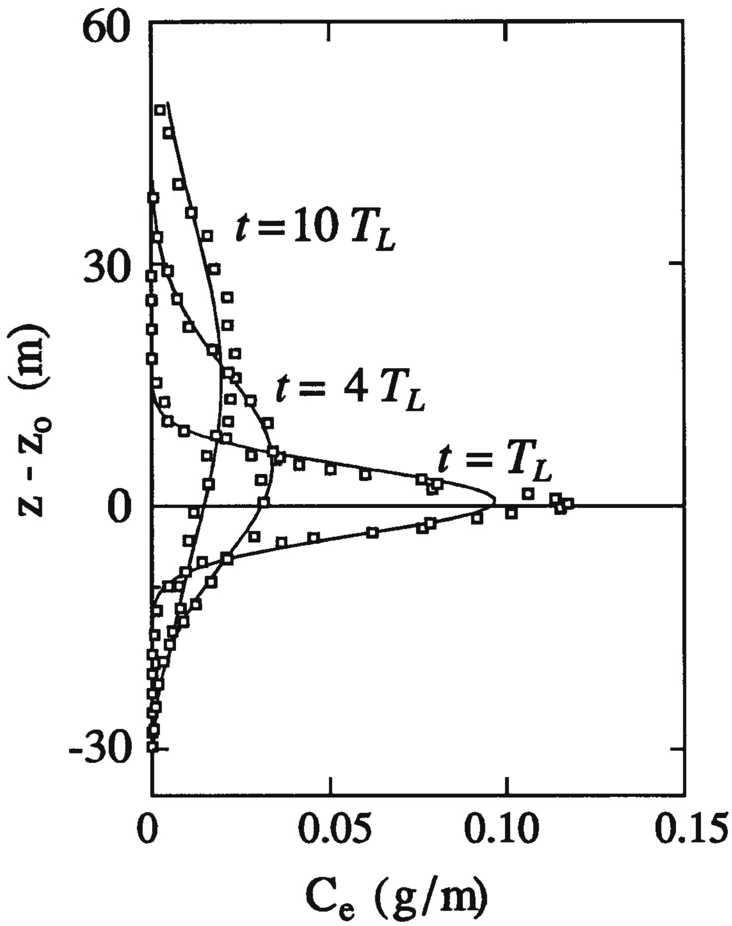

Figure D.1: Comparison of concentration profiles resulting from the release of 1 gram of mass at height z_o and time zero: (—) calculated using the analytical solution (D.21) and (□) simulated using the random flight technique.

or

$$SC_e(z,t;z_o,0)dt \tag{D.28}$$

$C_p(z;z_o)$, the total contribution from the plane source, can be found by integrating (D.28)

$$\begin{aligned} C_p(z;z_o) &= S\int_0^{t_f} C_e(z,t;z_o,0)dt \\ &= S\int_0^{t_f} \frac{1}{\sqrt{2\pi}\sigma_Z}\exp[-\frac{(z-\overline{Z})^2}{2\sigma_Z^2}]dt \end{aligned} \tag{D.29}$$

where $t_f = x_f/u$ and subscript p stands for this plane source. This integral can only be evaluated numerically.

Similarly, $F_p(z;z_o)$, the total contribution to the vertical flux at observing position $(0,z)$ from the plane source, can be found by integrating (D.27) with respect to t and multiplying by S, thus

$$F_p(z;z_o) = S\int_0^{t_f} F_e(z,t;z_o,0)dt \tag{D.30}$$

To evaluate (D.30), we use (D.27), (D.21) and (D.22) a new dummy variable ζ_t defined as

$$\zeta_t = \frac{z-\overline{Z}(z_o,t)}{\sigma_Z(z_o,t)} \tag{D.31}$$

With some lengthy algebra, it can be shown that

$$F_p(z;z_o) = \begin{cases} S[1-\Phi(\zeta_{tf})] & z > z_o \\ -S\Phi(\zeta_{tf}) & z < z_o \end{cases} \tag{D.32}$$

where

$$\zeta_{tf} = \frac{z-\overline{Z}(z_o,t_f)}{\sigma_Z(z_o,t_f)}$$

and

$$\Phi(\zeta_{tf}) = \frac{1}{\sqrt{2\pi}}\int_{-\infty}^{\zeta_{tf}} e^{-\zeta_t^2/2}d\zeta_t$$

Equations (D.29) and (D.32) show the evolution of the profiles of concentration and vertical flux as the fetch increases. Further work is needed to compare the results obtained from these equations with measurements (e.g. the experiment on the plane source disperion reported by Coppin *et al.* 1986) or those obtained from the conventional boundary layer theory.

The analytical expressions (Equations D.21, D.27, D.29 and D.32) enable the computation of the dispersion process to be carried out more rapidly, as compared to random flight techniques, and make some of the physical aspects of the dispersion process apparent. However, one should be aware of the simplifications made in the derivation (constant T_L, f, and u).

D.4 References

Batchelor, G.K.: 1964, 'Diffusion from sources in a turbulent boundary layer', *Archiv. Mechaniki Stosowanj.* **3,** 661-670.

Coppin, P.A., Raupach, M.R. and Legg, B.J: 1986, 'Experiments on scalar dispersion within a plant canopy. Part II: An elevated plane source', *Boundary-Layer Meteorol.* **35,** 167-192.

Durbin, P.A.: 1983, 'Stochastic differential equations and turbulent dispersion', NASA Reference Publication 1103.

Hunt, J.C.R. and Webber, A.H.: 1979, 'A Lagrangian statistical analysis of diffusion from a ground level source in a turbulent boundary layer', *Q. J. R. Meteorol. Soc.* **15,** 423-443.

Leclerc, M.Y., Thurtell, G.W. and Kidd, G.E.: 1988, 'Measurements and Langevin simulations of mean tracer concentration fields downwind from a circular line source inside an alfalfa canopy', *Boundary-Layer Meteorol.* **43,** 287-308.

Legg, B.J. and Raupach, M.R.: 1982, 'Markov-chain simulation of particle dispersion in inhomogeneous flows: The mean drift velocity induced by a gradient in Eulerian velocity variance', *Boundary-Layer Meteorol.* **24,** 3-13.

Legg, B.J., Raupach, M.R. and Coppin, P.A.: 1986, 'Experiments on scalar dispersion within a plant canopy. Part III: An elevated line source', *Boundary-Layer Meteorol.* **35,** 277-302.

Raupach, M.R.: 1989, 'A practical Lagrangian method for relating scalar concentrations to source distributions in vegetation canopies', *Q. J. R. Meteorol. Soc.* **115,** 609-632.

Raupach, M.R.: 1983, 'Near field diffusion from instantaneous sources in the surface layer', *Boundary-Layer Meteorol.* **27,** 105-113.

Taylor, G.I.: 1921, 'Diffusion by continuous movements', *Proc. Lond. Math. Soc.* **A20,** 196-211.

Wilson, J.D., Thurtell, G.W. and Kidd, G.E.: 1981, 'Numerical simulation of particle trajectories in inhomogeneous turbulence. I: Systems with constant turbulent velocity scale.', *Boundary-Layer Meteorol.* **21,** 295-313.

Appendix E

Wind and Turbulence Regimes in an Old Growth Douglas-fir Stand on a South-Facing Slope

Xuhui Lee and T. Andrew Black [1]

[1]Presented at the Annual Meeting of Canadian Society of Agrometeorology held on 24 July, 1990 in Penticton, British Columbia and submitted to Forest Science.

Abstract

This paper reports the results of the analysis of measured wind and turbulence regimes near the forest floor in an old growth Douglas-fir stand on a south facing slope in northern Vancouver Island. Primary instrumentation included one eddy correlation unit, which consisted of a 3-dimensional sonic anemometer, a krypton hygrometer and a fine wire thermocouple, and four home-made hot wire anemometers.

Anabatic and katabatic winds were observed within and outside the stand during clear weather. The high value of the ratio of the wind speed inside the stand to that outside (0.28) suggests the existence of a secondary maximum in the stand wind profile. The profile of the wind speed near the forest floor was well approximated by a logarithmic equation with an effective roughness length of 0.005 m. Turbulence intensity was found to be 0.7 for wind speed greater than 0.3 m/s. Skewness of the vertical velocity component was positive near the forest floor. Power spectra for the streamwise and lateral velocity components exhibited a bimodal distribution in contrast with a unimodal distribution for the spectrum of the vertical component. Latent heat flux near the forest floor was directed upward for all daytime and nighttime runs and was the main energy output component of the energy budget of the forest floor.

Keywords: eddy correlation, velocity statistics, energy budget

E.1 Introduction

Throughout much of Canada, old growth forests are important winter ranges for ungulates. For example, in the provincial and national parks and the ecological reserves of British Columbia, old growth forests occupy approximately 185,600 ha, covering 22% of the total area of the parks and reserves (Roemer *et al.* 1988). Yet little is known about the microclimate in the environment of old growth forests. As a part of the microclimate, wind and turbulence regimes are important in several respects. Wind speed and turbulence intensity affect both boundary layer and coat resistances of animals (McArthur and Monteith 1980, Campbell *et al.* 1980). High turbulence intensity coupled with the predominant eddy sizes (the turbulence length scale) similar to those of objects in the flow can greatly enhance heat and mass transfer from the objects (Chen *et al.* 1988). Knowledge of turbulent transfer processes near the forest floor is needed to understand the competitive role of understory vegetation (the food supply for many species of wild animals) in terms of water use and CO_2 uptake (Black and Kelliher 1989).

In order to understand the characteristics of air movement in old growth forests, an experiment was conducted in an old growth Douglas-fir stand (*Pseudotsuga menziesii* Mirb. Franco) on a south facing slope in 1989. The main objective of this paper is to describe the wind and turbulence regimes near the forest floor of this stand. Some specific concerns to be addressed included wind pattern, turbulence statistics, and spectral characteristics of the velocity components. In addition, the measurements of the energy budget will be briefly examined. The information documented in this report will be used in assessing the magnitude of heat loss from black tailed deer in old growth forests (Sagar *et al.* 1991).

E.2 Experimental Methods

E.2.1 Site Description

The experimental site was located on an extensive south facing, 30-40% slope in the Nimpkish Valley near Woss in northern Vancouver Island (50°65′N, 126°38′W). The valley is oriented approximately in an east-west direction and the valley sides reach an elevation of 500-700 m above sea level. The lower part of the slope was occupied by a second growth Douglas-fir stand, roughly 20 m tall, and the upper part by an old growth Douglas-fir stand over 200 years old, with dominant trees of about 30 m tall. The density of the old growth stand was 500-700 stems/ha. The understory vegetation was patchy, less than 0.7 m tall and mainly composed of salal (*Gaultheria shallon* Pursh.) and huckleberry (*Vaccinium parvifolium*).

Two locations were selected for the experiment: one approximately 100 m into the old growth stand, and the other, which served as a reference, at the outer edge of a widened portion of a logging road 50 m outside the old growth stand.

E.2.2 Instrumentation

At the interior location, an eddy correlation unit was mounted at a height of 2 m. It consisted of a 3-dimensional sonic anemometer (Applied Technologies Inc., Boulder, CO, Model BH-478B/3), a krypton hygrometer (Campbell Scientific Inc., Logan, UT, Model KH20, 1.021 cm path length) and a fine wire thermocouple (chromel-constantan, 13 μm in diameter). Profiles of wind speed and air temperature near the ground surface were measured using four home-made hot wire anemometers and four thermocouples (chromel-constantan, 26 μm in diameter), respectively, at heights of 0.2, 0.4, 0.8 and 2.0 m. For comparison and *in situ* calibration of the hot wire anemometers, a sensitive cup anemometer (C & F Casella Co., London, Model 3106/TG) was also mounted at the height of 2 m. The horizontal separation among the three types of wind speed sensors was approximately 5 m. A wind vane (Met One Inc., Grants Pass, OR, Model 024A) was mounted at a height of 2 m to monitor wind direction.

The hot wire anemometers were calibrated individually before the experiment using a turn-table system. The design of the hot wire anemometers was an improved version that of Kanemasu and Tanner (1968). The vertical supporting rod (1.7 mm in diameter) was 20 mm away from the vertically oriented heated ceramic tube (0.8 mm in diameter) so that measurements could be made for winds from all directions. The operating voltage was 2 V instead of the original 12 V. The voltage from a 12 V recreational vehicle battery was regulated down to four 2 V outputs in series so that 4 anemometers could be operated simultaneously. The heating wire had a resistance of about 10 Ω, the time constant was about 1 second, and the minimum detectable wind speed was about 0.05 m/s. The temperature difference between the ceramic tube and the air was on the order of 80 °C. Because of the robust construction and low power consumption (0.20 A), the hot wire anemometers were operated continuously.

Net radiation was measured with a net radiometer (Swissteco Instruments, Oberriet, Switzerland, Model S-1) mounted parallel to the slope surface at a height of 1.3 m. Another net radiometer of the same type was mounted on a tram system of 20 m path length for measuring spatially averaged net radiation (Black *et al.* 1991). The operation of the tram system was intermittent, but the results showed that the daytime total net radiation measured at a point with the first net radiometer well estimated the spatial average value. Heat flux into the soil was measured using four soil heat flux plates (two made by Middleton Instruments, South Melbourne, Model F, and two home-made) placed at a depth of 3 cm and two nickel wire integrating thermometers to correct for the change in heat storage in the surface soil layer.

The signals from the eddy correlation unit were sampled at 10 Hz by a data logger

(Campbell Scientific Inc., Model 21X with extended software II). The data logger was operated in two modes, mean and burst. In the former, statistics such as means, variance and covariance were calculated over 5 minute intervals and output every half hour. In the latter, the raw signals were sent via the data logger to a lap-top micro-computer (Zenith Data Systems Corp., St. Joseph, MI, Model ZWL-184-02 Supersport with a 20 Mb hard drive) for subsequent analysis. Sixty-seven 30-minute runs was made in the mean mode, fifty of which were in the daytime. Three 60-minute runs were made in the burst mode. Signals from the supplementary instruments were sampled by another data logger of the same type at 0.1 Hz. An array of means were generated every 5 minutes.

At the reference location, a vaned propeller anemometer (R.M. Young Company, Traverse City, MI, Model 05031) was operated at a height of 4.2 m. Wind speed and direction were averaged over 5-minute intervals.

The experiment started in late July and ended in the middle of August, 1989. The experiment was interrupted by three moderate to heavy rainfall events. Consequently, the forest floor was very wet during the experimental period.

E.2.3 Comparison of Anemometers

Figure E.1 compares measurements by the hot wire and the cup anemometers at the height of 2 m over the whole experimental period. In the low wind speed range, the hot wire sensor was superior to the cup sensor because of the inertial problem of the cup. Good agreement was achieved in the high wind speed range. Figure E.1 also shows that the calibration of the hot wire sensor did not shift during the experimental period.

To make the comparison between the hot wire sensor and the sonic sensor, 'cup' speed was calculated from the burst data for the sonic anemometer. The 'cup' speed was

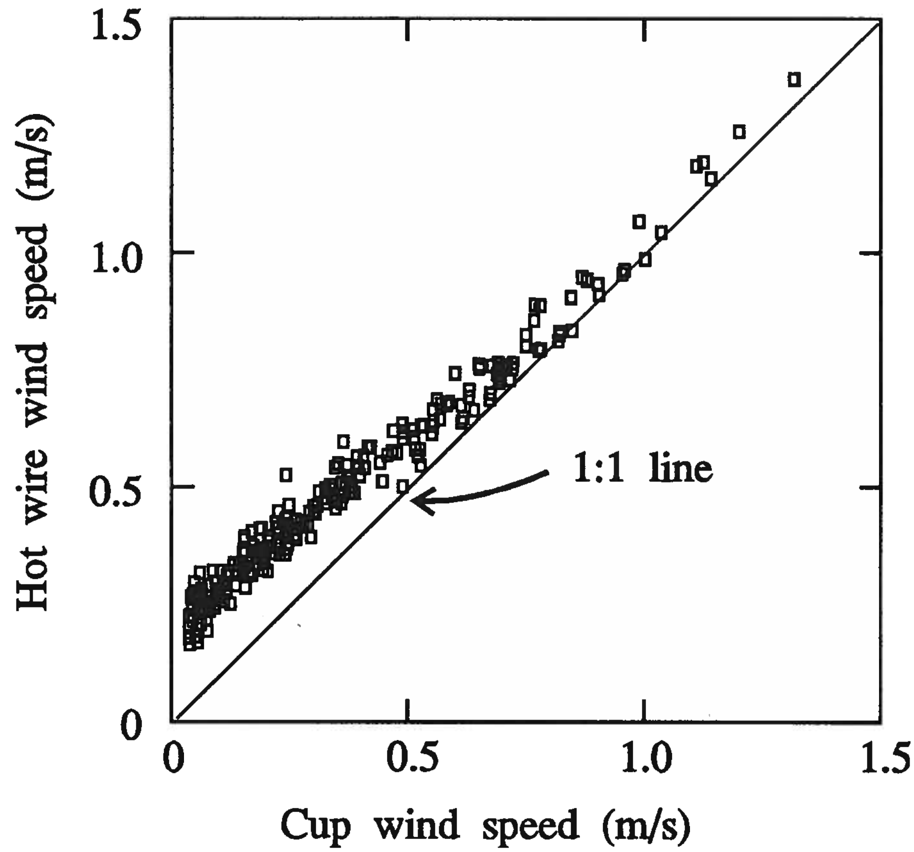

Figure E.1: Comparison of the 30-minute average wind speed measured with a hot wire anemometer with that measured with a cup anemometer at a height of 2 m in the old growth Douglas-fir stand near Woss during the entire experimental period of 1989.

defined as

$$V = \overline{\sqrt{u_1^2 + v_1^2}}$$

where u_1 and v_1 are the two instantaneous horizontal velocity components and the overbar denotes temporal average. The results are shown in Table E.1. There was a slight difference of 0.04 to 0.11 m/s, which might be a result of the underestimation by the sonic anemometer due to the shading effect of its transducers (Kaimal 1979, Baker 1989, Conklin *et al.* 1989).

On 14 and 16 August, the four hot wire sensors were mounted at the same height of 2 m for inter-comparison. The 5-minute average wind speeds agreed within 0.10 m/s. Generally, the hot wire system was reliable in measuring wind speed in low wind speed conditions.

E.2.4 Data Processing

E.2.4.1 Coordinate Rotation

Coordinate rotation was made in order to interpret properly the measurements of the eddy correlation unit. The new coordinate system was defined such that u was the streamwise component of the velocity vector, v the lateral component of the vector, and w the component of the vector normal to the slope surface. The statistical properties of turbulence were expressed in the new coordinate system.

E.2.4.2 Spectral Analysis

The power spectrum ϕ of the α component of the velocity (i.e. u, v, w) is defined as

$$\int_0^\infty \phi_{\alpha\alpha}(n)dn = \frac{1}{2}\overline{\alpha'^2}$$

where n is natural frequency in cycles per second (Hz) and $\overline{\alpha'^2}$ is the variance of α. The power spectra were calculated using a fast Fourier transform procedure written in Pascal

Table E.1: Comparison of the wind speed (m/s) at a height of 2 m measured by a hot wire anemometer (U) with the 'cup' speed measured by a sonic anemometer (V) on 9 August 1989 in the old growth Douglas-fir stand near Woss.

Run	Time (PST)	U	V
1a	10:00–10:30	0.76	0.73
1b	10:30–11:00	1.18	1.12
2a	13:15–13:45	1.39	1.31
2b	13:45–14:15	1.31	1.25
3a	22:15–22:45	0.50	0.41
3b	22:45–23:15	0.49	0.38

(Brigham 1988). The DC component and slope of the time series were removed before using the procedure.

E.3 Results and Discussion

E.3.1 Wind Regimes

E.3.1.1 Daily Pattern

On clear days there was a well defined anabatic (upslope, approximately 180°) and katabatic (downslope, approximately 0°) wind pattern both inside and outside the stand on this south-facing slope, as shown in Figures E.2 and E.3 for 9 August 1991. Driven by solar heating, the anabatic wind was well developed by around 08:00 PST. Wind speed increased with time and reached peak values of 3.5 and 1.9 m/s at the reference location and inside the stand, respectively, at 13:30 PST, when solar heating was greatest. After that wind speed decreased gradually. A transition occurred at 17:30 PST, when the upslope wind was replaced by a light downslope breeze. The nighttime wind speed fluctuated around 0.8 and 0.5 m/s at the reference location and inside the stand, respectively.

E.3.1.2 Comparison of Wind Speed inside and outside the Stand

The wind inside the stand was well coupled with that outside the stand despite the heavy overstory coverage, the correlation coefficient being 0.87 for 249 runs (Figure E.4). The positive offset of the regression equation shown in the figure was probably caused by the inertia of the vaned propeller anemometer at the reference location. Wind speed inside the stand was on average 28% of that outside the stand. This value is rather high, suggesting the existence of a secondary maximum in the profile of wind speed in the stand. Secondary maxima in the wind profiles have been frequently observed in the trunk space of forests (e.g. Shaw 1977). As a consequence of this maximum, gas and

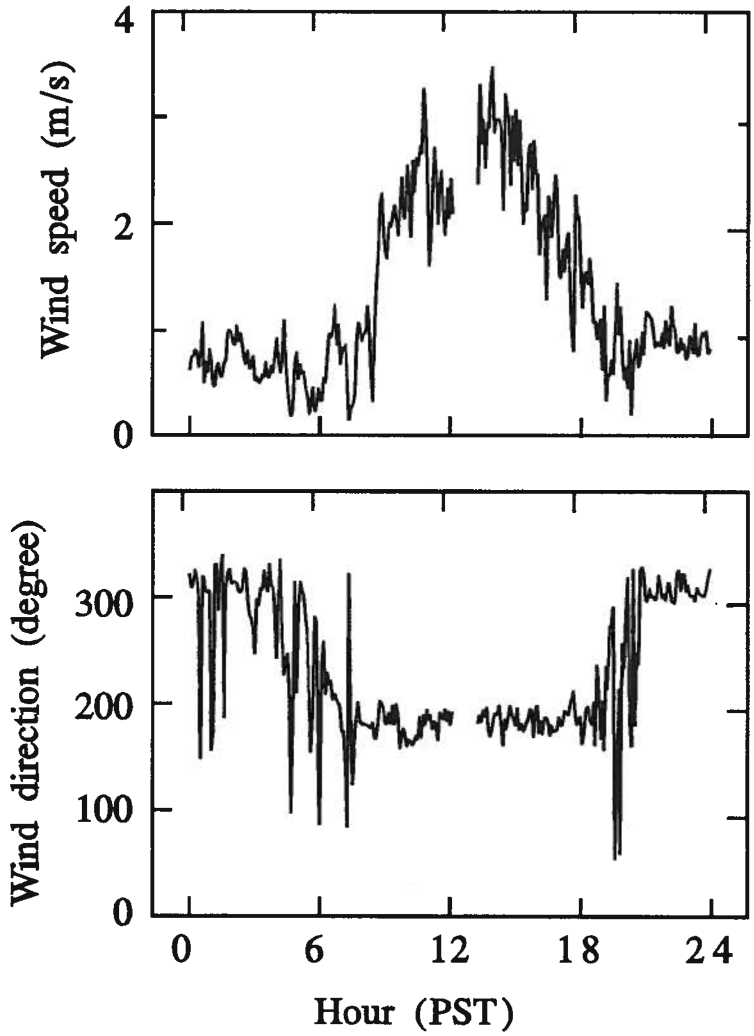

Figure E.2: Daily pattern of 5-minute average wind speed and direction observed on a clear day (9 August 1989) at a height of 4.2 m on the logging road outside the old growth Douglas-fir stand near Woss.

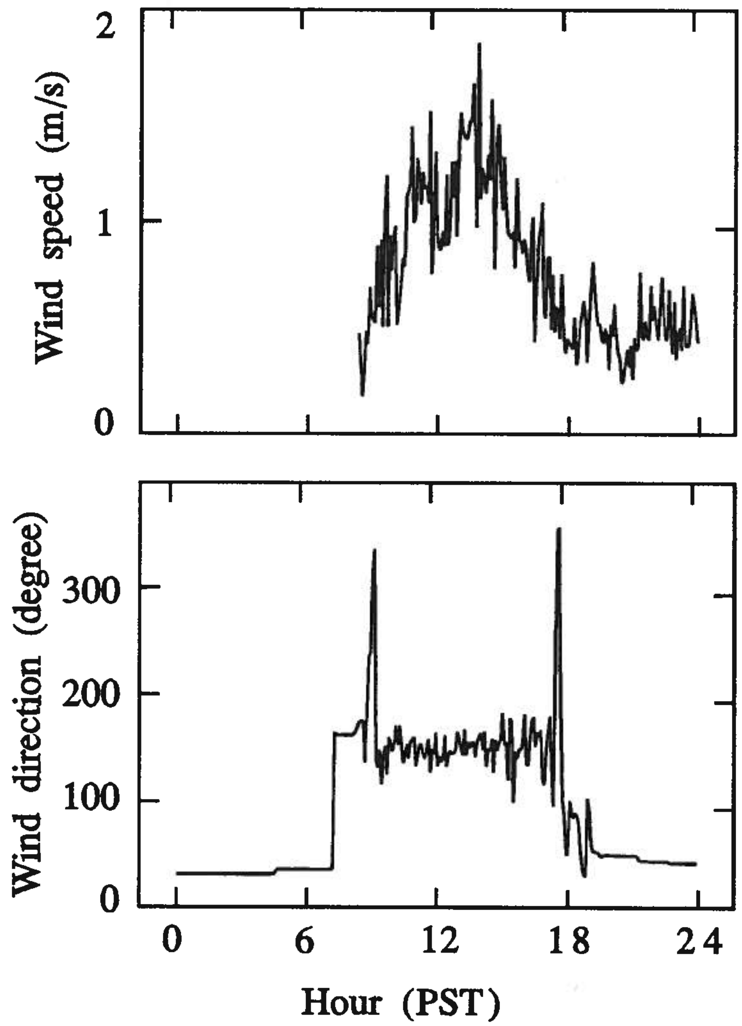

Figure E.3: Same as in Figure E.2 except at a height of 2 m inside the stand. The wind vane was stalled during the period between 0:00 and 7:00 PST.

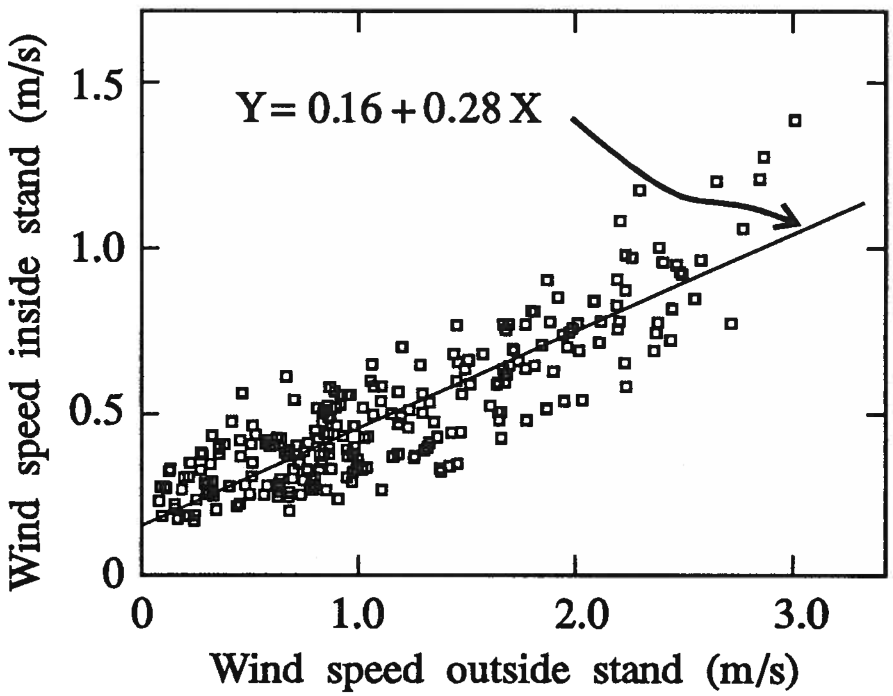

Figure E.4: Comparison of 30-minute average wind speed at a height of 2 m inside the old growth Douglas-fir stand near Woss with that at a height of 4.2 m outside the stand during the period from July 29 to August 19, 1989. Also shown is the equation for the best fit line.

heat exchange between the understory vegetation and the air, and the heat loss from animals are likely to be enhanced. In this sense, the old growth stand is not as good an 'insulating' environment as one may expect.

E.3.1.3 Wind Speed Profiles near the Forest Floor

For practical purposes, wind speed near the ground surface beneath a vegetation canopy is commonly described by (Wilson and Shaw 1977)

$$U(z)/U_r = \ln(\frac{z}{z_o})/\ln(\frac{z_r}{z_o}) \tag{E.1}$$

where $U(z)$ is the wind speed at height z measured with the hot wire anemometer, U_r is the wind speed at a reference height z_r (z_r = 2.0 m in this case), and z_o is an effective roughness length of the ground surface. In this study, the daytime wind speed increased approximately logarithmically with height (Figure E.5). As shown in this figure, the prediction of (E.1) with a value of 0.005 m for z_o agreed well with the daytime measurements. This value of z_o was smaller than expected, considering that there were scattered understory vegetation and dead debris on the forest floor. In other words, the forest floor was aerodynamically smoother than it appeared to be.

The nighttime wind speed was generally low. The nighttime profiles were slightly different in shape from the daytime profiles. For most of the nighttime runs, the wind speeds at 0.8 m and 0.4 m were of similar magnitude, while for some runs the wind speed at 0.4 m exceeded that at 0.8 m. This feature may be an indication of the thermally induced drainage flow on the slope during the nighttime.

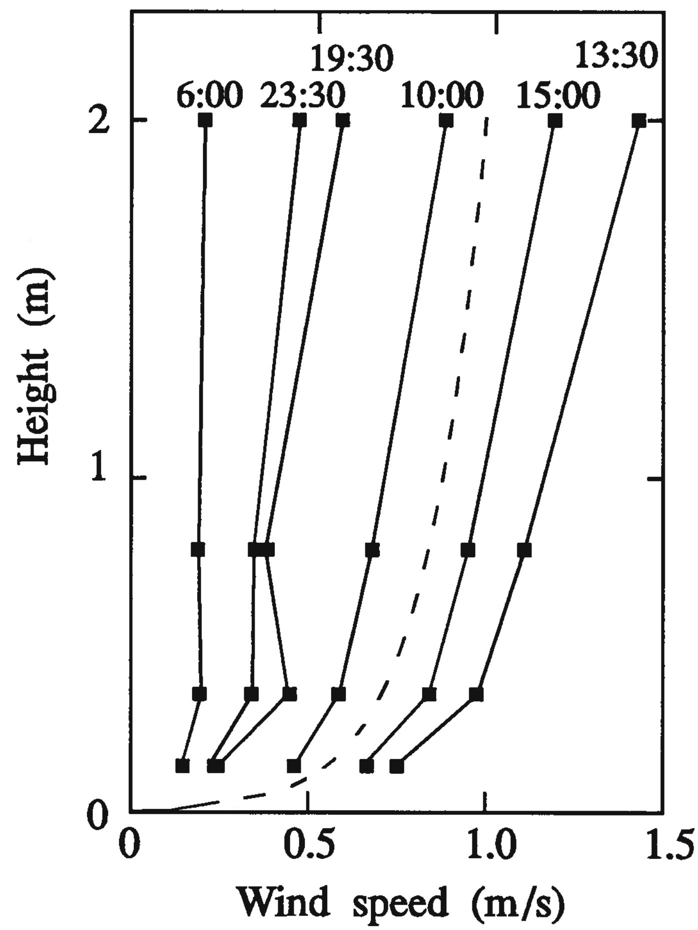

Figure E.5: Profiles of 30-minute average wind speed during the period from 09:30 PST 9 August to 06:00 PST 10 August 1989 near the forest floor of the old growth Douglas-fir stand near Woss. The time shown above each profile marks the end of the 30-minute run. The dashed line represents a logarithmic profile calculated from Equation(E.1) with a value of 0.005 m for z_o and a value of 1 m/s for U_r.

E.3.2 Turbulence Statistics

E.3.2.1 Variance and Momentum Flux

Information regarding variance of the velocity components is helpful for developing canopy flow models (e.g. Wilson and Shaw 1977, Wilson 1988) and for understanding of dispersion and diffusion processes in a plant canopy (Raupach 1987). The daytime averaged values for the u variance $(\overline{u'^2})$, v variance $(\overline{v'^2})$ and w variance $(\overline{w'^2})$ were 0.111, 0.094 and 0.008 m^2/s^2, respectively. The corresponding figures for the nighttime were 0.017, 0.014 and 0.004 m^2/s^2. The daytime ratios of $\overline{v'^2}/\overline{u'^2}$ and $\overline{w'^2}/\overline{u'^2}$ were, on average, 0.87 and 0.07, respectively. While the ratio $\overline{v'^2}/\overline{u'^2}$ was similar to that observed in the neutral surface layer (Panofsky and Dutton 1984) and in some other forest stands (e.g. Amiro 1990a and Baldocchi and Meyers 1988), the ratio of $\overline{w'^2}/\overline{u'^2}$ in the present study was much smaller. The small value was likely a consequence of the measurement being close to the ground (our sensor height/canopy height ratio was 0.07), and might have been related to the stratification of the air layer in the lower part of the stand. As pointed out later in this paper, daytime air temperature exhibited characteristically a moderate to strong inversion in the $0 < z < 2$ m layer. It is well established that in the surface layer the main contribution to w variance comes from smaller eddies and that the main contributions to u and v variances come from much larger eddies. Consequently, w variance obeys Monin–Obukhov scaling, i.e. a similarity theory that applies to the exchange processes in the atmospheric surface layer, while u and v variances do not (Panofsky and Dutton 1984). The spectral analysis presented later in this paper shows that the energy containing frequencies of the w variance were higher than those of the u and v variances by a factor of 10. In other words, turbulent energy was fed into the w component and the u and v components from eddies of quite different sizes. Vertical fluctuations were more subject to the local stratification in the lower part of the stand, because the size of the energy containing eddies was small, and hence were suppressed. On the other hand, streamwise and lateral fluctuations might be affected more by the external environment which was not necessarily stable, because the energy containing eddies were large.

Values of tangential momentum flux $-\overline{u'w'}$ varied from 0.035 to -0.015 m^2/s^2. Half the runs had negative values. Other researchers (Baldocchi and Hutchison 1987, Raupach *et al.* 1986, Chapter 2) have also reported negative momentum flux at the lower height within plant canopies. They suggested that the negative values, if real, might be associated with dispersive flux. Dispersive flux arises from the spatial correlation of quantities averaged in time but varying with horizontal position (Raupach and Shaw 1982). However, it is possible that the negative momentum flux reported here was a result of errors in the measurements or in performing the coordinate rotation on a steep slope.

E.3.2.2 Turbulence Intensity

Turbulence intensity is defined as

$$i = \frac{\sqrt{\overline{u'^2} + \overline{v'^2} + \overline{w'^2}}}{\overline{u}}$$

where $\overline{u}$ is the mean value of the streamwise velocity component. Figure E.6 plots the intensity (i) as a function of wind speed ($\overline{u}$). Much of the scatter occurred at wind speed less than 0.3 m/s, with the value of i occasionally exceeding 3.0. At higher wind speed, the intensity approached a constant value of approximately 0.7. This value was lower than that obtained by Baldocchi and Hutchison (1987) and Moritz (1989) near the forest floors of a deciduous forest and a pine forest, respectively, but similar to that obtained by Allen (1968) in a Japanese larch plantation.

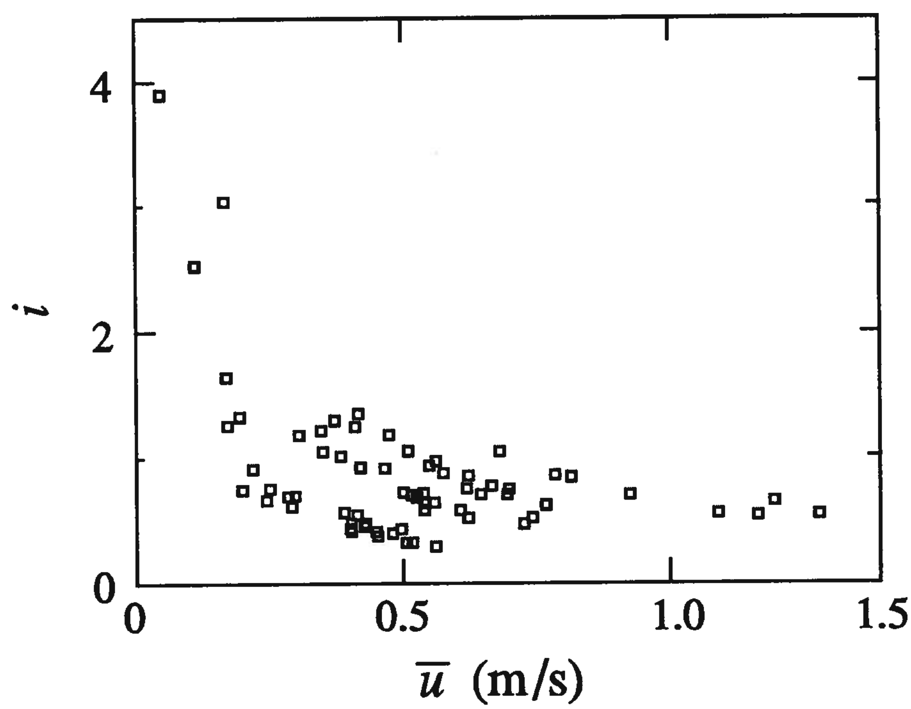

Figure E.6: Turbulence intensity (i) as a function of mean streamwise velocity ($\overline{u}$) at a height of 2 m inside the old growth Douglas-fir stand near Woss.

E.3.2.3 Higher Order Moments

Skewness and kurtosis were calculated from the the burst mode data obtained on 9 August 1989 (Table E.2). Skewness expresses the degree of asymmetry about the mean of a probability distribution. The values of skewness for the velocity components were not equal to zero, a value for the Gaussian distribution, and exhibited variability in magnitude for all three components and uncertainties in sign except for w component. The skewness of the w component was positive for all six 30-minute runs, implying active updraft motions. This seems to contradict the general picture that large scale downward movements are dominant in the plant canopy, making w skewness negative (e.g. Shaw and Seginer 1987, Raupach *et al.* 1986, Amiro and Davis 1988, Moritz 1989, Baldocchi and Hutchison 1987, Kelliher *et al.* 1991). However, Leclerc *et al.* (1991) found that w skewness in a deciduous forest canopy could become positive in strongly stable conditions.

Kurtosis is a measure of peakness or flatness of a probability distribution. For most of the runs, the values of the kurtosis of the velocity components were higher than 3, the value for the Gaussian distribution, but much smaller than those observed by other workers (e.g., Amiro and Davis 1988 and Raupach *et al.* 1986).

E.3.3 Power Spectra

The power spectrum of a quantity reveals the relative importance of eddies of different size in its variance. The spectra of the velocity components were calculated for the period 13:15–14:15 PST on 9 August (Figure E.7). The spectrum of the u component shows double peaks, the dominant one at 0.01 Hz and the less developed one at 0.5 Hz. A similar pattern was also found for the v component. This bimodal distribution is similar to the observations made by Allen (1968) for the streamwise velocity in a Japanese Larch plantation, with peaks occurring at 0.05 and 0.3 Hz, and the main contribution being

Table E.2: Turbulence statistics at a height of 2 m on 9 August 1989 in the old growth Douglas-fir stand near Woss, where $\overline{u}$ is the mean streamwise component of the velocity inside the stand and u_{ref} is the wind speed at the reference location outside the stand. The time of the runs is given in Table E.1.

Run	wind speed		variance			skewness			kurtosis		
	$\overline{u}$	u_{ref}	u	v	w	u	v	w	u	v	w
	m/s		m^2/s^2								
1a	0.67	2.38	0.14	0.12	0.01	0.58	0.17	0.12	3.99	2.79	3.53
1b	1.09	2.65	0.18	0.17	0.01	−0.54	−0.05	0.30	3.11	3.59	4.12
2a	1.28	2.91	0.29	0.18	0.02	−0.56	−0.08	0.47	4.39	3.23	4.50
2b	1.20	3.11	0.30	0.29	0.02	−0.26	0.72	0.82	2.62	4.10	4.67
3a	0.48	0.86	0.01	0.02	0.00	0.20	0.19	0.02	3.34	3.01	3.05
3b	0.43	0.86	0.02	0.02	0.00	−0.68	−0.22	0.08	3.95	2.51	3.09

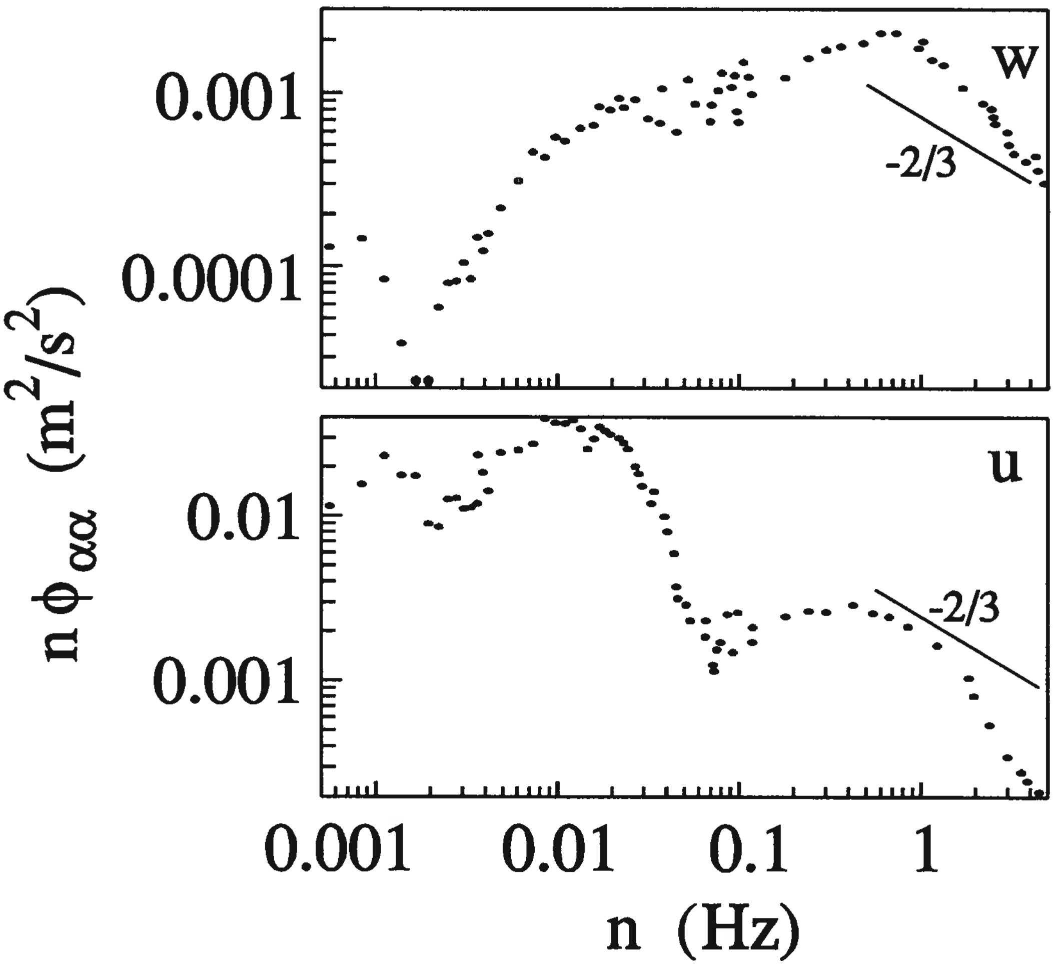

Figure E.7: Power spectra of the streamwise (u) and vertical (w) velocity components for the period 13:15–14:15 PST on 9 August 1989 at a height of 2 m in the old-growth Douglas-fir stand near Woss. Also shown is the slope predicted for the inertial subrange.

from the lower frequency peak. This means that near the forest floor there was less variance on small scales and that most of the streamwise and lateral variations of the air flow was associated with eddies of large scale.

Some researchers have suggested that turbulent wakes generated by the plant elements are responsible for the higher frequency peak in the power spectra inside canopies (Allen 1968, Seginer *et al.* 1976, Raupach *et al.* 1986, Amiro and Davis 1988). Some of them found that the secondary peak frequency could be predicted using (Seginer *et al.* 1976, Amiro and Davis 1988)

$$St = nd/\overline{u} \tag{E.2}$$

where d is an effective dimension of the plant elements, n is the frequency of the wakes, and St is the Strouhal number, which has a value of 0.21 for cylinders for Reynolds numbers between 6×10^2 and 6×10^3 (Schlichting 1968). In the present study, tree trunks were the main elements in the lower part of the stand. The diameter of the dominant trees was about 0.4 m. Using (E.2) with the value of 0.21 for St and a value of 1.2 m/s for $\overline{u}$, the frequency of the wakes of the tree trunks was found to be about 0.4 Hz, which is quite close to the secondary peak frequency. The vortices shed by the vertical cylinders, i.e. tree trunks, were mainly of vertical vorticity (Seginer *et al.* 1976), which would more likely show up in the u and v energy spectra. The u and v energy spectra may therefore be viewed as spectra combining the effects of wake production of the tree trunks and the low frequency fluctuations associated with large eddies.

The ratio of the size of vortices in the wake of the trunks to the characteristic dimension of the body of ungulates, e.g. mature black tailed deer, is approximately 1.0–2.3. According to the studies of Zijnen (1958) on heat transfer from cylinders in turbulent flow, ratios in this range would result in maximum heat loss. This implies that the size of vortices in the wake would be optimum to enhance heat transfer from the body of the deer.

In contrast, only one peak can be identified in the w power spectrum. The main contribution was from high frequencies, suggesting that the fluctuations in the w component were related to much smaller eddies. The peak of the w power spectrum occurred at around the secondary peak frequency of the u and v spectra. The separation between the energy containing frequencies of the u and v components and the w component near the forest floor has also been observed in several other cases (Baldocchi and Hutchison 1987, Amiro 1990b).

Besides resulting in the production of turbulent wakes, the drag force imposed on the canopy flow by plant elements short-circuits the energy cascade process, i.e. the continuous transfer of turbulence kinetic energy from larger to progressively smaller eddies (Shaw and Seginer 1985). The short circuit in the cascade, in combination with the invalidity of Taylor's frozen turbulence hypothesis in plant canopies and the energy loss due to the averaging over the path length between the transducers of the sonic anemometer, caused the power spectra to deviate from Kolmogorov's local isotropy law (Amiro and Davis 1988). This is evident from the slope of the high frequency range in Figure E.7 being steeper than $-2/3$, the slope predicted for the inertial subrange (Tennekes and Lumley 1972).

E.3.4 Energy Budget near the Forest Floor

The magnitudes of the energy budget components near the forest floor were rather small. The half-hourly values for net radiation flux (R_n), heat flux into the soil (G), sensible heat flux (H) and latent heat flux (λE) varied between –3 and 58, –5 and 10, –11 and 2 and 1 and 21 W/m^2, respectively. λE was positive (upward) for all 67 runs, which was expected since the forest floor was fairly wet during the experimental period. H was slightly positive in the nighttime and was negative (downward) for the majority of the runs (39 out of 50) in the daytime. The temperature profile near the forest floor constantly exhibited a moderate to strong inversion in the daytime, the gradient being as high as 0.3 °C/m, and a slight lapse in the nighttime. The directions of the temperature gradient resulted mainly from the radiative heating of the overstory in the daytime and cooling at night. These results suggest that very close to the floor of the tall forest, the scalar fluxes generally flowed down their respective gradients, although the phenomenon of counter-gradient flow has been frequently observed in the middle and upper parts of the forest stands (Denmead and Bradley 1985, Leclerc 1987, Amiro 1990a, Chapter 3). In fact, there existed a fair correlation between H and the temperature gradient calculated from the measurements at the heights of 2 m and 0.2 m, the correlation coefficient being 0.76 for the 67 runs.

Table E.3 shows the averaged values of the energy budget components for five periods. It can be seen that λE was the main output component of the energy budget of the forest floor during the daytime. The sum of the eddy fluxes ($H + \lambda E$) was slightly lower than the available energy flux ($R_n - G$), but overall the energy budget closure was satisfactory considering the small magnitudes of the components. The daytime courses of the energy budget components shown in Figure E.8 for 17 August 1989 are typical of those during the experimental period.

E.4 Concluding Remarks

On clear days, anabatic and katabatic winds were observed inside and outside the stand. The high value of of the ratio of wind speed inside the stand to that outside the stand (0.28) suggests that there existed a secondary maximum in the stand wind profile. This means that the old growth stand was not as good an 'insulating' environment as might be expected. The wind speed near the forest floor was well approximated by the logarithmic

Table E.3: Components (W/m^2) of the energy budget of the forest floor of the old growth Douglas-fir stand near Woss in August 1989. R_n is net radiation flux, G is the heat flux into the soil, H and λE are the eddy fluxes of sensible and latent heat, respectively. Also listed are the measure of energy budget closure (R_n–G–H–λE) and the average value of the global (horizontal surface) solar irradiance (S, W/m^2) outside the stand.

Date	9	9 to 10	10	17	18
Period (PST)	11:30–17:00	20:30–6:00	10:30–14:00	9:30–17:00	9:30–16:30
S	588	0	568	501	627
R_n	24	–3	21	23	26
G	3	–4	2	5	6
H	–3	1	–1	–2	–3
λE	17	1	13	8	13
R_n–G–H–λE	7	–1	7	12	10

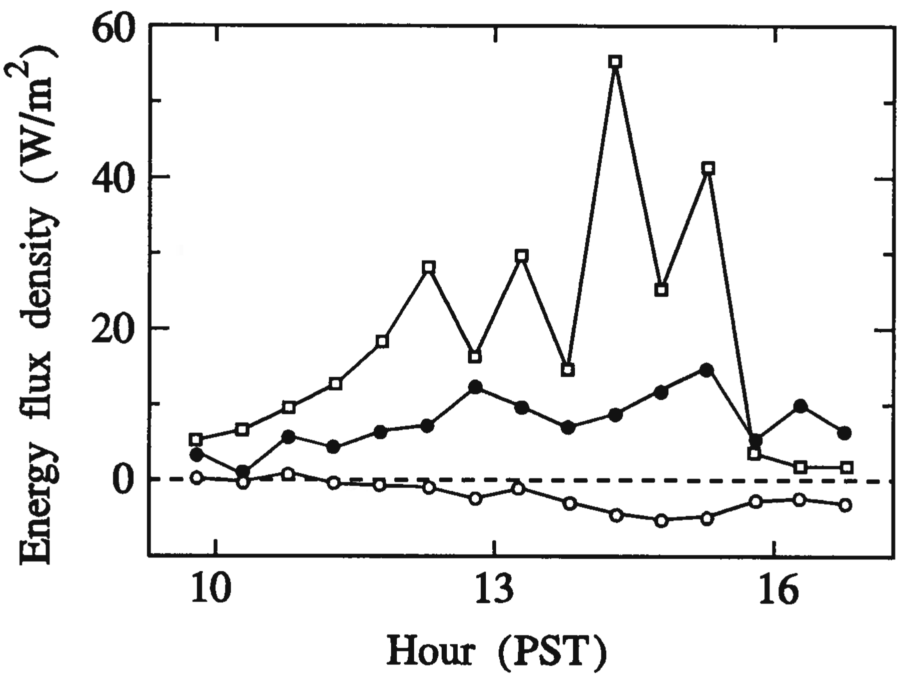

Figure E.8: Daytime courses of the energy budget components of the forest floor of the old growth Douglas-fir stand near Woss on 17 August 1989: (□) $R_n - G$, (○) H, and (•) λE. The sky was overcast.

wind profile equation with an effective roughness length of 0.005 m.

Turbulence intensity was a function of wind speed. The value of the intensity was about 0.7 for wind speed higher than 0.3 m/s. The skewness of the vertical velocity component was positive, implying active updraft movements near the forest floor. The power spectra for the streamwise and lateral velocity components exhibited a bimodal distribution, the main contribution being at the lower frequency peak. The sizes of the eddies corresponding to the higher frequency peak, probably the result of wakes produced by the tree trunks, were comparable to the trunk diameter of mature black-tailed deer. This may have implications in the turbulence enhancement of heat loss from the animal. Only one peak was identified in the spectrum for the vertical velocity component.

Latent heat flux was the main output component of the energy budget of the forest floor and was directed upward. Results showed that that eddy fluxes of sensible heat and water vapour near the forest floor generally flowed down their respective gradients.

E.5 Literature Cited

ALLEN, L.J. 1968. Turbulence and wind speed spectra within a Japanese larch plantation. J. Appl. Meteorol. 7:73-78.

AMIRO, B.D. 1990a. Comparison of turbulence statistics within three boreal forest canopies. Boundary-Layer Meteorol. 51:99-121.

AMIRO, B.D. 1990b. Drag coefficients and turbulence spectra within three boreal forest canopies. Boundary-Layer Meteorol. 52:227-246.

AMIRO, B.D. and P.A. DAVIS. 1988. Statistics of atmospheric turbulence within a natural black spruce forest canopy. Boundary-Layer Meteorol. 44:267-283.

BAKER, C.B. 1989. Experimental determination of transducer shadow effects on a sonic anemometer. Eighth Symposium on Turbulence and Diffusion, Preprint volume, American Meteorological Society, San Diego, CA, pp 104-107.

BALDOCCHI, D.D. and B.A. HUTCHISON. 1987. Turbulence in an almond orchard: Vertical variations in turbulent statistics. Boundary-Layer Meteorol. 40:127-146.

BALDOCCHI, D.D. and T.P. MEYERS. 1988. Turbulence structure in a deciduous forest. Boundary-Layer Meteorol. 43:345-364.

BLACK, T.A., J.M. CHEN, X. LEE, and R.M. SAGAR. 1991. Characteristics of shortwave and longwave irradiances under a Douglas-fir forest stand. Can. J. For. Res. 21:1020-1208.

BLACK, T.A. and F.M. KELLIHER. 1989. Processes controlling understory evapotranspiration. Phil. Trans. R. Soc. Lond. B324:207-231.

BRIGHAM, E.O. 1988. The Fast Fourier Transform and Its Applications, Englewood Cliffs, NJ.

CAMPBELL, G.S., A.J. McARTHUR, and J.L. MONTEITH. 1980. Windspeed dependence of heat and mass transfer through coats and clothing. Boundary-Layer Meteorol. 18:485-493.

CHEN, J.-M., A. IBBETSON, and J.R. MILFORD. 1988. Boundary-layer resistances of artificial leaves in turbulent air: I. Leaves parallel to the mean flow. Boundary-Layer Meteorol. 45:137-156.

CONKLIN, P.S., K.R. KNOERR, T.W. SCHNEIDER, and C.B. BAKER. 1989. A wind tunnel test of probe shadow effects on a sonic anemometer in two orientation. Eighth Symposium on Turbulence and Diffusion, Preprint volume, American Meteorological Society, San Diego, CA, pp 108-110.

DENMEAD, O.T. and E.F. BRADLEY. 1985. Flux-gradient relationships in a forest canopy. The Forest-Atmospheric Interaction, HUTCHISON, B.A. and B.B. HICKS (eds.). D. Reidel Publishing Co., Dordrecht, pp 421-442.

KAIMAL, J.C. 1979. Sonic anemometer measurement of atmospheric turbulence. Proceedings of Dynamic Flow Conference. Skovlunde, Denmark, DISA Electronic A/S, pp 551-565.

KANEMASU, E.T. and C.B. TANNER. 1968. A note on a heat transport anemometer. BioScience. 18:327-329.

KELLIHER, F.M., D. WHITEHEAD, K.J. McANENEY, AND M.J. JUDD. 1991. Partitioning evapotranspiration into tree and understorey components in two young *Pinus radiata* D. Don stands. Agric. Forest Meteorol. 50:211-227.

LECLERC, M.Y. 1987. Turbulence and turbulent diffusion inside and above vegetation. Ph.D. Thesis. University of Guelph, Guelph, Ontario.

LECLERC, M.Y., K.C. BEISSNER, R.H. SHAW, G. den HARTOG, and H.H. NEUMANN. 1991. The influence of buoyancy on third-order turbulent velocity statistics within a deciduous forest. Boundary-Layer Meteorol. 55:109-124.

McARTHUR, A.J. and J.L. MONTEITH. 1980. Air movement and heat loss from sheep. I: Boundary layer insulation of a model sheep, with and without fleece. Proc. R. Soc. Lond. B209:187-208.

MORITZ, E. 1989. Heat and momentum transport in an oak forest canopy. Boundary-Layer Meteorol. 49:317-329.

PANOFSKY, H.A. and J.A. DUTTON. 1984. Atmospheric Turbulence: Models and Methods for Engineering Applications, John Wiley & Sons, New York.

RAUPACH, M.R. 1987. A Lagrangian analysis of scalar transfer in vegetation canopies. Quart. J. R. Meteorol. Soc. 113:107-120.

RAUPACH, M.R. and R.H. SHAW. 1982. Averaging procedures for flow within vegetation canopies. Boundary-Layer Meteorol. 22:79-90.

RAUPACH, M.R., P.A. COPPIN, and B.J. LEGG. 1986. Experiments on scalar dispersion within a model plant canopy. Part I: The turbulence structure. Boundary-Layer Meteorol. 35:21-52.

ROEMER, H.L., J. POJAR, and K.R. JOY. 1988. Protected old-growth forests in coastal British Columbia. Natural Areas Journal. 8:146-159.

SAGAR, R.M., T.A. BLACK, X. LEE, and J.M. CHEN. 1991. Heat transfer relationships for deer in Douglas-fir stands. 20th Conference on Agricultural and Forest Meteorology and 10th Conference on Biometeorology and Aerobiology, American Meteorological Society, Salt Lake City, UT. Preprint volume. pp 129-132.

SCHLICHTING, H. 1968. Boundary-Layer Theory. 6th Edition, McGraw-Hill Book Company, New York.

SEGINER, I., P.J. MULHEARN, E.F. BRADLEY, and J.J. FINNIGAN. 1976. Turbulent flow in a model plant canopy. Boundary-Layer Meteorol. 10:423-453.

SHAW, R.H. 1977. Secondary wind speed maxima inside plant canopies. J. Appl. Meteorol. 16:514-523.

SHAW, R.H. and I. SEGINER. 1985. The dissipation of turbulence in plant canopies. Seventh Symposium on Turbulence and Diffusion, Preprint volume, American Meteorological Society, Boston, Massachusetts, pp 200-203.

SHAW, R.H. and I. SEGINER. 1987. Calculation of velocity skewness in real and artificial plant canopies. Boundary-Layer Meteorol. 39:315-332.

TENNEKES, H. and J.L. LUMLEY. 1972. A First Course in Turbulence, The MIT Press, Massachusetts.

WILSON, J.D. 1988. A second-order closure model for flow through vegetation. Boundary-Layer Meteorol. 42:371-392.

WILSON, R.N. and R.H. SHAW. 1977. A higher order closure model for canopy flow. J. Appl. Meteorol. 14:1197-1205.

Van der HEGGE ZIJNEN, B.G. 1958. Heat transfer from horizontal cylinders to a turbulent air flow. Appl. Sci. Res. A7:205-223.

Appendix F

Maps of the Browns River Research Site

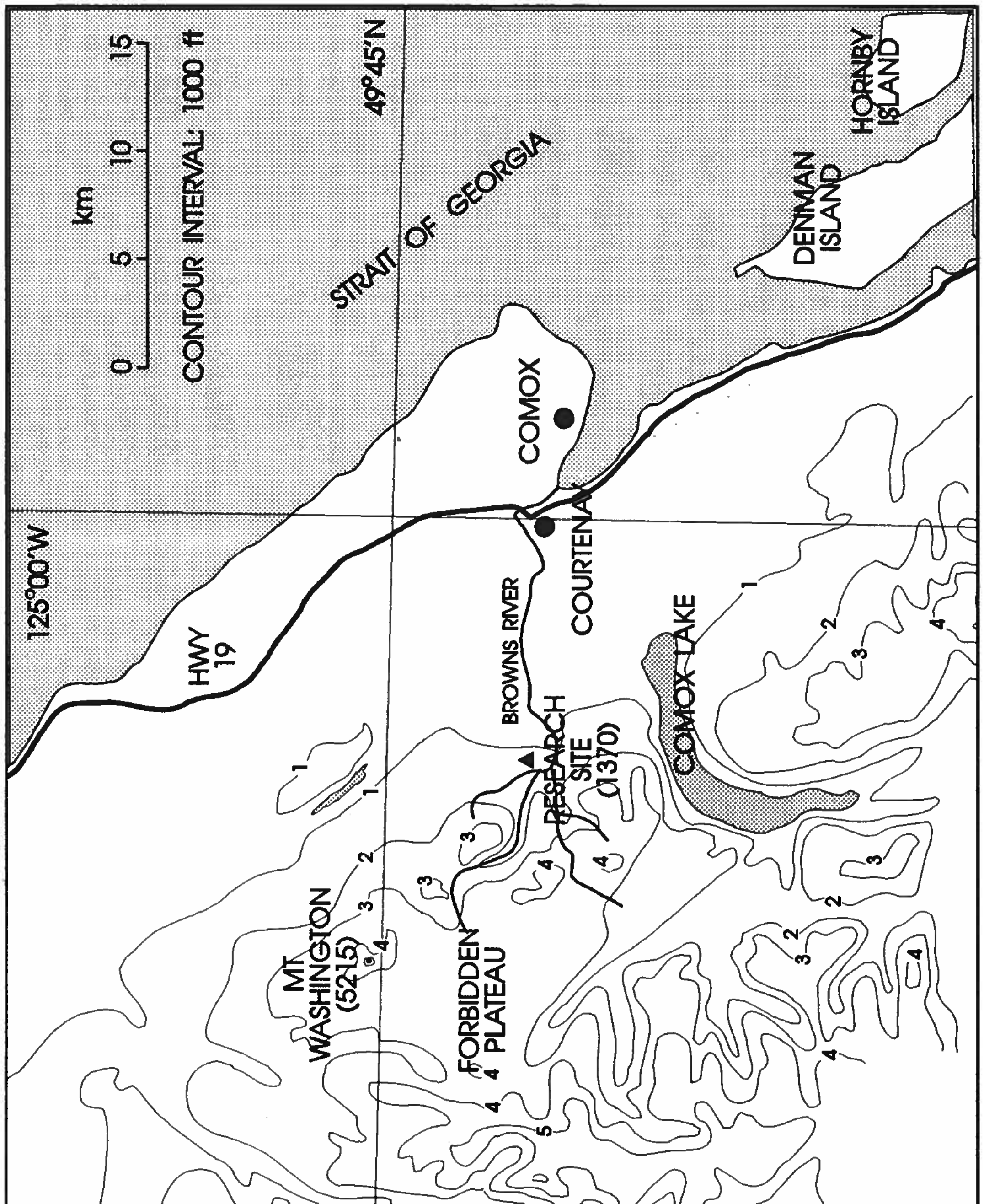

Figure F.1: Topographic map of the area around the Browns River Research Site. Contour elevations are in thousands of feet above mean sea level. The forest surrounding the site is second growth Douglas-fir of similar age which extends at least 5 km in all directions.

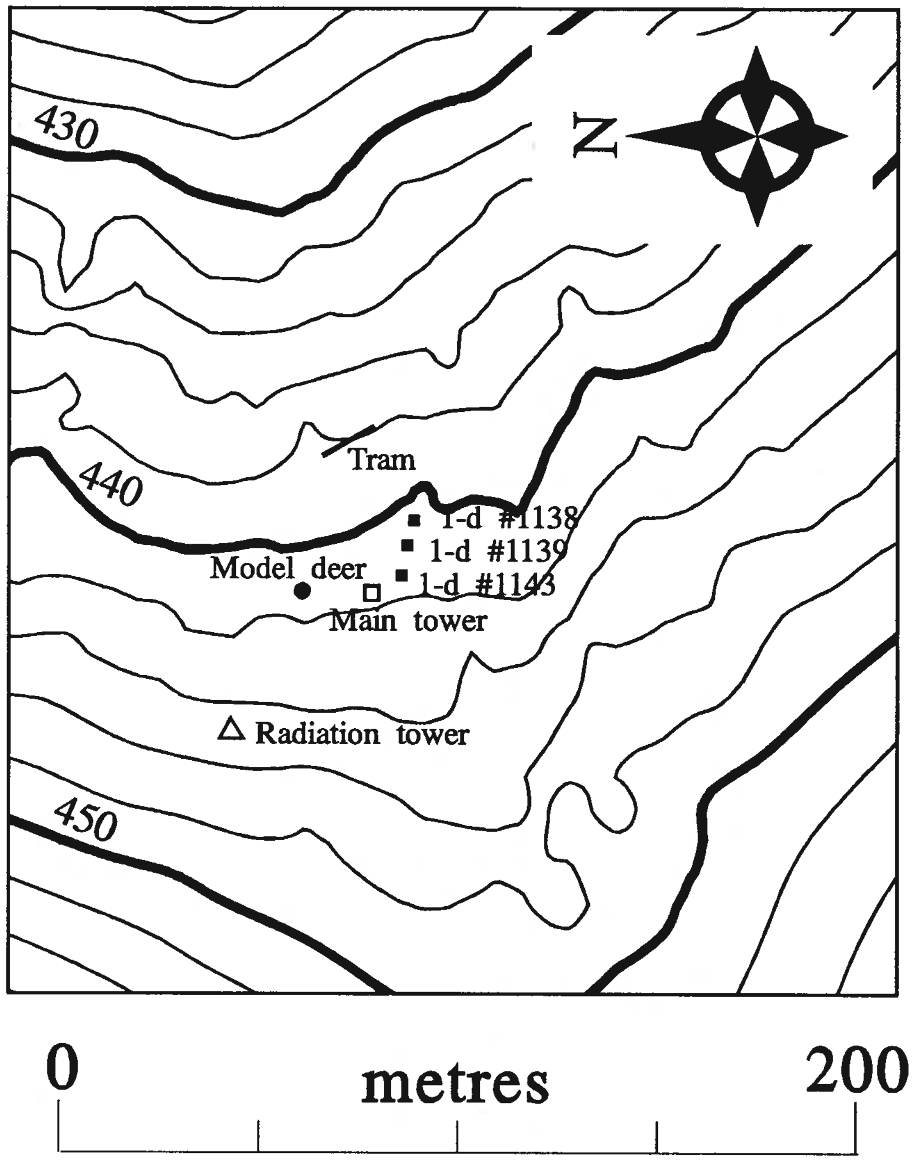

Figure F.2: Positions of the instruments used in the Browns River experiment: main instrument tower (□), tower for measuring diffuse solar irradiance above the stand (△), tram for radiation measurements (—), model deer (•), and one-dimensional sonic anemometer/thermometer units (■). Contour elevations are in metres above mean sea level.